EXPERIMENTAL ANALYSIS OF PRECAST SANDWICH PANELS WITH EPS CORE AND MORTAR WYTHES UNDER AXIAL LOAD

KAMIRÃ BARBOSA RIBEIRO

UNIVERSIDADE DE BRASÍLIA

FACULDADE DE TECNOLOGIA

BRASÍLIA/DF

JULHO – 2023

UNIVERSIDADE DE BRASÍLIA

FACULDADE DE TECNOLOGIA

DEPARTAMENTO DE ENGENHARIA CIVIL E AMBIENTAL

EXPERIMENTAL ANALYSIS OF PRECAST SANDWICH PANELS WITH EPS CORE AND MORTAR WYTHES UNDER AXIAL LOAD

KAMIRÃ BARBOSA RIBEIRO

ORIENTADOR: WILLIAM TAYLOR MATIAS SILVA

COORIENTADOR: RAMON SALENO YURE RUBIM COSTA SILVA

DISSERTAÇÃO DE MESTRADO EM ESTRUTURAS E CONSTRUÇÃO CIVIL

BRASÍLIA/DF

JULHO – 2023

UNIVERSIDADE DE BRASÍLIA

FACULDADE DE TECNOLOGIA
DEPARTAMENTO DE ENGENHARIA CIVIL E AMBIENTAL

EXPERIMENTAL ANALYSIS OF PRECAST SANDWICH PANELS WITH EPS CORE AND MORTAR WYTHES UNDER AXIAL LOAD

KAMIRÃ BARBOSA RIBEIRO

DISSERTAÇÃO DE MESTRADO SUBMETIDA AO DEPARTAMENTO DE ENGENHARIA CIVIL E AMBIENTAL DA FACULDADE DE TECNOLOGIA DA UNIVERSIDADE DE BRASÍLIA COMO PARTE DOS REQUISITOS NECESSÁRIOS PARA A OBTENÇÃO DO GRAU DE MESTRE EM ESTRUTURAS E CONSTRUÇÃO CIVIL.

APROVADA POR:

Prof. William Taylor Matias Silva, Dr. Ing.
(ENC/UnB)

EXAMINADOR INTERNO

Prof. Luciano Mendes Bezerra, PhD. (ENC/UnB)
EXAMINADOR INTERNO

Prof. Cleirton Andre Silva de Freitas, Dsc (UFCA)

EXAMINADOR EXTERNO

BRASÍLIA/DF, 28 DE JULHO DE 2023

FICHA CATALOGRÁFICA

RIBEIRO, KAMIRÃ BARBOSA
Experimental Analysis of Precast Sandwich Panels with EPS Core and Mortar Wythes Under Axial Load [Distrito Federal] 2023.

xxii, 116p., 210x297 mm (ENC/FT/UnB, Mestre, Estruturas e Construção Civil, 2023).
Dissertação de Mestrado – Universidade de Brasília, Faculdade de Tecnologia.
Departamento de Engenharia Civil e Ambiental
1. ???? 2. ??????
3. ???? 4. ???????
I. ENC/FT/UnB II. Título (Mestre)

REFERÊNCAI BIBLIOGRÁFICA

Ribeiro, Kamirã Barbosa (2023). **Análise Experimental de Painéis Sanduíche com Núcleo de EPS e Argamassa Armada à Compressão**. Dissertação de Mestrado em Estruturas eConstrução Civil, Publicação E.DM - 10A/22, Departamento de Engenharia Civil e Ambiental, Universidade de Brasília, Brasília-DF, 109p.

CESSÃO DE DIREITOS

AUTOR: Kamirã Barbosa Ribeiro

TÍTULO: EXPERIMENTAL ANALYSIS OF PRECAST SANDWICH PANELS WITH EPS CORE AND MORTAR WYTHES UNDER AXIAL LOAD

GRAU: Mestre ANO: 2023

Kamirã Barbosa Ribeiro
Qd.107, Lt.1, Cond. Alameda dos Eucaliptos, apto 604
71919-700 Brasília-DF – Brasil.
barbosakamira@gmail.com

AGRADECIMENTOS

A Deus, pela benevolência.

A todos os Orixás, dos quais o axé me deu um sentido de viver.

A minha mãe, pelo amor que não cabe em nenhuma linha deste mundo.

A meu pai, minha família, meus amigos e todos que me apoiaram.

Ameus avós, Scheilla e Newton, por serem um pilar da minha vida e por terem me ensinado tantos valores.

A meu orientador, Prof. William Taylor Matias Silva, pelo estímulo, prestatividade, e apoio intelectual e de todas as formas.

A meu coorientador Prof. Ramon Saleno Yure Rubim Costa Silva, pelo companheirismo, incentivo, gentileza e boas risadas.

Ao meu amigo Welington Vital da Silva, sem o qual esta dissertação não teria sido concluída, pelo exemplo de caráter, simplicidade, e fé.

A todos os estudantes e professores do PECC, em especial ao Prof. Luciano Mendes Bezerra, pela amizade, direcionamento, e alegria sem igual que compartilhamos nessa aventura da pesquisa.

Ao Gilson, técnico do laboratório, pelo irretocável trabalho e ética.

A todos os que são parte e dão vida ao Centro Espírita Assistencial Nossa Senhora da Glória, onde me sinto em casa e aprendi que não caminho sozinho. Saravá meus guias e mentores! Gratidão!

Dedicado à minha família

RESUMO

ANÁLISE EXPERIMENTAL DE PAINÉIS SANDUÍCHE COM NÚCLEO DE EPS E ARGAMASSA ARMADA À COMPRESSÃO AXIAL

Autor: Kamirã Barbosa Ribeiro
Orientador: William Taylor Matias
Silva, Dr. Ing
Programa de Pós-graduação em Estruturas e Construção Civil
Brasília, julho de 2023.

Os avanços na indústria da construção e a crescente necessidade de sistemas construtivos rápidos, sustentáveis e econômicos levaram à criação de vários novos elementos não estruturais e estruturais. Esse é o caso do sistema pré-fabricado, no qual se destaca a solução dos painéis sanduíche pré-fabricados (PSPFs). Nesse contexto e considerando as especificidades do processo construtivo dos Painéis Sanduíche Pré-fabricados no Brasil, este trabalho concentrou-se em avaliar o comportamento mecânico sob carga axial desses painéis. O trabalho relata os resultados de três painéis pré-fabricados de sanduíche de camada fina testados sob carga axial. O reforço dos painéis e os conectores de cisalhamento no estado atual dos painéis pré-fabricados de sanduíche no contexto da construção civil são avaliados. O autor mediu o deslocamento em duas alturas distintas do painel, bem como ao longo da largura do painel, para fornecer o comportamento carga-deslocamento no nível da seção transversal e ampliar os dados experimentais sobre o assunto. Além disso, foram feitas interpolações com esses deslocamentos registrados nos painéis, a fim de ilustrar o perfil carga-deslocamento ao longo de sua altura. Os resultados dos testes desenvolvidos nesta pesquisa mostraram boa concordância com os resultados disponíveis na literatura. Além disso, como as equações de resistência de painéis de concreto estão relacionadas ao comportamento compressivo de painéis pré-fabricados de sanduíche, uma breve revisão de fórmulas empíricas também é oferecida aqui. Além disso, dados empíricos, desde 2005, sobre testes de carga concêntrica e excêntrica disponíveis na literatura também são relatados e compilados. Testes axiais adicionais em paredes de alvenaria não armada também foram realizados, medindo deslocamentos em duas alturas distintas das paredes. Os resultados experimentais em PSPFs mostraram concordância entre as equações propostas na literatura, indicando que os maiores deslocamentos no nível da seção transversal não foram observados no meio da largura do painel e que o grau de composição foi amplamente alcançado.

Palavras-chave: Painéis sanduíche, Carga axial, Resistência última, Compressão em escala real.

ABSTRACT

EXPERIMENTAL ANALYSIS OF PRECAST SANDWICH PANELS WITH EPS CORE AND MORTAR WYTHES UNDER AXIAL LOAD

Author: Kamirã Barbosa Ribeiro
Advisor: William Taylor Matias
Silva, Dr. Ing.
Postgraduate Program in Structures and Civil
ConstructionBrasilia, July of 2023.

The advances in the construction industry and the growing necessity for fast, sustainable, and cost-effective construction systems have led to the creation of several new non-structural as well as structural elements. This is the case for the precast system, for which the solution of Precast Sandwich panels (PCSPs) stands out. In this context and given the specificities of the constructive process of the Precast Sandwich Panels in Brazil, this work has focused on assessing the mechanical compressive behavior of those panels under axial load. This work reports the results of three thin wythe precast sandwich panels tested under axial load. Panel reinforcement and shear connectors in the current state of precast sandwich panels in the civil construction context are evaluated. The author measured displacement at two distinct panel heights as well as along the panel width to provide load-displacement behavior at the cross-section level and broaden the experimental data on the subject. Further interpolations were made with those displacements registered in the panels, in order to illustrate the load-displacement profile of them along their```` height. The test results developed in this research showed good agreement with the results available in the literature. In addition, as concrete-wall panel strength equations have been linked to the compressive behavior of precast sandwich panels, a brief review of empirical formulae is also offered herein. Moreover, empirical data, since 2005, on both concentrical and eccentrical load testing available in the literature is also reported and compiled. Further axial tests on unreinforced masonry walls were carried out, also measuring displacements at two distinct wall heights. Experimental results on PCSPs showed agreement between equations proposed in the literature among that the largest displacements at cross-section level have not been observed in mid-width of panel and that the degree of composition was highly achieved.

Keywords: Precast Sandwich Panel; Axial Load; Ultimate Load; Full scale Compression Test.

Table of Contents

LIST OF FIGURES

LIST OF TABLES

LIST OF ACRONYMS AND ABBREVIATIONS

ABNT	Associação Brasileira de Normas Técnicas
ACI	American Concrete Institute
ABAQUS	Finite Element Engineering software
CFC	Chlorofluorocarbon
DCA	Degree of Composite Action
EPS	Expanded Polystyrene
FRP	Fyber Reinforced Polymer
HBM	German Technology Company
I	Inner surface of masonry wall or inner wythe of sandwich panel
IF	Instituto Federal
LABEST	Laboratory of Structures of University of Brasília
LVDT	Linear Variable Differential Transformer
O	Outer surface of masonry wall or outer wythe of sandwich panel
PA	Panel
PCI	Precast/Prestressed Concrete Institute
PCSP	Precast Sandwich Panel
SIPs	Structural Insulated Panels
VIPs	Vacuum Insulation Panels
W	Unreinforced Masonry Walls Tested

LIST OF SYMBOLS

I_e	Equivalent inertia
M_{cr}	Cracking moment
M_a	Maximum bending moment acting on the span
I_g	Moment of inertia of the gross concrete area
I_{cr}	Moment of inertia of transformed concrete section
I_{exp}	Experimentally determined moment of inertia
w	Distributed load for unit width of the panel
L	Span length of applied load
E_c	Concrete Young's module
Δ	Deflection value which specifies the point that defines the representative line of the initial stiffness of the uncracked panel
I_{nc}	Moment of inertia of the non-composite panel
I_c	Moment of inertia of the fully composite panel
κ	Percentage of composite action
M	Total moment
σ	Stress on each fiber
y	distance of centerline to the beginning of the wythe
E_s	Steel Young's module
$EI_{section}$	Calculated stiffness of the section
ρ	Curvature radius
d_0	Total section thickness
d_i	Core layer thickness
N	Number of steel area per steel layers
A_s	Steel area for unit
W	Panel height
$\sigma_{cracking}$	Cracking stress of concrete or module of rupture
M_{ult}	Total resistant moment calculated
T_{bm}	Traction force contribution of the superior layer
T_s	Contribution of the traction force of the reinforcement in the ferrocement mesh
T_{wn}	Contribution of the traction force due to the reinforcement present in the web
a	Depth of the compression block
h	Section height
H	Wall height
t_w	Wall thickness
f'_c	Contribution of the tensile strength of the armor present in the web
A_g	Gross concrete area
k	Coefficient associated to the support conditions
φ	Safety coefficient
P_u	Ultimate load
t	Wall thickness
f_{cu}	Characteristic cube strength of concrete
A_c	Gross area of the wall panel section
f_y	Characteristic yield strength of steel
A_{sc}	Area of compression steel
L	Wall width
F_a	Direct allowed compression tension
w	Concrete specific weight
h	Height between panel supports
t_e	Area of section perpendicular to the load application
P_u	External applied force
F_{cc}	Resultant force in compressed wythe
F_{sc}	Resultant force in compression reinforcement
F_s	Resultant force in tension reinforcement

b	Panel width
s	Simplified neutral axis
f_{sc}	Stress in the compression reinforcement
f_s	Stress in the tension reinforcement
d_1	Depth of the reinforcement A_{sc}
d_2	Stress in the tension reinforcement A_s
N_{Rd}	Resistant design force
f_d	Design compressive strength of masonry unit
A	Gross cross-section area of wall
R	Coefficient which accounts for the slenderness of the wall
φ_s	Reduction coefficient
h_{ef}	Effective height, chosen according to the support conditions
t_{ef}	Effective thickness, chosen according to the support conditions
l_{ef}	Effective span, chosen according to the support conditions
P_n	Resistant force
A_n	Net cross-section area of section
f'_m	Characteristic compressive strength of units
r	Radius of gyration of masonry unit
f_{bk}	Concrete block characteristic strength
$f_{bk,est}$	Estimated concrete block characteristic strength
Ψ	Coefficient for calculation of characteristic block strength according to number of samples tested
t_1	Thickness of each mortar wythe
t_2	Thickness of the insulation layer
c	mortar cover
f_u	Ultimate strength of steel
ε_{cu}	Ultimate strain at failure

CHAPTER 1

1 INTRODUCTION

Precast Sandwich Panels (PCSPs) are a constructive system composed of two or more concrete or mortar wythes separated by an insulation layer, which is normally expanded polystyrene (EPS). The layers are connected to each other through shear connectors, ribs, or both. They can be used or not for structural purposes, and are known to have efficient thermal, acoustic, and mechanical characteristics. The structural applications of PCSPs are bearing walls, channels, water reservoirs, among others (BERTINI, 2002). An example of a PCSP with horizontal steel bars as shear connectors is presented in Figure 1.1 below.

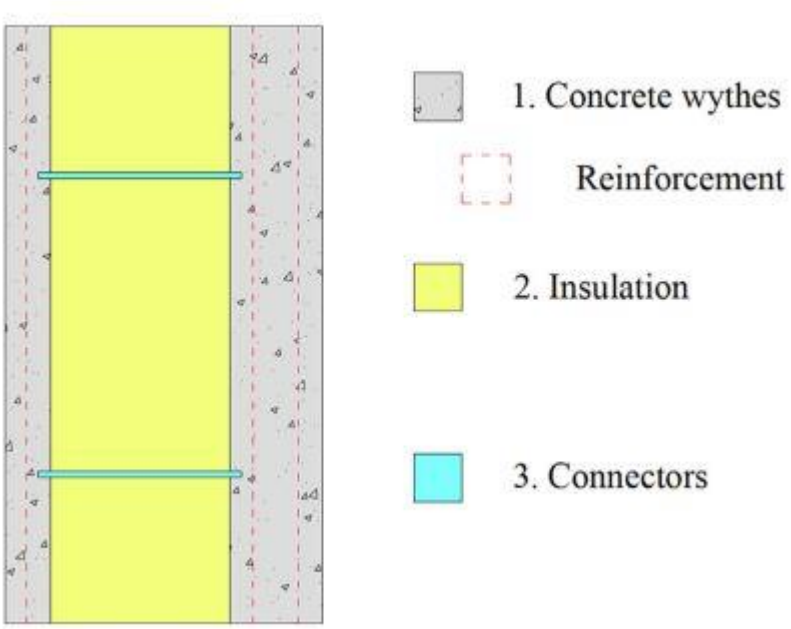

Figure 1. 1 - Example of PCSP vertical view. Modified from: O'HEGARTY *et al*. (2020).

From a more general perspective, sandwich systems are not restricted exclusively to the application of the aforementioned panels. The basic structure of sandwich panels follows the same pattern, consisting of two external faces and a core, usually composed of lightweight material that presents sufficient stiffness in the direction normal to the plane of the faces. In this way, with the association between the dissimilar materials, the beneficial and desired properties for specific applications of their use are combined, being able to increase the behavior of the panel. With regard to their use, prior to 1960, a major restriction on the aerospace field can be

highlighted, with the Second World War being a landmark event in the use of technology. The dissemination and expansion of the field of applications in other areas, such as civil construction, automobile, and naval industries, intensified from this period onwards (CIB WORKING COMMISSION, 2001).

It is possible, however, to cite the use of Structural Insulated Panels (SIPs) prior to this period, having been employed in the 1930s in the United Kingdom, and manufactured in 1947, with plywood and bearing functionality (AMRAN *et al.*, 2020). Other uses and specificities of the use of sandwich panels prior to the date mentioned above are found in literature. For example, the "Tilt-up" construction system, started in the United States in 1906, stands out. In that system, concreting of the horizontal panel consisted of stages, initially molding the lower layer of 50 mm with sand positioned above, and subsequent concreting of the upper bed, arranged above the intermediate layer of sand. Finally, the sand was washed, generating an air mattress between the concrete layers, and the panel was then erected vertically. Another system can be attributed to Swedish builders in 1933, through the provision of additional layers of lightweight concrete and mortar, aiming at better thermal performance. In 1946, E.I du Pont de Nemours Company manufactured panels with a gypsum core for industrial constructions (FONSÊCA, 1994). An example of a SIP built with Carbo Fiber shear connectors is presented in Figure 1.2 below.

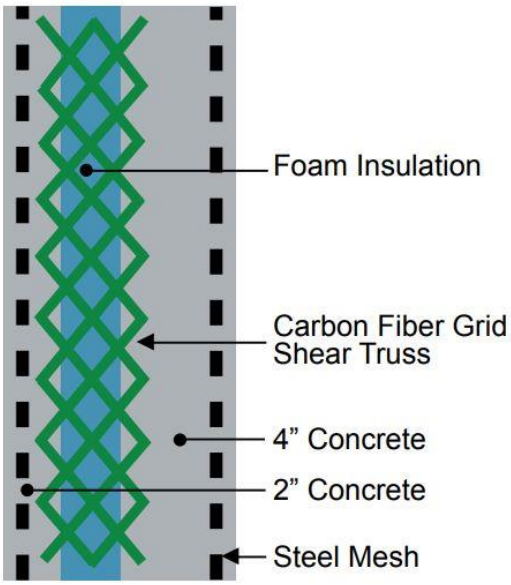

Figure 1. 2 -SIP built with Carbon Fiber shear connectors. Modified from: GLEICH (2007).

EINEIA *et al.* presented, in 1991, a state of the art of concrete sandwich panels. In the work, the authors define them as a system composed of two layers of

concrete separated by an insulating core, interconnected by some type of shear connector. The authors claim it to be the most thermally efficient among the several types of wall systems (EINEIA *et al.*, 1991). Much of the thermal efficiency of concrete sandwich panels is due to the presence of the insulating layer, usually composed of expanded polystyrene (EPS).

The evolution towards what is modernly conceived as a constructive system of concrete sandwich panels, is described from the 1960s by GLEICH. According to the author, the projects started in this decade with the use of "Double Tee" profiles (they consisted of ribs along the length of the panel, which resemble gutters), which later evolved into smooth and flat profiles. In this period, the use of fully composed mechanical action stands out. Steel trusses were also later incorporated into the designs. The development of panels with non-composite mechanical action would only take place from 1980 onwards, with the introduction of the use of non-steel trusses, compromising structural performance to the detriment of better thermal insulation (GLEICH, 2007). An assembly system built by connecting the frames through three-dimensional trusses, composed of welded steel wires, is detailed by another author, in addition to the mention of the first patent of the constructive system of sandwich panels with steel wires, made by Victor Weisman, in 1967, in California (PICKARD, 1990).

PAWAR *et al.* analyze the advantages and disadvantages, among alternative categories of construction systems, in the scope of application in light housing in India. Among them are 3D precast concrete construction system (volumetric precast); prefabricated concrete construction system assembled in loco; prefabricated sandwich panel system; monolithic concrete construction system, among others. In the case of sandwich panels, considered a prominent solution among the investigated methods, they describe two construction methods, including the installation of prefabricated panels in the industry or the erection of panels produced in situ. Greater quality control, low cost, and speed in execution are some of the main advantages listed in the work, while the formation of cracks due to improper execution of projected mortar, deterioration due to prolonged exposure to sunlight, when concreted in-situ, are specific disadvantages of the constructive system. In addition, in general, both analyzed technologies share challenges in their use, such as: limitations in the shape and size of prefabricated elements, due to the need to lift or transport the panels;

difficulty in changing the architectural layout, in case of renovations; demand for more specialized labor (PAWAR *et al.*, 2022).

As innovative manufacturing methods continue to develop, most academic work has focused on reducing the size and weight of PCSPs, benefiting transportation, installation, and cost. However, the design of thin sandwich panels is related to several structural and thermal challenges and future questions, such as steel bridging, optimization of geometry, combined thermal performance of insulations, and maintenance of the composite action of the wythes (O'HEGARTY *et al.*, 2021). From the mechanical point of view, regarding the compressive behavior of the PCSPs, the experimental investigations conducted in the literature have been restricted so far to the evaluation of panels with wythe thickness bigger than 35 mm. This limit is present in a few specimens evaluated in (GARA *et al.*, 2012; CARBONARI *et al.*, 2013). Another lacking element in the literature is the influence of the aspect ratio of real-scale panels on the mechanical behavior of the PCSPs and the experimental analysis of displacements along the cross-section, as the results obtained to this point have limited themselves to the displacement at one single point in each cross-section. Therefore, it will be fundamental that experimental and numerical models validate the behavior of the sandwich panels under such unfavorable and extreme conditions, both mechanically and physically. In this context, the present research is fundamental in the further advance, evaluation and understanding of the mechanical behavior of this desired new, thinner, sandwich panels, as the ones tested in this work have been restricted to a layer thickness of wythes equal to 25 mm, which represents specimens with at least 10 mm thinner wythes as all literature experimental data.

The range of application of this new, thinner panels can be for example the recladding of mid-20th century buildings which are requiring retrofit. The new cladding, when done by thin sandwich panels, can reproduce the ancient visual aspect of the building in its finishing, by adding only a little additional weight to the structure. Another possibility is the production of high thermally efficient panels, with low U-value (high R-value), which can be used to improve future building thermal performance (O'HEGARTY *et al.*, 2021).

Other interesting perspective related to the construction system per say and its configuration is the restricted focus given to the fact that the insulation layer is

responsible for the absorption of part of the water of freshly cast mortar or concrete in the wythes. This, together with the lack of embedment of the shear reinforcement, known as shear connectors, can cause problems in a long-term perspective, because this reinforcement, absolutely fundamental to the mechanical behavior of the panels, may have its strength and functionality reduced through a process of corrosion due to this humidity absorption.

1.1 General objectives

The present work consists of an experimental study of masonry walls and sandwich panels with EPS core layers and external layers constituted by mortar reinforced with welded steel meshes, and steel shear connectors, in bars. The objective of this work is to evaluate the behavior of sandwich panels under axial compression, providing technical and scientific support for their design and safe use under such loading conditions, given the current and growing use and interest, nationally and internationally, in the constructive system investigated, and the technology employed.

1.2 Specific objectives

As specific objectives, the following aspects of the research can be described:

- Evaluation of the correspondence of theoretical and experimental validity of the proposed empirical and analytical formulations, associated with the design of sandwich panels in the literature.
- Experimental evaluation of the compressive behavior under centered axial loading of the sandwich panel with EPS core, reinforced mortar in electro welded mesh, and shear connectors in bars, built according to the particular constructive system of PCSPs adopted in Brazil.

CHAPTER 2

2 LITERATURE REVIEW

2.1 Constructive process of the PCSPs

Prefabricated sandwich panels, or PCSPs (Precast Sandwich Panels) for short, are typically constructed with a total thickness exceeding 300 mm and have weights of approximately 500 kg per m^2 of panel area. The manufacturing process primarily involves the initial construction of wooden or steel formwork, followed by the assembly of steel reinforcement and poured concrete. Shear connectors and insulation are then placed after the concrete has been poured while still fresh (O'HEGARTY & KINNANE, 2020). The typical precast process, although beneficial for quality and construction speed, presents some challenges regarding the alignment and connection of elements since they need to be assembled and subsequently connected (PAWAR *et al.*, 2022).

After the PCSPs are manufactured, they are transported to the site. At this point, the foundations are already built, and the ground floor is leveled. For small construction sites, it is common to mark and align the position of walls and foundations using a system of wooden stakes. The central axes of the walls are delimited by a line drawn on top of the footings, and steel bars, usually 8 mm in diameter and spaced along the length of the wall locations, are placed on them (SANTANA *et al.*, 2020).

The thermal and acoustic performance of sandwich panels is achieved using insulation materials (materials defined as having thermal conductivity $\lambda < 0.065$ m^2/mW). Many of these materials are filled with air because the base material occupies only a small fraction of the volume. This, together with the porous material's restrictive characteristic, leads to poor convective process inside the material and low conductivity values (CASINI, 2016). Expanded polystyrene (EPS) is commonly used in panel applications and has properties such as vapor barrier, thermal insulation, and high impact resistance (SULONG *et al.*, 2019). The benefit of using insulation layers in wall systems with materials like EPS is that the overall weight of the walls is reduced, resulting in decreased weight on the foundations and improved performance of the claddings. The most common types of insulation are cellular insulators, as described

above, and the gas used can be air, chlorofluorocarbon (CFC), carbon dioxide, among others, while the insulators themselves are generally expanded polystyrene (EPS), polyurethane, and polyisocyanurate.

Regarding the varieties of shear connectors, they are subdivided according to the achieved mechanical behavior, whether they transmit shear in one or two directions of the panels. When acting through unidirectional shear, they can typically fall into one of the following categories: 1) concentrated unidirectional shear connectors, consisting of small bent bars that traverse the insulation layer and are anchored in the outer mortar or concrete layers; 2) continuous unidirectional connectors, which can be steel trusses, continuous curved bars, or expanded perforated plate connectors. For bidirectional shear, the commonly used options are: 1) crown anchors (bent bars to create a three-dimensional connection); 2) concrete blocks (bridges across insulation layers, connecting concrete or mortar layers); 3) cylindrical connector (PAWAR *et al.*, 2022). Non-composite connectors are considered incapable of transferring shear between wires. They are usually plastic pins, fiber composite connectors, steel clamps, continuous welded ladders, according to the PCI Committee (Precast/Prestressed Concrete Institute Committee, 2011).

Thermal issues have been associated with steel bridging through shear connectors. Another problem faced is the possible bowing, due to the repeated thermal cycles that occur daily. This effect can affect the mechanical behavior and decrease the stiffness of the panel over time (BUSH & STINE, 1994). A validated finite element model accounted for the thermal bridge as 71% of the total heat transmittance for thin sample panels. Model validation was done through analysis of panels composed of 20 and 40 mm fiber reinforced concrete strands, which incorporate Vacuum Insulated Panels (VIPs) and rigid foam insulation elsewhere connected with Fiber Reinforced Polymer (FRP) connectors. The usual value is around 20% for standard PCPs (O'HEGARTY *et al.*, 2020). Shear connectors play a crucial role in panel behavior. It is customary practice to fix them with special devices, providing stability and facilitating the assembly of the reinforcement between the panels.

In the face of increasingly evident climate change, with the Earth warming at an unprecedented rate and resulting in natural disasters, the construction industry faces a new challenge. This challenge is to build new and cost-effective construction systems to meet the enormous demand for affordable housing, along with new sustainable

practices. The construction systems must be structurally stable, allow for quick and easy assembly with unskilled labor, provide good thermal and acoustic insulation to improve comfort for occupants while minimizing energy consumption. They should also make use of prefabricated elements produced on an industrial scale, with quality control, material reuse, minimal waste, and easy transportation and assembly. Therefore, traditional construction systems such as concrete, steel, or reinforced concrete prefabrication only partially meet some of these requirements. Due to the inadequacies of existing traditional building construction systems for small-scale residential constructions, there is a need for new types of building techniques that meet current needs along with the increasingly demanding requirements of material reuse and sustainability principles. Therefore, in recent years, there has been a significant increase in constructions using wall systems with expanded polystyrene core reinforced concrete or mortar sandwich panels, which are widely used to meet the purposes of cost-effective construction, with versatile applications in affordable housing, fast construction, and adherence to new sustainable practices to mitigate environmental impacts. For construction purposes, the required size of the EPS panel is pre-cut to match the wall dimensions that meet the architectural conditions of the building. Next, the coated steel wire mesh is installed and attached to both sides of the EPS panel, and it is joined using shear connectors that pass through the EPS core. Then, the panels are transported to the construction site according to the construction plan. The concreting of the walls initially involves the projection of mortar or shotcrete onto the steel mesh, followed by the finishing of the wall with the execution of structural mortar plaster. The construction steps for the execution of sandwich walls cast in situ are presented in Figure 2.1.

Figure 2. 1 - Constructive steps for execution of sandwich walls cast in situ.

On the other hand, the construction of popular houses using this constructive system with walls in RCSP, has applied two techniques for the execution of the slabs.

In the first solution, the builders are supporting the slab directly on the wall cast in situ, avoiding the execution of a beam at the end of the wall. This immensely reduces the construction cost, as it does not need to execute the formwork on the wall. Figure 2.2 shows the construction steps using this technique.

Figure 2. 2 - Execution of slab directly supported on sandwich wall panes cast in situ.

The other solution used in the construction of low-income housing in Brazil with PCSPs, consists of the execution of a load distribution beam at the upper end of the walls, with the execution of a formwork and the concreting of a reinforced beam, to carry out the assembly of the slab. This beam executed at the end of the wall works to evenly distribute the efforts of the slab to the reinforced mortar layers, avoiding eccentricities and crushing of the concrete in the wall-slab connection. Figure 2.3 shows the construction stages with the execution of the end beams on the cast in situ walls using this construction system.

Figure 2. 3 - Execution of slab directly supported on sandwich wall panes cast in situ.

After the construction of the houses using the two construction systems, it has been observed that the use of the first constructive solution without the use of beams at the end of the walls, has generated several problems for the builders, mainly after the first year of use of the building. Several appearances of cracks have been observed in the connections between slabs and walls cast in situ. Figure 2.4 shows some of the main cracks found in buildings close to the connection between the panel-slab.

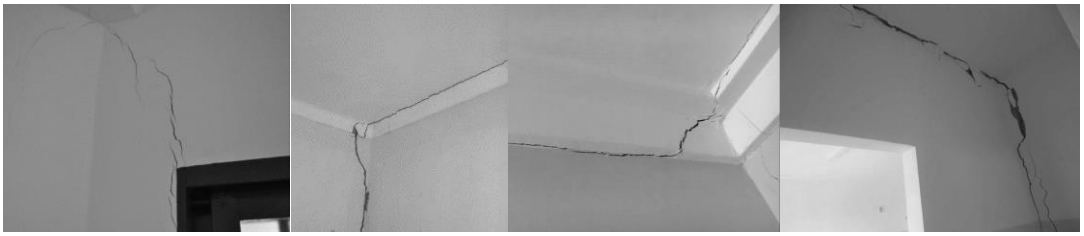

Figure 2. 4 - Cracks found in the connection of wall-slab of houses without distribution beam at wall top.

2.2 Mechanical behavior of the PCSPs

2.2.1 *Degree of composite action*

From a mechanical perspective, the panels are divided according to the degree of composite behavior exhibited by the walls. They can be categorized as fully composite (resisting bending forces in a manner similar to a solid section), partially composite (where there is incomplete shear transfer and subsequent stress distribution as in composite sections), and non-composite panels (where the shear connectors are not capable of transferring shear longitudinally, resulting in each layer acting independently). Sandwich panels behave as composite structures, with the core playing a crucial role. In addition to maintaining the correct positioning of its constituent elements, the core is responsible for load transfer between the resisting layers. For low-stifness insulation materials like EPS, this load transfer is predominantly conducted by the connectors, and the degree of composite behavior of the panel depends on the efficiency of these connecting elements.

Al-RUBAYE *et al.* describe the development of the calculation procedure for sandwich panels. In 1971, an ACI committee established a calculation method based on the use of an "effective section," where shear transfer through the insulation core was previously disregarded. Although conservative, the procedure was straightforward. In the 1990s, the degree of composite behavior exhibited by the external layers started to be evaluated and investigated. However, there is no universally accepted method to ensure a specific degree of composite behavior, whether it is fully or partially composite. The shape, quantity, and spacing of connectors are based on empirical recommendations from each manufacturer (AL-RUBAYE *et al.*, 2017). The deformation profiles for sections with different degrees of composite behavior are illustrated in Figure 2.5.

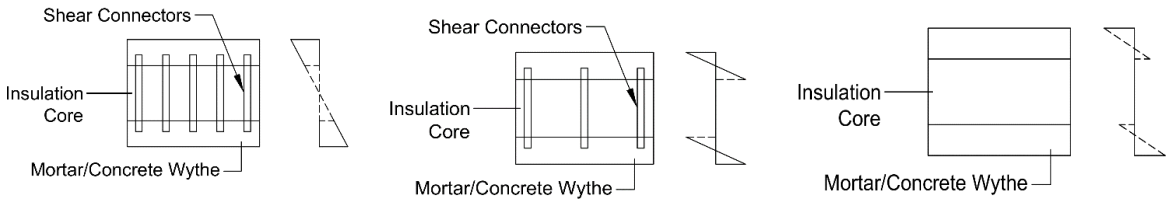

a) **b)** **c)**

Figure 2. 5 - Deformation profile by layer, for each degree of panel composition: a) Fully composite; b) Partially composite; c) Noncomposite.

EINEA *et al.* drew attention to a series of tests conducted at the University of Oklahoma in 1989, where concrete penetration through the perforations created in the insulation layer by shear connectors had an impact on the stiffness of the connectors, affecting shear transfer and thermal efficiency of the tested panels. The authors also reported experiments conducted by Wade, where the degree of composite behavior could be increased through the use of porous insulation layers. However, to ensure that the mechanical action remained composite, the use of EPS was recommended to ensure a more durable composition between layers (EINEA *et al.*, 1991). The degree of composite behavior of sandwich panels is typically determined through experimental tests, evaluating the efficiency of the connectors, as well as through analytical and numerical studies. Based on the level of composite action, panels are classified as fully composite, partially composite, or non-composite. Figure 2.5 illustrates the strain diagrams of the cross-section for each panel type.

An experimental evaluation conducted in 2003 aimed to determine the influence of three types of mechanisms on shear transfer in the behavior of sandwich panels. The considered shear transfer mechanisms were solid regions of concrete through the insulation layer (where the external layers are directly connected at specific points by removing part of the central insulation layer), shear connectors made of steel bars bent in an M shape, and adhesion between the insulation layer and the concrete or reinforced mortar layers. The experimental program is presented in Figure 2.6, followed by another one showing load-deflection curves from flexural tests on the panels in Figure 2.7. Theoretical curves were created considering the assumption of a fully composite and non-composite section. For the linear region, the calculation of inertia is performed considering the gross section, with the concrete layers acting together or independently, respectively, in the case of a fully composite or non-composite panel. The determination of the theoretical cracking load is based on considering that cracking will occur when the applied load generates a tensile stress equal to the adopted by the American Concrete

Institute (ACI) modulus of rupture expression. The expression used to determine the theoretical inertia after cracking, derived from a formulation by Nilson for cracked prestressed beams, is also presented. Finally, the equation used for calculating experimental inertia is provided (PESSIKI & MLYNARCZYK, 2003).

Panel	M-tie connector	Concrete–insulation bond	Solid regions of concrete	Primary variable
1	Yes	Yes	Yes	Prototype panel
2	Yes	No	No	Fraction of composite action provided by M-tie connector
3	No	No	Yes	Fraction of composite action provided by solid concrete regions
4	No	Yes	No	Fraction of composite action provided by bond between insulation and concrete

Figure 2. 6 - Experimental program evaluated. Modified from: PESSIKI & MLYNARCZYK, 2003.

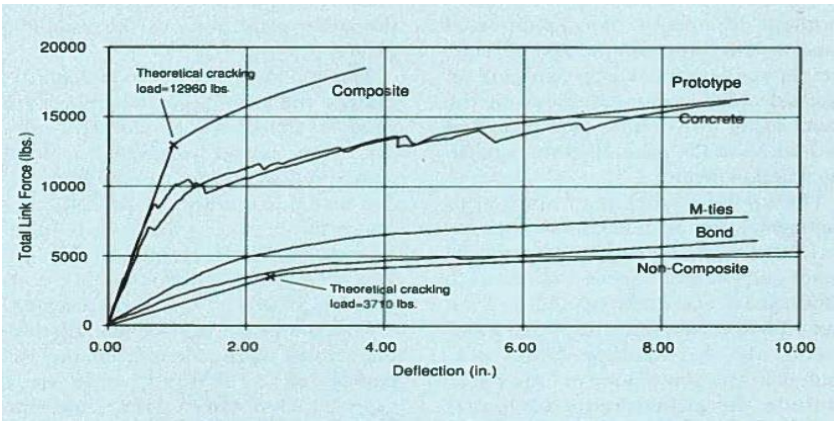

Figure 2. 7 - Load-deflection curves of the panels in the experimental program and of theoretical formulations. Modified from: PESSIKI & MLYNARCZYK, 2003.

$$I_e = I_g \left(\frac{M_{cr}}{M_a}\right)^3 + \left[1 - \left(\frac{M_{cr}}{M_a}\right)^3\right] I_{cr} \quad (1)$$

Where:

I_e = Equivalent inertia;

M_{cr} = Cracking moment;

M_a = Maximum bending moment acting on the span;

I_g = Moment of inertia of the gross concrete area;

I_{cr} = Moment of inertia of transformed concrete section.

$$I_{exp} = \frac{5wL^4}{384\Delta E_c} \quad (2)$$

Where:

I_{exp} = Experimentally determined moment of inertia;

w = Distributed load for unit width of the panel;

L = Span length of applied load;

E_c = Concrete Young's module;

Δ = Deflection value which specifies the point that defines the representative line of the initial stiffness of the uncracked panel;

In general, a substantial portion of sandwich panels exhibit partially composite mechanical behavior. Therefore, it has been widespread practice to evaluate the degree of composite behavior in terms of its proximity to fully composite or non-composite behavior. This measure can be well assessed in percentage terms. Thus, the following expression is adopted to quantify this effect (LEE & PESSIKI, 2008).

$$\kappa = \frac{I_{exp} - I_{nc}}{I_c - I_{nc}} \quad (3)$$

Where:

I_{exp} = Experimentally determined moment of inertia;

I_{nc} = Moment of inertia of the non-composite panel;

I_c = Moment of inertia of the fully composite panel;

Recently, design concepts have led to the use of FRP (Fiber Reinforced Polymer) as shear connectors in sandwich panels. These connectors have high stiffness and mechanical strength compared to steel, but with lower thermal conductivity. HODICKY *et al.* conducted a series of 46 push-through shear tests on concrete-coated sandwich panels with EPS cores, with and without FRP truss shear connectors. For panels without shear connectors, it is interesting to note that the observed failure modes consist of two possibilities: shear cracking in the EPS core or cracking in the EPS core accompanied by slippage due to loss of bond between the concrete layers and the EPS.

In the case of panels with connectors, failure occurred either due to tension in the tension diagonals of the trusses or buckling of the compressed bars. The tests show that an increase in core thickness reduces the shear flow for the same quantity of shear connectors, while an increase in connector spacing promotes an increase in shear flow (HODICKY *et al.*, 2014).

Comparatively, the use of steel truss connectors is less efficient than FRP trusses in terms of achieving a high degree of composite behavior between the panel layers, approaching full composite behavior. Regarding the use of insulation material, it has been found that EPS exhibits a higher shear flow compared to other materials such as extruded polystyrene (XPS). In tests to evaluate the degree of composite behavior in panels with fiberglass connectors subjected to wind pressure and suction loadings, it was found that failure occurred in the concrete layer when the shear resistance of the connectors was sufficient until rupture, while connector failure occurred in the opposite case (CHOI *et al.*, 2015). Other types of connectors are also proposed in the literature, such as the use of steel plates, which serve as spacers and anchorage for the steel bars in the concrete layers, restricting torsion and lateral displacement due to eccentricities. However, the plates depend on the combined action of the two concrete layers and their reinforcement, which makes it difficult to develop independent behavior between them. An image of the system can be seen in Figure 2.8 (KINNANE *et al.*, 2015).

Figure 2. 8 - Shear connector made of steel plate. Modified from: KINNANE *et al.*, 2015.

ACHARJEE *et al.* performed numerical analyses using finite element method with the commercial software ABAQUS to determine the influence of door and window openings on the mechanical behavior and cracking of sandwich panels

simulating a rectangular building measuring 4m x 3m with a height of 3.3 m. To determine the degree of composite behavior of individual panels (1000mm x 1000mm), modeled with polystyrene as the insulation layer, steel meshes as reinforcement in the outer layers, and shear connectors in the form of bars crossing the polystyrene perpendicularly to the mesh, a numerical simulation was conducted to investigate the response of the panel to a three-point bending test. The influence of the presence and diameter of the shear connectors can be observed in the load-displacement curve generated by the program, in Figure 2.9. Increasing the gradation of the connectors shows a positive effect on enhancing the composite behavior of the panel. In the figure below, DCA in a) stands for "Degree of Composite Action," and b) presents the curves of finite element models for sandwich panels with different mechanical properties of the reinforcement bars, including the shear connectors (ACHARJEE *et al.*, 2022).

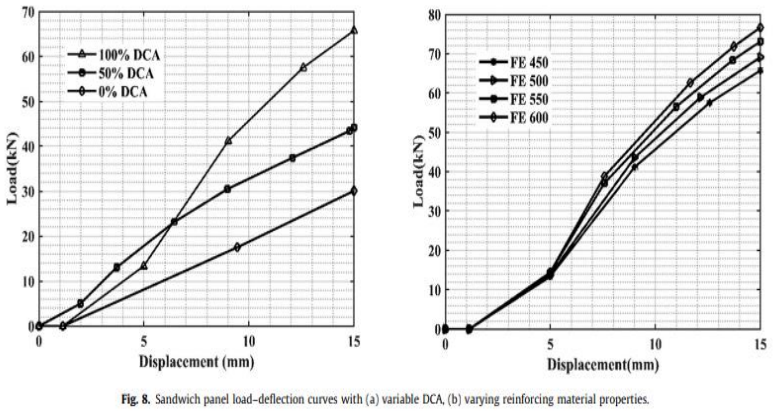

Fig. 8. Sandwich panel load–deflection curves with (a) variable DCA, (b) varying reinforcing material properties.

Figure 2. 9 - Load versus deflection curves for different degrees of: a) composite action; b) reinforcement properties. Modified from: ACHARJEE *et al.*, 2022.

2.2.2 *Flexure mechanical behavior of PCSPs*

ELLIS & CUMMINGS presented an initial design procedure for sandwich panels subjected to flexure. They analyzed the mechanical behavior of a symmetric section by performing an elastic analysis of the composite action of the core and concrete layers (as shown in Figure 2.10). The onset of cracking is adopted as the ultimate strength limit, at a stress of approximately 300 psi (about $6.9x10^3$ Pa). The moment is calculated as the sum of the stresses in each layer, resulting in equation 4. By replacing the moment of inertia of each layer with the integral of y over the area of each layer, an expression for the equivalent moment of inertia of the panel is obtained,

as shown in equation 7. The cracking moment or design limit can then be determined using equation 8 by substituting the stress with the modulus of rupture of the concrete (ELLIS & CUMMINGS, 1970).

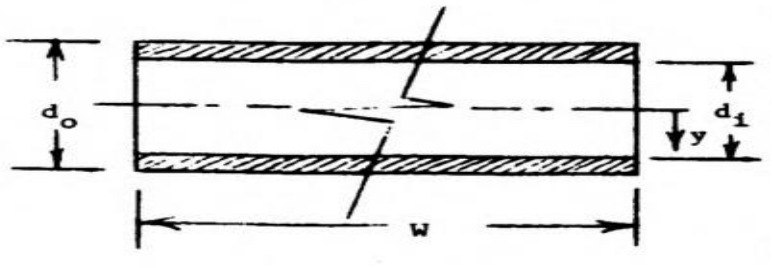

Figure 2. 10 - Cross-section profile and parameters for the calculation of the resistant capacity to flexure of the panel. Modified from: ELLIS & CUMMINGS, 1970.

$$\int \sigma y dA \tag{4}$$

$$\int \sigma y dA = \int \frac{E_c y dA}{\rho} + \int \frac{E_s y dA}{\rho} \tag{5}$$

$$M = \frac{EI_{section}}{\rho} \tag{6}$$

$$EI_{section} = w\left(\frac{1}{12}E_c\left({d_0}^3 - {d_i}^3\right) + 2NA_s d(E_s - E_c)^2\right) \tag{7}$$

$$M = \frac{2\sigma_{cracking} EI_{section}}{E_c d_0} \tag{8}$$

Where:

M = Total moment;

σ = Stress on each fiber;

y = Distance of centerline to the beginning of the wythe;

E_c = Concrete Young's module;

E_s = Steel Young's module;

$EI_{section}$ = Calculated stiffness of the section;

ρ = Curvature radius;

d_0 = Total section thickness;

d_i = Core layer thickness;

N = Number of steel area per steel layers;

A_s = Steel area for unit;

W = Panel height;

$\sigma_{cracking}$ = Cracking stress of concrete or module of rupture.

Regarding compressive strength, stability, and therefore stifness is mentioned as determining factors (ELLIS & CUMMINGS, 1970). In the 1970s, CHONG & HARTSTOCK conducted a series of studies in the area of sandwich panels formed by a rigid polyurethane core and cold-formed light steel faces. In 1979, CHONG, WANG, and GRIFFITH extended the analytical solutions for the deformation and displacement of panels subjected to flexure with multiple spans. The results agreed with the experimental tests conducted (CHONG *et al.*, 1979). BASANBUL *et al.* analyzed the flexural strength of 12 sandwich panels composed of: 20 mm thick ferrocement layers, reinforced with steel wires; varying numbers of shear reinforcements formed by rib connections of the ferrocement layers through the central layer; additional steel reinforcements in the skeleton or mortar connections, with a polystyrene core. An approach considering the panels as concrete sections was adopted, using equations and the conventional method of designing concrete beams by simplifying the stresses into rectangular stress blocks, as adopted in the ACI code. The theoretical and experimental results for the maximum resisted moment differed by a maximum of 29.6%. However, the theoretical results varied between conservative values or against safety. The expressions for the ultimate moment, in the case where the depth of the compression block a) is smaller than the thickness of the upper outer concrete layer (t_p), are presented below (BASANBUL *et al.*, 1991). The schematic section with the forces considered for the calculation is presented in Figure 2.11.

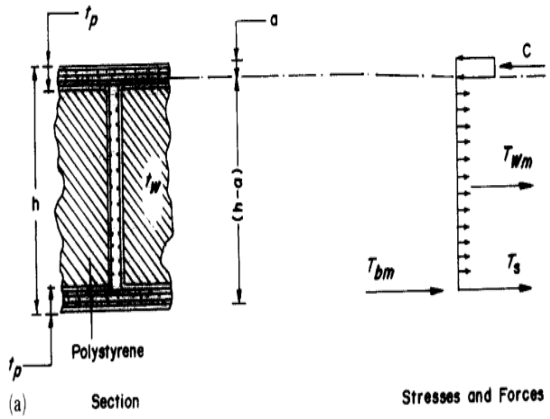

Figure 2. 11 - The position of the compression and traction forces in the ferrocement sandwich panel. Modified from: BASANBUL *et al.*, 1991.

$$M_{ult} = T_{bm}\left(h - \frac{t_p}{2} - \frac{a}{2}\right) + T_s\left(h - \frac{t_p}{2} - \frac{a}{2}\right) + T_{wm}\left(h - \frac{a}{2}\right) \quad (9)$$

Where:

M_{ult} = Total resistant moment calculated;

T_{bm} = Traction force contribution of the superior layer;

T_s = Contribution of the traction force of the reinforcement in the ferrocement mesh;

T_{wn} = Contribution of the traction force due to the reinforcement present in the web;

a = Depth of the compression block;

h = Section height;

From the historical perspective of the development of design criteria and sizing of sandwich panels, two trends can be observed regarding flexural behavior. The first trend is the use of simplified elastic methods or methods that restrict the analysis of the structure to stages prior to cracking. These methods are conservative and counterproductive from an economic point of view, as they limit the structural utilization of the panels to values below their full load-carrying capacity. The second trend is the adaptation of calculation methods established in other areas. An example of this is the work mentioned above, developed by BASANBUL *et al.* (1991), which involves the resolution and application of beam elasticity equations to describe the flexural mechanical behavior and obtain analytical expressions based on specific support conditions and considered cases, as done by CHONG *et al.* (1979). However, in the first case, it is found that the influence on the strength for the various configurations of reinforcement, connectors, and other combinations of panel construction arrangements cannot be described by the calculation model. In the second case, the solutions are specific, and for the case of axial loading, no formulations are suggested by these authors.

2.2.3 *Compressive behavior and empirical design equations of PCSPs*

Sandwich panels can serve many purposes. Among the different applications they are used for are thermal and/or acoustic insulation, load-bearing capacity (able to withstand compression forces), ceiling and floor systems, and combinations of these uses, among others. In the case of thermal insulation, from a historical perspective, the development of analyzing their behavior under compression is intertwined with the development of structural analysis of solid concrete walls.

Seddon (1956) is mentioned in literature as one of the pioneers in the study of solid concrete walls. He made contributions to the analysis of these walls with supports restricted to the lower and upper ends of the walls and influenced the calculation procedures adopted in the British standard BS8110. In the 1970s, a series of studies conducted by Oberlender (1973), Pillai and Parthasarathy (1977), and Kripanarayanan (1977) contributed to determining empirical expressions that included the effects of slenderness and eccentricity on wall strength and estimated their compressive capacity. These equations resulted in the expressions used in the codes of ACI, starting from the early versions of ACI-318, since 1971.

Seddon (1959) investigated the strength of simply supported and doubly reinforced walls with small eccentricities (limited to one-third of the thickness) and varying slenderness ratios (from 18 to 54) and a constant aspect ratio (1.5). Oberlender (1973) conducted tests on walls with single and double reinforcement with slenderness ratios ranging from 8 to 28 and varying aspect ratios (1 to 3.5). Pillai and Parthasarathy (1977) focused on panels with single-layer reinforcement, also with varying proportions and slenderness ratios (16 to 31.5 and 5 to 30, respectively). All of these studies included tests with different concrete strengths, but high-performance concretes were not used (DOH *et al.*, 2001). In 1977, Kripanarayanan showed that the equation from the ACI-310-71 Building Code, 1971 edition, for the strength design method (Eq. 10) could be divided into two parts. A parameter k was also included to account for the effect of distinct types of support conditions (KRIPANARAYANAN, 1977). The resulting equation used from 1989 by ACI-89 is illustrated in the equation below (Eq. 11).

$$P_u = 0.55\varphi f'_c A_g \left[1 - \left(\frac{H}{40t_w}\right)^2\right] \quad (10)$$

$$P_u = 0.55\varphi f'_c A_g \left[1 - \left(\frac{kH}{32t_w}\right)^2\right] \quad (11)$$

Where:

H = Wall height, in inch;

t_w = Wall thickness, in inch;

f'_c = Contribution of the tensile strength of the armor present in the web, in psi;

A_g = Gross concrete area, in $inch^2$;

k = Coefficient associated to the support conditions. Equal to l for walls unrestrained against rotation and equal to 0.8 to walls restrained against rotation;

φ = Safety coefficient, equal to 0.7 for compression members;

P_u = Ultimate load, in pounds;

Thus, it is essential to understand the experimental limitations to which the expressions created for the analysis of solid concrete walls were subjected, as they have been cited since then as a means of designing sandwich panels under compression. These initial equations were limited to the influence of slenderness as a means of predicting the load-bearing capacity and disregarded aspects such as the type and quantity of reinforcement used, second-order effects, unrestricted eccentricities in load application, aspect ratio (the ratio between the height and length of the base of the walls), among other factors. Although BENAYOUNE *et al.* (2007) reported that in the works of Pillai and Parthasarathy, little influence of the amount of reinforcement on the ultimate compressive strength of solid concrete walls was observed (BENAYOUNE *et al.*, 2007). SAHEB & DESAYI conducted an extensive series of tests to determine the influence of aspect ratio, quantity of horizontal and vertical reinforcement used, and slenderness ratio on the compressive behavior of unrestrained reinforced concrete walls. It was found that for compressive loads applied with an eccentricity of one-sixth of the thickness of the tested solid reinforced concrete walls, with base and top pinned supports, the amount of vertical reinforcement linearly influenced the ultimate strength. The increase is 55%, for an increase of vertical reinforcement ratio of 0.175% to 0.850% for walls with a slenderness ratio of 12, and 45% for walls with a slenderness

ratio of 24. However, the rate of horizontal reinforcement showed no change in the final capacity of the tested walls. Regarding the aspect ratio, an influence on the mode of failure was observed, changing it from predominantly concrete crushing to crushing accompanied by significant lateral deflection. A reduction of 16.6% in the ultimate compressive strength was observed with an increase in the aspect ratio from 0.67 to 2. New expressions were proposed, considering the incorporation of the mentioned parameters (SAHEB & DESAYI, 1981). Therefore, the need for experimental investigations to evaluate the validity of applying the expressions for reinforced concrete walls to the design of sandwich panels becomes evident. The equations related to the empirical formulations, mentioned in the work of BENAYOUNE *et al.* (2007), obtained for concrete walls are presented below. Regarding the units used in the equations, they should be consistent with each other, such that units can be used in either system or the american units standard, knowing that the results obtained will be relative to the force units used in each case. Respectively, the equations refer to the formulations by Leabu, Obelender, Pillai and Parthasarathy, and Saheb and Desayi.

$$P_u = 0.2 f_{cu} A_c \left[1 - \left(\frac{H}{40t}\right)^3\right] \tag{12}$$

Where:

H = Wall height;

t = Wall thickness;

f_{cu} = Characteristic cube strength of concrete;

A_c = Gross area of the wall panel section;

P_u = Ultimate load;

$$P_u = 0.6 f_{cu} A_c \left[1 - \left(\frac{H}{30t}\right)^2\right] \tag{13}$$

Where:

H = Wall height;

t = Wall thickness;

f_{cu} = Characteristic cube strength of concrete;

A_c = Gross area of the wall panel section;

P_u = Ultimate load;

$$P_u = 0.57\varphi f_{cu} A_c \left[1 - \left(\frac{kH}{50t}\right)^2\right] \quad (14)$$

Where:

φ = Safety coefficient, equal to 0.7 for compression members;

H = Wall height;

k = Coefficient associated to the support conditions. Equal to l for walls unrestrained against rotation and equal to 0.8 to walls restrained against rotation;

t = Wall thickness;

f_{cu} = Characteristic cube strength of concrete;

A_c = Gross area of the wall panel section;

P_u = Ultimate load;

Finally, the equation proposed by Saheb and Desayi suggests two different expressions, depending on the value of the aspect ratio (H/L), with the first one for aspect ratios less than 2 and the second one for aspect ratios greater than or equal to 2. The use of the equation is limited to eccentricities smaller or equal to one-sixth of the wall thickness and slenderness ratio (H/t) ≤ 32.

$$P_u = 0.55\varphi\left(f_{cu}A_c + \left(f_y - f_{cu}\right)A_{sc}\right)\left[1 - \left(\frac{kH}{32t}\right)^2\right]\left[1.2 - \frac{H}{10L}\right] \quad (15)$$

$$P_u = 0.55\varphi\left(f_{cu}A_c + \left(f_y - f_{cu}\right)A_{sc}\right)\left[1 - \left(\frac{kH}{32t}\right)^2\right] \quad (16)$$

Where:

φ = Safety coefficient, equal to 0.7 for compression members;

H = Wall heigth;

t = Wall thickness;

f_{cu} = Characteristic cube strength of concrete;

f_y = Characteristic yield strength of steel;

A_c = Gross concrete area;

A_{sc} = Area of compression steel;

k = Coefficient associated to the support conditions. Equal to l for walls unrestrained against rotation and equal to 0.8 to walls restrained against rotation;

L = Wall width;

P_u = Ultimate load, in pounds;

Therefore, it is essential to understand the experimental constraints to which the expressions created for the analysis of solid concrete walls were subjected, as they have been cited since then as a way of designing sandwich panels under compression.

In the same year as the use of the expressions mentioned in the previous paragraph, whose evolution is described above, Adam *et al.* (1971) presented a calculation method based on stress checks. This work standardized the design calculation procedure for precast concrete panels in the United States at that time, whether they were solid, sandwich, or other types. For the case of vertical compression, the following expressions were proposed based on compression stresses. The first one was limited to the use of stresses lower than 11 percent of the compressive strength of the concrete used, while the second one was restricted to higher stresses (OLSEN, 2017). This is the oldest association found in the literature between the behavior of these two structural elements and the historical reason for the association between the equations of solid walls and the description of the behavior of sandwich panels.

$$F_a = 0.225 f'_c \left[1 - \frac{\sqrt{f_c'}}{w^{1.5}} \left(\frac{h}{9t_e}\right)^2\right] \tag{17}$$

$$F_a = 5w^{1.5} \sqrt{f_c'} \left(\frac{t_e}{h}\right)^2 \tag{18}$$

Where:

F_a = Direct allowed compression tension, in psi;

f'_c = Concrete compressive strength resistência at 28 days of age, in psi;

w = Concrete specific weight, in pcf;

h = Height between panel supports, in inch;

t_e = Area of section perpendicular to the load application;

Recently, two studies have correlated experimental test data of sandwich panels under axial loading with expressions used for reinforced concrete walls found in the literature. BENAYOUNE *et al.* (2007) conducted tests on sandwich panels with shear connectors in a 45-degree diagonal pattern, with aspect ratios ranging from 1.2 to 2 and slenderness ratios between 10.77 and 20. The authors found that the expressions used, except for one, were conservative. Among these expressions, the most conservative was Equation 11. The observed failure mode was concrete crushing at one or both ends of the panels, and the cracking loads varied between 44% and 79% of the ultimate strength. AHMAD & SINGH evaluated six compression specimens of sandwich panels, for which the expressions derived from reinforced concrete walls were found to be non-conservative and, in some cases, even predicted lower strengths than the experimental values (BENAYOUNE *et al.*, 2007; AHMAD & SINGH, 2021). Therefore, BENAYOUNE *et al.* (2007) proposed an equation that considered the presence of compression reinforcement, which refers to the vertical bars in the steel mesh used in the wythes. This equation is presented in Eq. 19, along with another equation proposed in the literature specifically for compression in sandwich panels, extracted from MOHAMAD *et al.* (2012) and cited as Eq. 20.

$$P_u = 0.4 f_{cu} A_c \left[1 - \left(\frac{kH}{40t}\right)^2\right] + 0.67 f_y A_{sc} \tag{19}$$

Where:

H = Wall heigth;

t = Wall thickness;

f_{cu} = Characteristic cube strength of concrete;

f_y = Characteristic yield strength of steel;

A_c = Gross concrete area;

A_{sc} = Area of compression steel;

k = Coefficient associated to the support conditions. Equal to l for walls

unrestrained against rotation and equal to 0.8 to walls restrained against rotation;

P_u = Ultimate load;

$$P_u = 0.4 f_{cu} A_c \left[1 - \left(\frac{kH}{40\left(t - \frac{t}{20}\right)} \right)^2 \right] + 0.6 f_y A_{sc} \quad (20)$$

Where:

H = Wall heigth;

t = Wall thickness;

f_{cu} = characteristic cube strength of concrete;

f_y = characteristic yield stength of steel;

A_c = Gross concrete area;

A_{sc} = Area of compression steel;

k = Coefficient associated to the support conditions. Equal to l for walls unrestrained against rotation and equal to 0.8 to walls restrained against rotation;

P_u = Ultimate load.

Regarding the evaluation of the influence of some basic factors that raise interest in this recent structural concept of sandwich panels, we can mention the parametric assessment of numerous factors presented in the work of CARBONARI *et al.* (2012). The authors assessed, among other factors, the effect of varying the thickness of the EPS (80 mm and 120 mm) on the strength of panels with wythes of the same thickness (15 mm), while varying the strength of the mortar between 4.6 MPa, 17.15 MPa, and 39.6 MPa. The results are shown in Figure 2.12. This trend, however, may not be valid for specimens at full scale, given the considerable number of factors that can influence results at full scale, such as size and scale effects, among others.

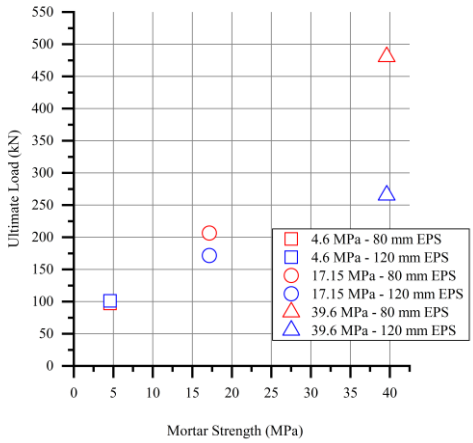

Figure 2. 12 - Results of compressive strength for varying eps thickness and mortar strength. Plot with results from data of: CARBONARI *et al.*, 2012.

Given the results above, which suggest that for higher slenderness ratios, the strength of panels with an EPS thickness of 80 mm is greater than those with 120 mm, they evaluated the influence of further increasing the EPS thickness (80, 120, 160, 200, 240 mm) for the same mortar strength of 39.6 MPa. The results show a decrease in compressive strength with increasing EPS thickness in this case. The authors also evaluated the same variation in EPS thickness as shown in the figure 2.12, but with the addition of specimens with a thickness of 240 mm, with different thicknesses of wythes, namely 25 mm and 15 mm respectively, and with mortar having a strength of 39.6 MPa. These results are presented below (Figure 2.13) and show that for slenderness ratios close to 1, the differences in strength are negligible, but for higher slenderness ratios, the higher strength varies between specimens with equal and different wythe thicknesses.

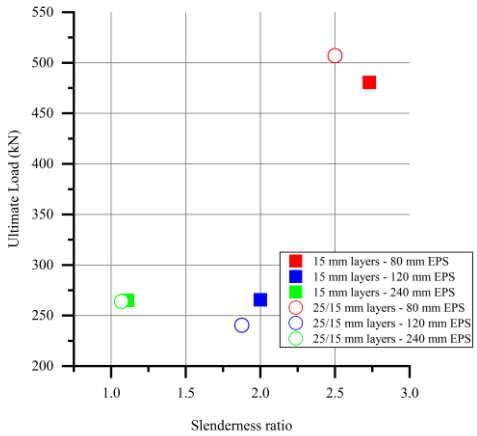

Figure 2. 13 - Results of compressive strength for varying eps thickness and different thickness of wythes. Plot with results from data of: CARBONARI *et al*., 2012.

In addition to the attention given to the experimental results of sandwich panels under compression, academic studies have focused on the development of numerical models for their mechanical description. Studies that performed finite element modeling of the panels under such loading conditions are discussed, along with works involving experimental and numerical analysis, as well as the general procedures adopted for creating finite element models. In general, the mentioned experimental tests are limited to the analysis of panels with a length on the order of 1200 mm. It is also observed in some studies that a two-dimensional finite element modeling tends to show good agreement with experimental results. This trend is possibly due to the limitation in the length of the tested specimens, which in turn may limit the effects of the aspect ratio on the compressive mechanical behavior. Therefore, it is necessary to experimentally verify this hypothesis. The numerical verification of three-dimensional models validated with experimental data, adapted, and analyzed for panels with unusual aspect ratios, can also provide preliminary information on the subject. However, it is evident that experimental confirmation of such results is required. The two-dimensional numerical models found in the literature follow the following procedures, with their corresponding results also presented: 1) Adoption of two-dimensional isoparametric elements (plane stress state) to model the concrete layers, along with two-dimensional bar elements for the truss used as shear connectors. Total Lagrangian formulation is used to account for large displacement effects, as well as nonlinear solutions obtained through the Newton-Raphson method. The ultimate strength results showed differences of at least 9.1% compared to experimental results, while the displacement results were

approximately 17.6% lower than the test data after cracking (BENAYOUNE *et al.*, 2007); 2) Following the same modeling approach described above, applying eccentricity in the model and comparing it to the results of eccentrically loaded panels, a difference of at least 6.7% was found in both the experimental and numerical ultimate strength, and a variation of less than 2.4% in the initial displacement results, and more than 10% at panel failure (BENAYOUNE *et al.*, 2006); 3) Model with beam elements in the concrete layers, with internal connection of internal nodes to shear elements ("Shear elastic link"). Physical nonlinearity of the concrete layers was assumed using a nonlinear constitutive law, and a perfect elastoplastic bilinear constitutive model was assumed for the steel shear connectors. The numerical results showed better agreement than for centrally loaded panels. Differences of up to 38% between experimental and numerical results were found for eccentrically loaded panels. Further analyses were conducted to evaluate the influence of the panel mechanic composition degree on the ultimate strength by altering the stiffness of the shear link elements (GARA *et al.*, 2012); 4) Modeling of the concrete layers with two-dimensional isoparametric elements (plane stress state), and the truss bars used as shear connectors with two-dimensional bar elements. Geometric and physical nonlinearity considerations were adopted using the total Lagrangian formulation and the Newton-Raphson method to implement the nonlinear solutions. During the initial stage, the deflection corresponded to about 28.2% of the experimental values, while the strength results differed by at least 10.53% (AMRAM *et al.*, 2018). A three-dimensional model was evaluated for slender panels under eccentric compression (ALCHAAR & ABED, 2020). It was observed as a general practice in the generation of numerical finite element models that the mechanical behavior and interaction of the insulation layer with the outer layers have been disregarded, except in the work of GOH *et al.* (2016).

Attention has been given to the use of lightweight prefabricated sandwich panels. Among the solutions presented in the literature, one of them is the use of foam concrete. RAHMAN & JAINI conducted experimental tests on two sandwich panels with shear connectors in steel trusses with diameters of 6 and 9 mm, as well as vertical longitudinal reinforcement in the concrete layers, with a layer of polystyrene insulation. The experimental results showed a mode of failure by crushing of the concrete. It was found that 3-D numerical models using a combination of finite element method and discrete element method in ABAQUS software resulted in more effective models than

those created using only finite elements. Constitutive models based on Mohr-Coulomb were used for the foam concrete layers, and the Von-Mises criterion was used for the shear connectors and vertical reinforcement. Conformity between displacement profiles, mode of failure, and load-carrying capacity between the numerical model and experimental results were found (RAHMAN & JAINI, 2013).

GOH *et al.* also developed numerical models for lightweight prefabricated sandwich panels using foam concrete and a polystyrene insulation core. They used data from literature to create constitutive models for polystyrene. Tests were conducted to determine the properties of the foam concrete used in the external layers and the regular concrete used in the distribution beam, using the Concrete Damaged Plasticity Model. Additionally, tensile tests were performed on the steel shear connectors and main reinforcement. The numerical results were validated by comparing them with two experimental results from the literature for panels under concentric compression loading, with a slenderness ratio of 20, polystyrene layers of 20 mm, and varying concrete layer thicknesses. It was found that the perfect quasi-static model (without incorporating initial eccentricity) consistently represented the displacement, mode of failure, and load-carrying capacity of the compared panels. The load-carrying capacity showed a divergence of 14.58% and 3.78% between the numerical and experimental results. Regarding the model with initial eccentricities between one-twentieth and one-sixth of the panel thickness, better accuracy was found for an adopted eccentricity of one-twelfth of the panel thickness. Comparing the perfect models and models with initial eccentricity, greater conformity with the experimental results for load-carrying capacity was found (GOH *et al.*, 2016). Some data from the experimental results found in the literature for the compressive strength of tested sandwich panels have been summarized and compiled in Table 2.1.

Table 2.1 - Experimental results of axially 1oaded precast sandwich panels in literature.

Authors	Type of isolation material	Insulation material thickness (mm)	Total thickness (mm)	Slenderness ratio	Aspect ratio	Cracking Load (kN)	Failure Load (kN)
Benayoune *et al.* (2007)	EPS	50.00	130.00	10.77	1.17	848.00	1425.00
		40.00	120.00	11.67	1.17	927.00	1398.00
		50.00	130.00	13.85	1.50	689.00	1330.00
		40.00	120.00	15.00	1.50	565.00	1295.00
		50.00	130.00	18.46	2.00	743.00	1250.00

		40.00	120.00	20.00	2.00	588.00	1182.00
Benayoune *et al.* (2006)	EPS	50.00	130.00	10.77	1.17	531.00	1028.00
		40.00	120.00	11.67	1.17	578.00	1051.00
		50.00	130.00	13.85	1.50	472.00	985.00
		40.00	120.00	15.00	1.50	411.00	913.00
		50.00	130.00	18.46	2.00	324.00	852.00
		40.00	120.00	20.00	2.00	305.00	749.00
Gara *et al.* (2012)	Poliestireno	80.00	150.00	18.00	2.41	-	701.00
		80.00	150.00	18.00	2.41	-	783.00
		120.00	190.00	14.21	2.41	-	806.00
		120.00	190.00	14.21	2.41	-	844.00
		160.00	230.00	11.74	2.41	-	855.00
		160.00	230.00	11.74	2.41	-	907.00
		80.00	150.00	18.00	2.41	-	736.00
		80.00	150.00	18.00	2.41	-	765.00
		80.00	150.00	18.00	2.41	-	375.00
		80.00	150.00	18.00	2.41	-	401.00
		120.00	190.00	14.21	2.41	-	460.00
		120.00	190.00	14.21	2.41	-	545.00
		160.00	230.00	11.74	2.41	-	524.00
		160.00	230.00	11.74	2.41	-	630.00
		80.00	150.00	18.00	2.41	-	461.00
		80.00	150.00	18.00	2.41	-	591.00
Amran *et al.* (2018)	EPS	25.00	105.00	28.57	2.50	-	759.90
		25.00	125.00	24.00	2.50	620.00	839.50
		35.00	150.00	20.00	2.50	540.00	1048.60
		45.00	175.00	17.14	2.50	720.00	1231.10
		50.00	200.00	15.00	2.50	740.00	1515.10
		60.00	225.00	13.33	2.50	980.00	1602.70
		25.00	125.00	24.00	2.50	620.00	762.20
		25.00	125.00	24.00	2.50	840.00	1147.80
Ahmad & Singh (2021)	EPS	80.00	150.00	6.67	1.67	-	545.60
		80.00	150.00	6.67	1.67	-	505.60
		80.00	150.00	6.67	1.67	-	660.70
		80.00	180.00	5.56	1.67	-	880.10
		80.00	180.00	5.56	1.67	-	713.50
		80.00	180.00	5.56	1.67	-	742.80
Carbonari *et al.* (2013)	wavy EPS	80.00	110.00	2.73	0.60	-	98.00
		80.00	110.00	2.73	0.60	-	96.00
		120.00	150.00	2.00	0.60	-	110.00
		120.00	150.00	2.00	0.60	-	91.00
		80.00	110.00	2.73	0.60	-	493.00
		80.00	110.00	2.73	0.60	-	468.00
		120.00	150.00	2.00	0.60	-	288.00
		120.00	150.00	2.00	0.60	-	243.00
		160.00	190.00	1.58	0.60	-	419.00

		160.00	190.00	1.58	0.60	-	352.00
		200.00	230.00	1.30	0.60	-	303.00
		200.00	230.00	1.30	0.60	-	276.00
		240.00	270.00	1.11	0.60	-	293.00
		240.00	270.00	1.11	0.60	-	237.00
		80.00	110.00	2.73	0.60	-	543.00
		80.00	110.00	2.73	0.60	-	471.00
		120.00	150.00	2.00	0.60	-	253.00
		120.00	150.00	2.00	0.60	-	228.00
		80.00	110.00	2.73	0.60	-	264.00
		80.00	110.00	2.73	0.60	-	-
		80.00	110.00	2.73	0.60	-	208.80
		80.00	110.00	2.73	0.60	-	204.00
		80.00	110.00	2.73	0.60	-	191.00
		80.00	110.00	2.73	0.60	-	152.00
		80.00	197.00	2.41	0.86	-	732.00
		80.00	200.00	3.98	1.50	-	528.00
		80.00	200.00	2.42	0.89	-	802.00
		80.00	200.00	3.89	1.48	-	589.00
		80.00	199.00	2.36	0.85	-	587.00
		80.00	200.00	3.85	1.45	-	672.00
		60.00	177.00	2.71	0.88	-	795.00
		60.00	178.00	4.39	1.48	-	723.00
		60.00	177.00	2.64	0.85	-	652.00
		60.00	177.00	4.35	1.45	-	650.00
		40.00	157.00	3.01	0.87	-	631.00
		40.00	157.00	4.94	1.49	-	691.00
		100.00	145.00	3.29	0.87	-	131.00
		60.00	105.00	7.39	1.42	-	132.00
		100.00	190.00	13.42	2.13	-	480.00
		60.00	150.00	17.00	2.13	-	530.00
Goh *et al.* (2016)	Poliestireno	20.00	100.00	28.00	3.73	-	668.00
		20.00	125.00	22.40	3.73	-	685.00
		20.00	100.00	28.00	3.73	-	531.00
		20.00	100.00	28.00	3.73	-	557.00
		20.00	100.00	28.00	3.73	-	575.00
		20.00	100.00	28.00	3.73	-	586.00
		20.00	100.00	28.00	3.73	-	599.00
		20.00	100.00	28.00	3.73	-	614.00
Mohamad *et al.* (2012)	Poliestireno	20.00	100.00	18.00	2.40	200.00	345.00
		20.00	100.00	18.00	2.40	315.00	446.00
		20.00	100.00	20.00	2.67	295.00	421.00
		20.00	100.00	20.00	2.67	385.00	545.00
		20.00	100.00	28.00	3.73	487.00	695.00
		20.00	100.00	28.00	3.73	455.00	645.00
		45.00	125.00	22.40	3.73	205.00	289.00

		45.00	125.00	22.40	3.73	520.00	745.00
		20.00	100.00	25.00	3.33	315.00	445.00
		20.00	100.00	25.00	3.33	315.00	445.00
		20.00	100.00	25.00	3.33	375.00	534.00
		20.00	100.00	25.00	3.33	605.00	864.00
		120.00	200.00	12.50	3.33	295.00	463.00
		120.00	200.00	12.50	3.33	515.00	855.00
Amran *et al.* (2016)	EPS	25.00	125.00	14.00	1.46	320.00	962.70
		25.00	125.00	16.00	1.67	340.00	923.70
		25.00	125.00	18.00	1.88	480.00	881.30
		25.00	125.00	20.00	2.08	540.00	838.60
		25.00	125.00	22.00	2.29	520.00	773.50
		25.00	125.00	24.00	2.50	620.00	762.20
		25.00	125.00	24.00	2.50	-	-
		25.00	125.00	24.00	2.50	-	-

2.2.3.1 Influence of slenderness ratio on mechanical behavior of PCSPs

As experimental programs developed so far regarding the resistance of PCSPs under axial load dealt with a wide number of parameters, such as type of shear connector reinforcement, wythe reinforcement, concrete strength, geometrical properties (slenderness ratio, aspect ratio), condition of application of load (with or without eccentricity), a graphical compilation of experimental data does not necessarily show the information gathered thoroughly. However, associated with further description of the results, they are a powerful analysis tool. Therefore, in Figure 2.14 one can observe a point plot of the results compiled from (BENAYOUNE *et al.*, 2006; AHMAD & SINGH, 2021; CARBONARI *et al.*, 2013; GARA *et al.*, 2012; AMRAN *et al.*, 2016; AMRAN *et al.*, 2019). The mortar compressive strength used in (BENAYOUNE *et al., 2006*) was obtained by test cubes specimens, resulting in a 31.8 MPa concrete strength. For results in (CARBONARI *et al.*, 2013) the micro-concrete compressive strength was also obtained from a test on cube specimens (70 mm), and the average concrete strength at 28 days of cure was 44 MPa. The mortar used in the wythes had a compressive strength of 25 MPa. In GARA *et al.* (2012) concrete resistance was obtained through both prismatic specimens as well as specimens extracted after concrete casting of the wythes (cored ones). The average resistances obtained were respectively 21.95 MPa (prismatic specimens) and 25.10 MPa (cored specimens). In AMRAN *et al.* (2016) foamed concrete was used in the wythes, having a mean compressive resistance of 24.83 MPa, while the reference panels, built with

normal concrete so that to compare both panel results, had a compressive strength equal to 26.66 MPa. AMRAN *et al.* (2018) and AMRAN *et al.* (2019) had the same experimental data used, therefore only results of AMRAN *et al.* (2016) and AMRAN *et al.* (2019) are presented in the figure. The sandwich panels evaluated in those works had foamed concrete strength of the same strength as the one used in AMRAN *et al.* (2016), but different geometrical configurations. Figure 2.14 shows the influence of the slenderness ratio on the ultimate load. The ultimate load of the panels is shown per unit of width meter of the panel to represent the data better, as the different experimental programs have built panels with various widths. Small-scale panels tested from experimental data have not been considered in the figure, because of the wide variation in the mortar, eps, and wythe thickness and the consequent large scatter of that data. The results which investigated the influence of eccentricity of applied load in compressive behavior have been displayed separately in Figure 2.15.

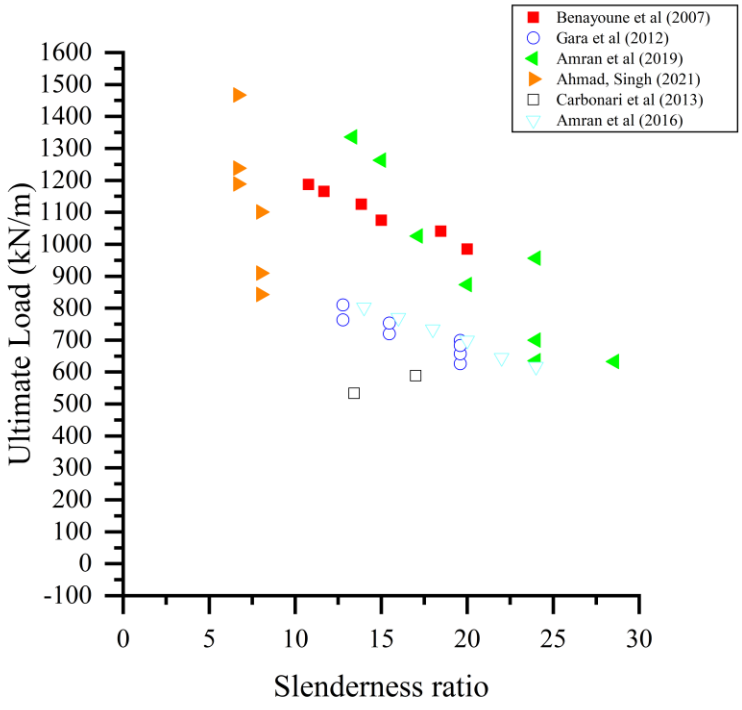

Figure 2. 14 - Ultimate load per unit width against slenderness ratio.

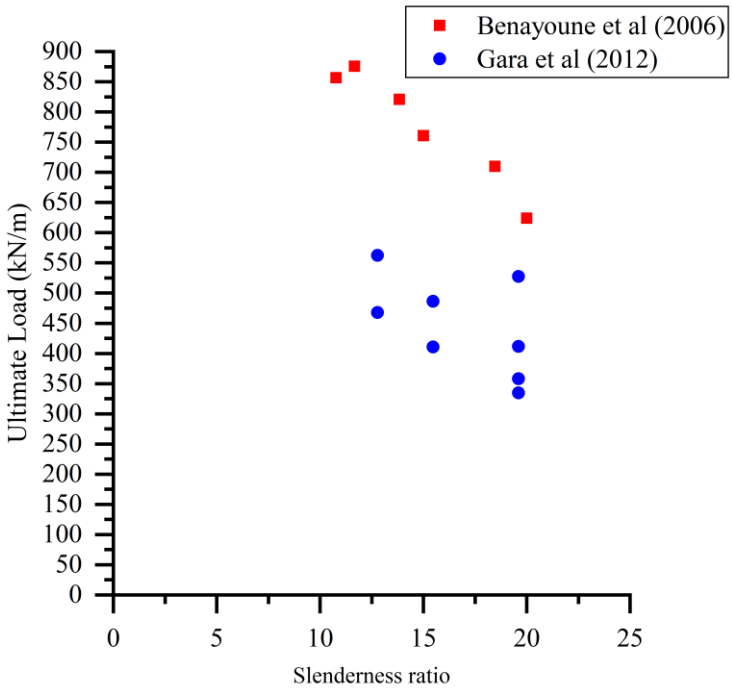

Figure 2. 15 - Ultimate load per unit width against slenderness ratio for eccentric load application.

2.2.3.2 Influence of load eccentricity on mechanical behavior of PCSPs

In the literature, the influence of eccentric axial load application compared to concentric axial load has been investigated in the papers of BENAYOUNE *et al.* (2006) and BENAYOUNE *et al.* (2007), as well in the paper of GARA *et al.* (2012).

For the first two set of works, the experimental program has focused on the determination of the load-deformation response, strain characteristics, crack patterns, failure mode, truss-shaped shear connectors strain, and effectiveness of the solid concrete-wall formulae to represent the ultimate strength results obtained experimentally for the precast sandwich panels. For each given height and width of the panels in the program, two different specimens were cast with exactly same wythe thickness, however the insulation layer was not maintained with constant thickness but varied in 10 mm from one another. The influence of this variation in the EPS core is further detailed in the text, with respect to each of the measurements cited above.

The panels in both BENAYOUNE *et al.* (2006) and BENAYOUNE *et al.* (2007) were constructed exactly the same, using a square welded mild steel mesh reinforcement with 200 x 200 mm openings, assembled with both longitudinal and

transverse mild steel bars of 6 mm diameter, while the shear connectors used between the inner and outer wythes were continuous truss-shaped mild steel bars, also of 6 mm diameter, throughout the panel height, placed evenly spaced four times over the panel width. The concrete mean compressive and tensile strengths were, respectively, 31.8 and 2.25 MPa, while the elasticity modulus was 25.32 kN/ mm^2. The panels were fixed at the base and pinned at the top bottom during loading. The surface aspect of the insulation EPS core was flat.

Those works have found that despite the increase of insulation core layer for the pairs of panels cast with all other geometrical parameters the same, the variation in the load-deformation response was almost insignificant (however this thickness increase was only 10 mm). This tendency was also present for the sandwich panels which were loaded eccentrically. Considering the general load-deformation response, however, the magnitude of deflection has almost doubled when the panels were loaded eccentrically. In the load-deflection along panel PA5 height the magnitude of lateral deflection was less than 10 mm. For the geometrically equivalent panel to PA5, but eccentrically loaded, the maximum deflection recorded during loading was 21.2 mm. The deflections behaved linearly until the first crack appeared, in both loading cases. The strain characteristics under axial load in the wythes have shown to have a small discontinuity (insignificant with respect to the order of the strains) across one wythe to another and varied linearly though each of the wythes thickness in the mid-height. The discontinuity increased as the load got close to the failure load. This discontinuity may be due to the fact that cracks appeared at different loads for the inner and outer wythes. As eccentricities took place, the discontinuity was negligible in the strains from one wythe to the other and the wythes have still shown to behave linearly in each wythe. Regarding the percentage of first crack load to ultimate load, the panels axially loaded ranged from 44% to 79%, whereas the eccentrically loaded panels ranged from 38% to 54%. Finally, the failure mode under axial load is observed by crushing of concrete in one or both bottoms of the panels, with only additional horizontal cracks along the whole panel height and inclined cracks near the top edge for the panel PA6. For eccentrically loaded panels, mainly vertical cracks were formed, and the panels failed due to compression. In panels PE5 and PE6 additional horizontal cracks were present in the unloaded wythe, and attributed to flexure effects since they failed under more pronounced deflections (BENAYOUNE *et al.*, 2006; BENAYOUNE *et al.*, 2007).

Figure 2.16 below shows the strain profiles in the concrete wythes for both loading cases.

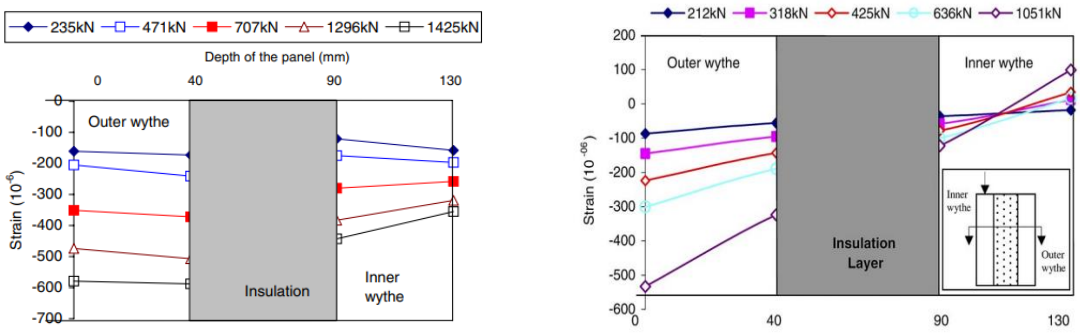

a) b)

Figure 2. 16 - Strain profile in concrete wythes: a) for axial load; b) for eccentric load. Source: Benayoune *et al*. (2006), Benayoune *et al*. (2007).

GARA *et al.* (2012) have tested sixteen panels under compression, being half axially loaded and half eccentrically loaded. All panels were 2940 mm height, 1120 mm width and 35 mm thick in the concrete layers. The panels varied in eps thickness, being built two specimens with either 80, 120 or 160 mm wavy eps core (designated, respectively, by WP08, WP12 and WP16), for each load case. The rest of the panels topologies were made with eps thickness of 80 mm, one being cast with a non-undulated EPS and the other with half the number of shear connectors (represented respectively by WPN08 and WPH08). They were cast with capping beams at the top and bottom of the panels. Those beams were reinforced with four 8 mm diameter steel bars and with U-shaped connectors of 6 mm diameter steel bars at each 200 mm of panel width. The reinforcement of the panels consisted of wire meshes with 3 mm diameter steel bars, and of shear connectors placed perpendicular to the panel height axis. Two additional panels were built for each load case, one intending to evaluate the influence of the surface of the eps layer, and the other to determine the influence of the number of shear connectors (had half the quantity of shear connectors). The sandwich walls were restrained at the top, while having a cylindrical pin at the base. The test results show that for mid-height, the panels with 120 mm eps thickness achieved higher stiffness under axial load, that eccentricity reduced all panels stiffness compared to axial load and that the influence in lateral deflection at mid-height of eps having non-undulated face was practically the same as reduction of shear connectors number to half. Another important remark is that the influence of slenderness ratio in the ultimate

load was observed to increase when the load application was eccentric. For the panels under axial load, the decrease in mean ultimate load for panels with 12,78 slenderness ratios to the ones with 15,47 and 19,6 was respectively 6,36% and 15,77%, while for the panels eccentrically loaded this reduction was observed to be 12,82% and 32,75%. Figure 2.17 shows the results of lateral deflection obtained for the panels in the experimental program. The dashed lines represent the panels evaluated eccentrically. The number 2 represents panel typology WP08, number 3 represents panel typology WP12, number 4 stands for panel typology WP16, while X.2 and Y.2 stands for the panel typologies WPN08 and WPH08 tested under axial load, but X.1 and Y.1 represent same panel typologies yet under eccentric load.

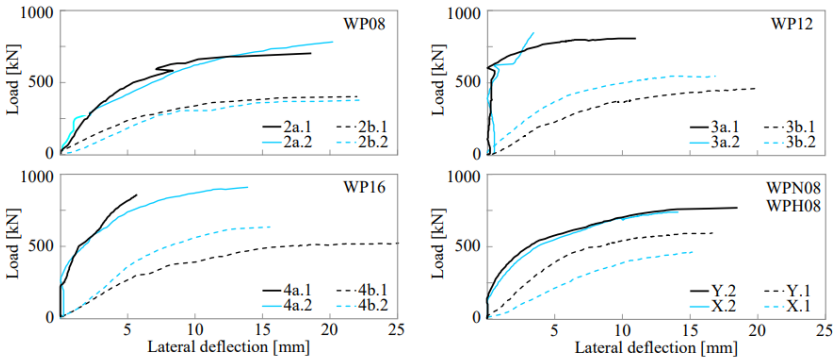

Figure 2. 17 - Axial and eccentric compression tests: load-lateral deflection diagrams at mid-height of the panel. Source: GARA *et al.* (2012).

The authors concluded that the lateral profiles of measured deflections of the two external layers (of the same thickness) presented a remarkably similar behavior, in the works of BENAYOUNE *et al.* (2006, 2007), with maximum deflections of approximately 10 mm, at half height. Ultimate strength reduction of only 11% was observed with an increasing slenderness ratio from 10 to 15, while a decrease of 38% was observed for increasing 10 to 20 of slenderness index. A high degree of composition was also found, and the mode of failure was by concrete crushing. Cracking load presented quite variable values, between 38 and 55% of the panels resistance (BENAYOUNE *et al.*, 2006). Another study evaluated the influence of eccentricity on the compressive strength of sandwich panels. Sixteen panels, with a smooth and corrugated polystyrene core and steel shear connectors (inserted perpendicularly to the face of the cores in straight bars), and with a height of 2940 mm by a length of 1120 mm were assessed, among which 8 with eccentric loading and 8 with concentric loading. Regarding the support condition fixed to the base, they found

that in the presence of eccentricities, the ultimate resistance also follows a linear decrease with the increase in the slenderness index (the specimens evaluated had a slenderness ratio between approximately 12 and 20). That is, given the similarity of the slenderness analyzed in the two studies, there is evidence of experimental difference between the behavior under eccentric compression for panels with the different types of shear connectors cited (metallic trusses and steel bars), given the non-proportional decrease of resistance between the intervals of 10 to 15 and 10 to 20 of slenderness index, in the case of the first mentioned work. Finally, the failure modes observed by GARA *et al.* varied between concrete crushing accompanied by buckling, for the concentrically loaded panels, and failure due to the rupture of the steel meshes present in the concrete layers in the eccentrically loaded panels. Eccentrically tested panels behaved as partially composite (GARA *et al.*, 2012).

Figure 2.18 below describes the symbols and meanings of each variable used in the formulation and the resultant equations achieved and the process to get to them.

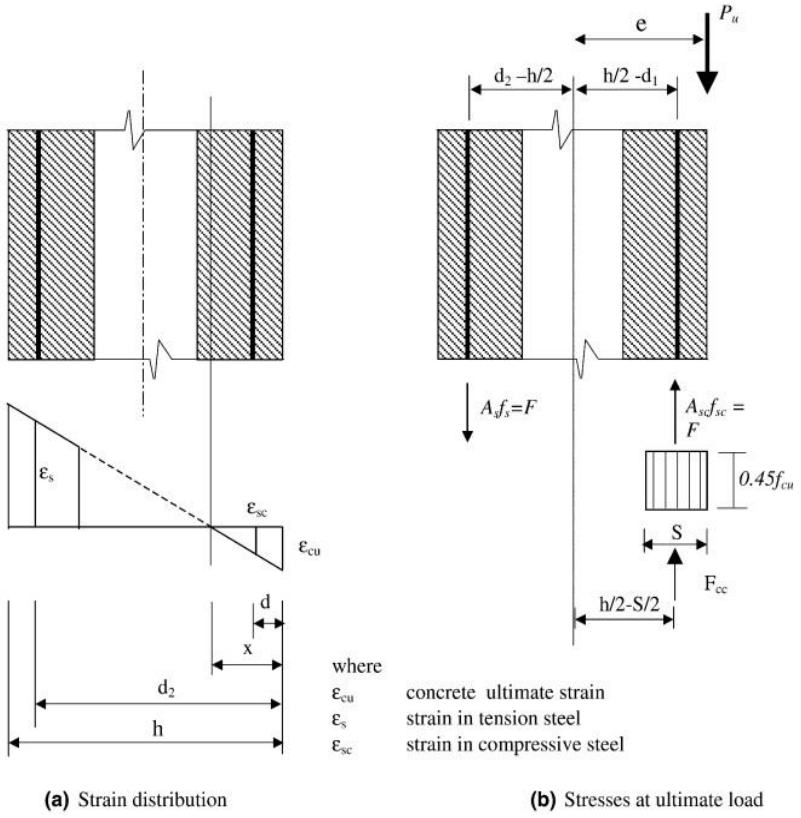

Figure 2. 18 - Force diagram and strain profile used to formulate analytical expression for eccentrically loaded sandwich panels. Source: BENYOUNE *et al.* (2006).

For the sake of equilibrium, the applied force acting on the section must equal the internal forces due to the tension and compression in the vertical bars of the wire

mesh plus the forces in the wythe subjected to compression. Therefore, using the assumptions mentioned above, the equilibrium turns into the below expressions (Eq. 21 and Eq. 22).

$$P_u = F_{cc} + F_{sc} - F_s \tag{21}$$

$$P_u = 0.45 f_{cu} bs + f_{sc} A_{sc} - f_s A_s \tag{22}$$

Where:

P_u = External applied force;

F_{cc} = Resultant force in compressed wythe;

F_{sc} = Resultant force in compression reinforcement;

F_s = Resultant force in tension reinforcement;

f_{cu} = Concrete compressive cube strength;

b = Panel width;

s = Equal to 0.9 times the depth neutral axis from the most compressed fiber;

f_{sc} = Stress in the compression reinforcement;

f_s = Stress in the tension reinforcement;

Through the expression developed above, it is possible to determine the neutral axis depth from the most compressed fiber. Then, with this information, one set the process to calculate the resistant moment of the section. It is done by setting the equilibrium of moments in the section. The equations that represent it are given below (Eq. 23 and Eq. 24).

$$M_u = P_u e \tag{23}$$

$$M_u = F_{cc}(h/2 - s/2) + F_{sc}(h/2 - d_1) + F_s(h/2 - d_2) \tag{24}$$

Where:

M_u = Resistant moment of the section;

F_{cc} = Resultant force in compressed wythe;

F_{sc} = Resultant force in compression reinforcement;

F_s = Resultant force in tension reinforcement;

h = Thickness of the wall;

s = Equal to 0.9 times the depth neutral axis from the most compressed fiber;

d_1 = Depth of the reinforcement A_{sc};

d_2 = Stress in the tension reinforcement A_s;

2.2.3.3 On the use and influence of capping beams on compressive strength of PCSPs

The cast of capping beams in one or both bottoms of the precast sandwich panels for axial compression tests has not been a standard procedure in the literature experimental programs (BENAYOUNE *et al.*, 2007; BENAYOUNE *et al.*, 2006; CARBONARI *et al.*, 2013; AHMAD & SINGH, 2021; AMRAN *et al.*, 2017; AMRAN *et al.*, 2016; AMRAN *et al.*, 2019; GARA *et al.*, 2012). It has even been advised to associate the experimental results under axial load with capping beams with appropriate constructive procedures, in which there are presence of capping beams or similar connections between the panels and the floors (GARA *et al.*, 2012). This difficulty, whether the literature results adequately represent the engineering practice, is enhanced by the fact that both types of connections are used in the site, with or without capping beams. Analyzing the experimental programs, it is also noticeable that none of them directly evaluated the influence of the capping beam with control groups. There are works where: 1) all panels tested under axial load are cast with capping beams at both ends (AHMAD & SINGH, 2021; GARA *et al.*, 2012; MOHAMAD *et al.*, 2017; MOHAMAD *et al.*, 2012) small-scale and real scale panels were tested under axial load, but capping beams as steel reinforcement hoops were used only for the real scale panels (CARBONARI *et al.*, 2013); 3) real scale panels were experimentally evaluated, however they did not have capping beams at any end (BENAYOUNE *et al.*, 2007; BENAYOUNE *et al.*, 2006; AMRAN *et al.*, 2017; AMRAN *et al.*, 2016; AMRAN *et al.*, 2019).

The details of the capping beams used in axial or eccentrical load are described here: in AHMAD & SINGH (2021) they were made of reinforced concrete respectively with size 600 mm x 100 mm x 150 mm and 600 mm x 100 mm x 180 mm. The first ones being used for the panels with 150 mm and 180 mm thick panels. They were cast at both panel ends and had four 8 mm diameter bars as longitudinal reinforcement, two numbers of 6 mm diameter stirrups, and U-shape anchor bars as a means to integrate them to the rest of the panels. The authors justified their insertion in the panels for avoidance of stress concentration and local crushing, as well as uniform distribution of

the load. Panels were tested under both axial and eccentrical load; in GARA *et al.* (2012), they had four 8 mm diameter bars as longitudinal reinforcement, and 6 mm diameter bars with 200 mm spacing as the stirrups. Capping beams were present at both ends; in MOHAMAD *et al.* (2017) the authors conducted axial load tests, where the capping beam cast in the panels was made using normal concrete from grade 25, with thickness of 50 mm. The authors justified their use to prevent premature cracking at both panel ends in the foamed concrete layer; in MOHAMAD *et al.* (2012) capping beams of 100 mm thick were cast at both ends with normal concrete.

The wide range of both geometrical (height, width, slenderness ratio, aspect ratio, etc) and mechanical (compressive strength, yield strength, young's module of both mortars, concrete, or reinforcement) of the experimental data cited makes it difficult to evaluate what kind of influence the presence of capping beams has on the resistance, and in other important mechanical aspects of the precast sandwich panels in compressive behavior.

2.2.4 Historical development of masonry walls

The use of masonry walls as resistant element dates back to the beginning of human civilization. It is considered the first form of shelter construction after the use of tents by nomadic humans (SILVA, 2007). The major advantage of masonry construction is its ability to combine multiple functionalities in a single element. It can simultaneously divide spaces, provide structural support, thermal and acoustic insulation, as well as fire protection, while being cost-effective and durable. It also allows for various finishes and easy implementation of different geometric configurations (HENDRY, 2004).

From a historical perspective, the development of masonry materials was highly influenced by the natural availability associated with the local environment. Therefore, civilizations located near rivers utilized alluvial deposits for brick manufacturing. For example, in Mesopotamia, bricks made from dried river mud were used. On the other hand, civilizations near mountains and rocky outcrops used stone structures, as seen in ancient Egypt, located in the rocky region of the Nile. Clay bricks dating back to 10000 years, and there's evidence that even as far as 12000 years. They have been found in various locations, including Babylon, Spain, and South America.

During the time of the Roman Empire, clay bricks could be manufactured by sun-drying or firing, with a waiting period of 5 or 2 years, respectively, before they could be used in construction. In 1858, the invention of the Hoffmann kiln is known to have accelerated the brick manufacturing process at that time. Initially, solid concrete masonry units were made, which reduced their popularity due to their weight. The development of techniques for manufacturing hollow blocks dates back to 1866 (DRYSDALE *et al.*, 1993).

However, the widespread use of masonry began around 1920 due to the first scientific investigations based on experimental tests. Another series of tests in Europe in 1951 was also crucial in expanding the use of this construction system, leading to the construction of a 13-story building in Switzerland using non-reinforced masonry, with internal walls 15 cm thick and external walls 37.5 cm thick. In Brazil, the implementation of this construction system was slow and started around 1966 with the construction of four-story buildings using hollow concrete blocks (JUSTE, 2001).

The Second World War also played a significant role in the dissemination of masonry construction. The extensive destruction caused by the war necessitated the rational, quick, and effective reconstruction of buildings. In Brazil today, walls with thicknesses of 14 cm and 19 cm are allowed in tall buildings, with design considerations based on the slenderness limits specified in the building codes. Regarding the design, the behavior and compressive strength of walls are crucial factors (LOPES, 2014).

Masonry as structural element involves the use of concrete blocks with structural functionality, capable of withstanding flexural and compressive forces, as well as combined actions of both. Sandwich panels can serve various purposes. Part of the uses include thermal and/or acoustic insulation, load-bearing capacity (resisting compressive forces), ceiling, flooring, or combinations of these applications, among others. In terms of historical perspective, the development of compression behavior analysis in sandwich panels is intertwined with the overall structural analysis of solid concrete walls.

2.2.5 Factors which influence the compressive strength of masonry walls

It is standard practice, established in standards such as ABNT NBR 16868-Alvenaria estrutural – Parte 3: Métodos de Ensaio, to correlate the compressive strength

of a full-scale wall with the compressive strength of a prism. For example, for masonry walls made of 190 mm blocks, the mentioned standard specifies that the characteristic strength of the wall should be considered as 70% of the compressive strength of the prism (f_{pk}) or 85% of the small wall (f_{ppk}). Small walls are defined by the same standard as walls with a length equivalent to at least two blocks or bricks and a height equivalent to five times the thickness of the block or brick, but not less than 70 cm, and they should have an odd number of courses along the height. Prisms are defined as a unit consisting of two stacked blocks with a mortar joint. Therefore, it is common in experimental studies to evaluate the relationship between the compressive strengths of prisms, small walls, and full-scale walls, as well as their associated efficiencies (ratios between the strengths of two elements), based on the investigated parameters.

In general, the significant factors that influence the strength of masonry walls can be divided with respect to each component of the masonry. Regarding the block properties, the following factors are determinative: geometry, compressive and tensile strength, and absorption. Regarding the mortar, the influencing factors include its strength, water retention, and joint thickness. Regarding the relationship between these elements, the stiffness relationship between the block and mortar is crucial. According to Mohamad (1998), an analysis of literature results indicates that there is a tendency for the prism strength to increase (non-linearly) with an increase in mortar strength when there is no change in the blocks used. However, the results suggest that such a trend does not hold for blocks with low strength. As expected, an increase in the block strength also leads to an increase in prism strength (non-linearly) (SILVA, 2007).

One of the key factors in masonry strength is the evaluation of prism behavior based on the type of bedding used. ZAHRA *et al.* investigated the influence of bedding mortar arrangement on the compressive strength of concrete blocks and prism blocks. Prisms were tested with bedding mortar only on the face shells of the blocks in the direction of their length ("Face shell bedding mortar") and with bedding mortar along all walls of the blocks ("Full mortar bedding"), whether transverse or longitudinal. The observed failure modes were predominantly vertical cracks throughout the prism (in the case of prisms with "Full mortar bedding") and failure at the transverse faces of the blocks, except when the mortar used had lower characteristic strength (M2 mortar), which caused the faces of the blocks to fail first (in the case of prisms with "Face shell bedding mortar"). The authors found a reduction in prism strength of up to 15% with

the decrease in bedding thickness in prisms with bedding only on the transverse faces of the blocks compared to prisms with all faces bedded (ZAHRA *et al.*, 2021).

In the case of ungrouted prisms, when the block is stiffer than the mortar, and the prism is subjected to compression, the bedding mortar has a greater tendency for lateral expansion than the block. Consequently, the restriction of movements between the two materials induces the presence of lateral stresses in both the mortar and the block. When the compressive strength of the mortar in the multiaxial state is greater than the tensile strength of the block, vertical cracks appear at approximately 60% of the final strength of the prism, with predominantly horizontal expansion for the mortars. However, a nearly linear stress-strain relationship is still observed in the pre-cracking and post-cracking behavior. Conversely, when the compressive strength of the mortar in the multiaxial state is lower than the tensile strength of the block, localized failures occur in the mortar, and non-linear behavior of the materials is observed from around 40% of the final strength of the prism. A schematic representation of the stress state and prism behavior in these two cases is presented in Figure 2.19. The failure of the mortar is more decisive than the failure of the block in the overall behavior of the prism (NALON *et al.*, 2022).

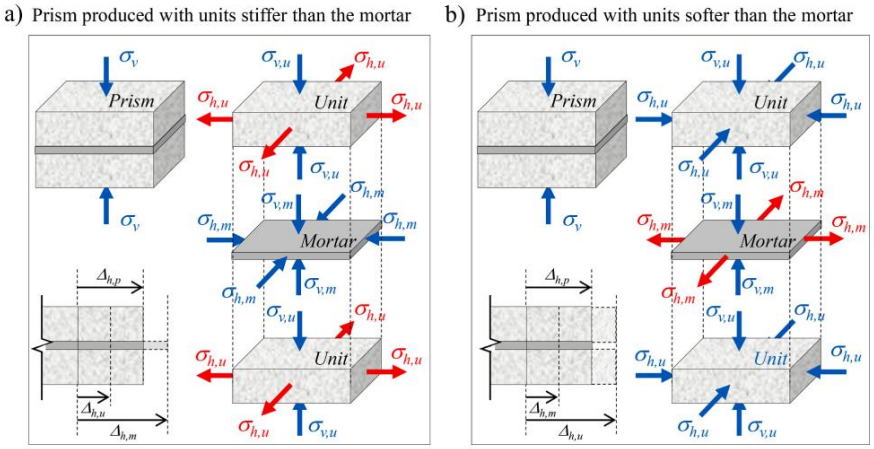

Figure 2. 19 - Stresses in prism according to the relation between mortar and unit stiffness. Source: NALON *et al.*, 2002.

MOHAMAD *et al.* present the historical development of a failure criterion for prisms. According to the authors, initially, a consideration of equilibrium between lateral and compressive stresses between the block and mortar, together with the assumption of a linear failure envelope based on Mohr-Coulomb theory, led to the Hilsdorf criterion. However, the model disregards the influence of deformations and, in the case of high-strength blocks, predicts overly conservative results. Other

theoretical models have been proposed, but the authors highlight some encountered difficulties. Among them, the failure mechanism of hollow concrete blocks is a stepwise process rather than an abrupt and defined failure (MOHAMAD *et al.*, 2017).

Regarding the influence of buckling on the compressive strength of masonry walls, there is a considerable number of studies evaluating the stability of masonry walls with various slenderness ratios and eccentricity in load application. However, analytical solutions are based on a limited and specific number of stress-strain curves and support conditions (SANDOVAL *et al.*, 2011). It is worth mentioning that the anisotropic behavior of masonry walls, resulting from the combined behavior of materials with different physical and mechanical properties, has been evaluated and modeled through the formulation of macro models, such as the model proposed by Grzyb and Jasinski, using homogenization methods (GRZYB & JASINSKI, 2022).

2.2.6 Compressive strength of masonry walls

A series of empirical equations have been proposed in different standards for the design of masonry walls. In the case of unconfined compression of unreinforced masonry, four different expressions from different standards are presented here. The formulations are based on a certain number of geometric and mechanical parameters of the blocks (such as net area, compressive strength, radius of gyration, among others) chosen as determinants, and incorporate factors that account for the effect of wall slenderness on compressive strength, initial eccentricities. These factors depend primarily on the slenderness, effective heights (dependent on support conditions), and effective thicknesses of the blocks.

The Brazilian standard ABNT NBR 16868-Alvenaria estrutural – Parte 1: Projeto provides the following equation for the design of unreinforced masonry walls and columns subjected to compression. The second equation represents the reduction coefficient R (due to wall slenderness), where λ represents the ratio between the effective height (which depends on the actual height of the masonry and support conditions). The slenderness limit index for unreinforced structures should be limited to 24. However, for single-story residential buildings, higher values up to 30 are allowed, provided that the masonry strength reduction factor is considered equal to 3. In the case of columns, the value of N_{Rd} should be multiplied by 0.9.

$$N_{Rd} = f_d AR \quad (25)$$

Where:

N_{Rd} = Resistant design force;

f_d = Design compressive strength of masonry unit;

A = Gross cross-section area;

R = Coefficient which accounts for the slenderness of the wall, equal to $\left[1 - \left(\frac{\lambda}{40}\right)^3\right]$;

A figure depicting the variation of the reduction coefficient R as a function of slenderness is presented as Figure 2.20.

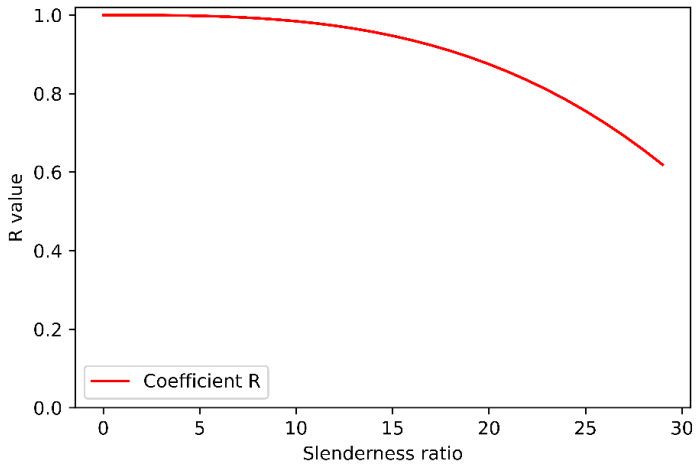

Figure 2. 20 - Coefficient R variation versus slenderness ratio.

The European standard Eurocode 6: Design of Masonry Structures – Part 3: Simplified calculation methods for unreinforced masonry structures establishes a procedure for calculating the compressive strength of unreinforced masonry. This procedure is based on the compressive strength of the masonry unit, the reduction coefficient due to eccentricity (Φ_s), wall buckling, and initial eccentricity effects. The standard provides the following values for the reduction coefficient for different types of walls: intermediate walls, walls acting as lateral supports of floors, and walls at the top floor that also act as lateral supports of floors. The smaller value between the two equations and 0.4 is adopted. The effective height (h_{ef}) depends on the support conditions and the reduction factor (ρ_n), which is defined based on the wall's restraint

or stiffness and the story height. The value of l_{ef} also depends on the support conditions, and the effective thickness (t_{ef}) depends on the number of masonry layers used in the wall and their respective thicknesses. The expressions for the reducing coefficient (φ_s) follows below (Eq. 26 and Eq. 27).

$$\varphi_s = 0.85 - 0.0011\left(\frac{h_{ef}}{t_{ef}}\right)^2 \tag{26}$$

$$\varphi_s = 1.3 - \frac{l_{ef}}{8} \leq 0.85 \tag{27}$$

And the expression for ultimate design strength is given below (Eq. 28).

$$N_{Rd} = \varphi_s f_d A \tag{28}$$

Where:

φ_s = Reduction coefficient, given by lesser value of the described equations above and 0.4;

f_d = Concrete block compressive strength;

A = Transverse cross-section area of wall;

h_{ef} = Effective height, chosen according to the support conditions;

t_{ef} = Effective thickness, chosen according to the support conditions;

l_{ef} = Effective span, chosen according to the support conditions;

Two figures with the variation of the reduction coefficient φ_s for each case above are presented as Figure 2.21 and Figure 2.22, as a function of slenderness and effective span.

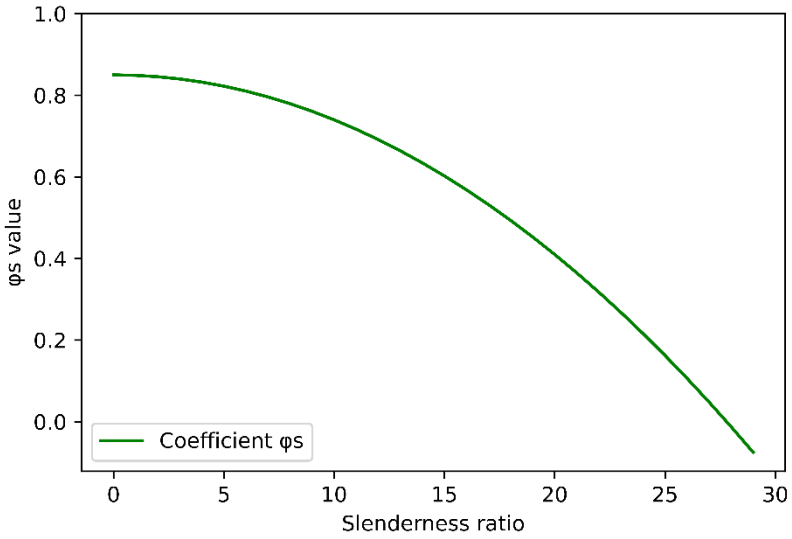

Figure 2. 21 - Coefficient φ_s variation versus slenderness ratio, given by equation 26.

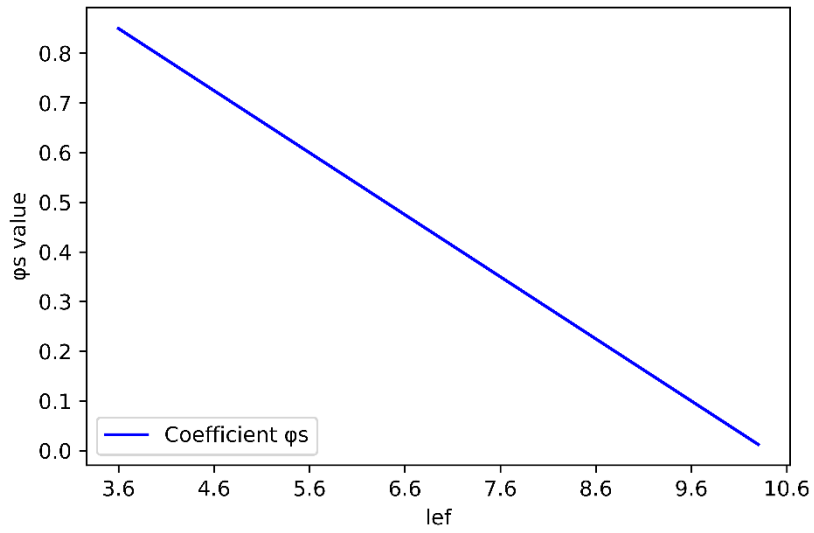

Figure 2. 22 - Coefficient φ_s variation versus l_{ef}, given by equation 27

The American standard ACI 530-02 establishes two equations for the compression design of non-reinforced masonry, depending on the ratio between its height and the radius of rotation of the block. In the first case (Eq. 29), the cited quotient has values not greater than 99, and in the second case (Eq. 30), for quotients above 99.

$$P_n = 0.80\left(0.80A_n f'_m\left[1-\left(\frac{h}{140r}\right)^2\right]\right) \quad (29)$$

$$P_n = 0.80\left(0.80A_n f'_m\left(\frac{70r}{h}\right)^2\right) \quad (30)$$

Where:

P_n = Resistant force, in pounds;

A_n = Net cross-section area of section, in $inch^2$;

f'_m = Characteristic compressive strength of units, in psi;

h = Wall height, in inch;

r = Radius of gyration of masonry unit, in inch;

CHAPTER 3

3 EXPERIMENTAL PROGRAM

In this chapter, a description of the experimental program carried out in this work is thoroughly given. The chapter is subdivided into sections about the experimental tests conducted on the unreinforced masonry walls, and later on the precast sandwich panels. First, the experimental devices are specified, along with their use control, positioning, numbering, identification, and experimental devices abbreviation maintained throughout the experiments. This is exposed so that further investigations may be able to reestablish the conditions in which the tests were conducted, therefore allowing future repetition or extension of the current research, as well as they clarify the mechanical conditions under which results were obtained and interference of those conditions on the data. Then the description and mechanical evaluation of the materials used in each of the specimens is commented. Further information is available about the geometry and construction of the specimens evaluated, such as the mechanical boundary conditions which were considered in the experiments.

Before the subsections described above are presented, a schematic figure of the reaction frame used to load both unreinforced masonry walls and precast sandwich panels is shown as Figure 3.1. The specimens are centrally positioned on the reaction frame at the Structures Laboratory (LABEST), at the University of Brasília. Regarding the use of the hydraulic actuator, the use varied from an actuator with a capacity of 500 kN to one with 1000 kN capacity, chosen to apply the axial load. The frame has a clear height of 5000 mm, with a clear width of 1700 mm. In a effort to guarantee better distribution in the application of the load, a layer of 30 mm of neoprene was used between the train track and the walls and panels. Further details of the experimental “Setup” are added in the next subsections.

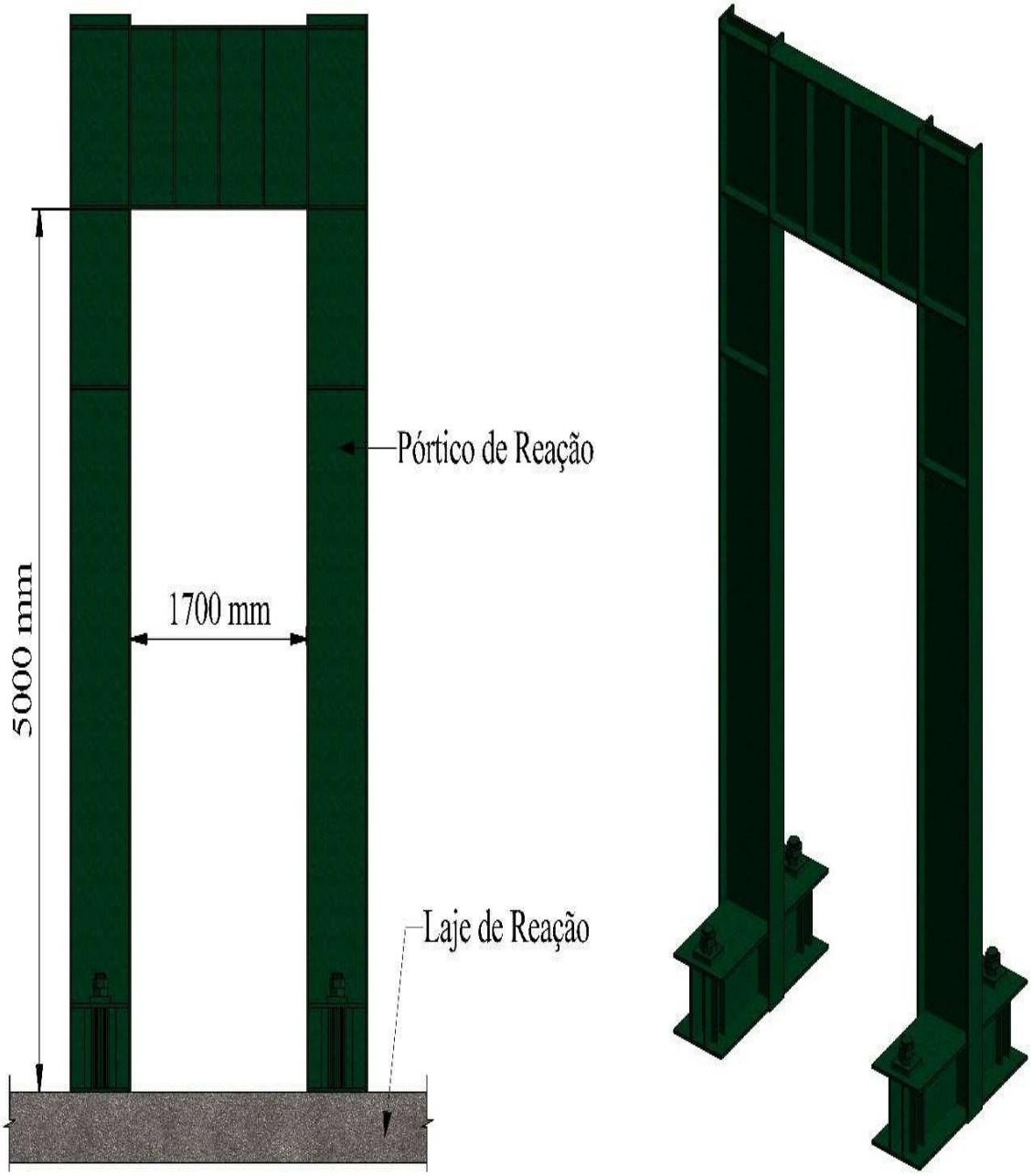

a) b)

Figure 3. 1 - Reaction Frame; a) Front view of the frame; b) Frame perspective.

3.1 Experimental devices

Data acquisition is conducted using two Spider 8 modules, with data reading and storage performed by HBM's Catman program. The load control system, which comprises the control table and actuator, is an Enerpac load application system, with an oil flow outlet hose (quick coupling for the oil flow outlet), and inlet hose of the oil flow (quick coupling to enter the oil flow). The data acquisition system is shown in Figure 3.2.

Figure 3. 2 - Data acquisition system.

3.2 Tests on unreinforced masonry walls

3.2.1 Masonry walls geometry

According to the Brazilian standard which regulates the projects and the tests on masonry walls (ABNT NBR 16868 – Parte 3), the size and geometry of the specimen subjected to evaluation should be representative of the real wall considered, based on the actual structure built. However, for the cases where it is not possible to do so, the standard determines that the minimum dimensions of the specimen are required to be 1.20 m x 2.60 m (width x height).

Therefore, the masonry walls in this experimental program were chosen so that they satisfy this minimum condition. For the thickness, the walls have been built to possess the same thickness as the concrete masonry blocks, which means they have been cast without any surface layer of mortar or grout. As there is a need to settle the masonry units with mortar, the mortar layer's thickness was adopted so the total width achieved was the one required (1.2 m). Table 3.1 compiles the geometric dimensions of the three masonry walls specimens tested. Figure 3.3 illustrates the details of the walls.

Table 3.1 - Dimensions of the masonry walls specimens.

Wall	H(m)	B(m)	t(m)
W1	2.60	1.20	0.090
W2	2.60	1.20	0.090
W3	2.60	1.20	0.090

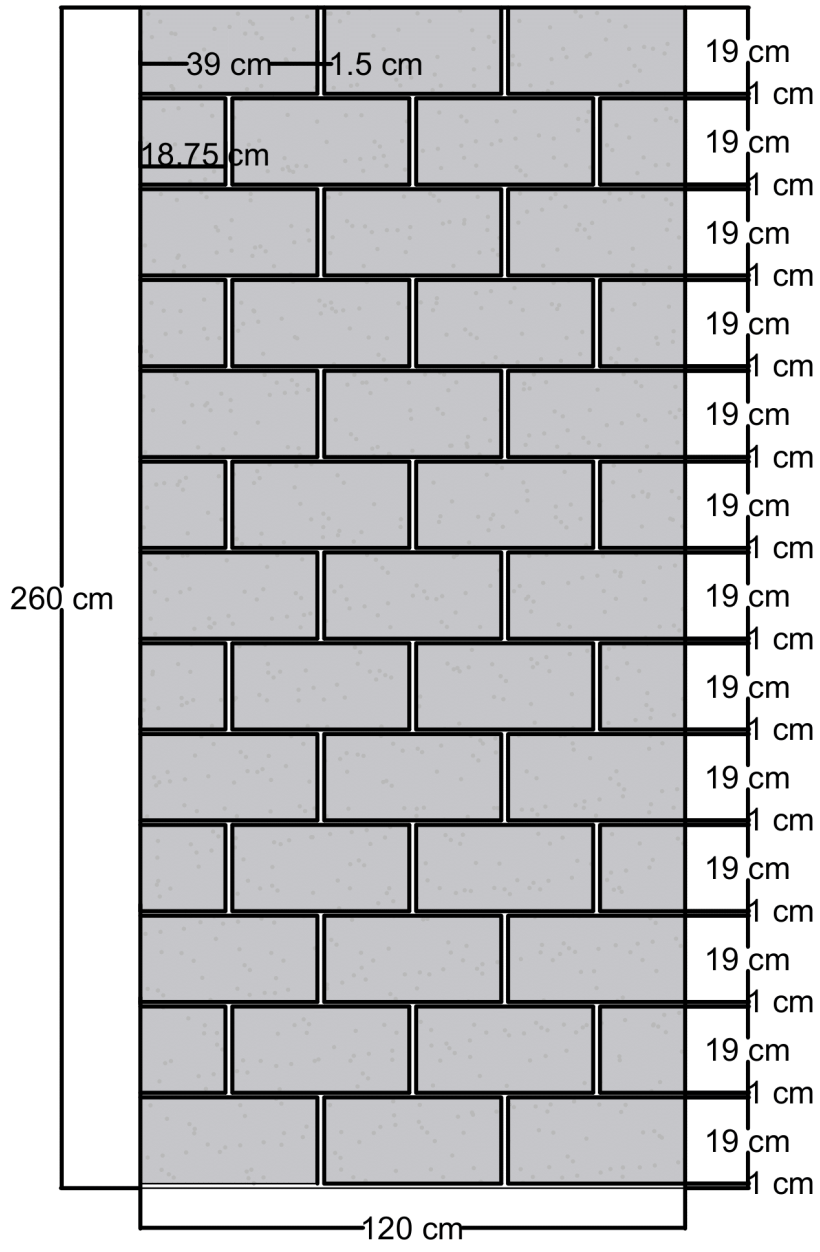

Figure 3. 3 - Masonry walls detail.

3.2.2 First Masonry wall setup

The experimental setup for the masonry walls specimens presents some common aspects regarding the positioning of the LVDTs, but for each of the masonry

specimens evaluated there is also aspects to which the experimental setup changes with respect to the LVDTs positioning. This basic instrumentation will also be used in all masonry specimens.

It consists of 2 LVDts positioned at 2/3 of the wall height and 5 LVDTs positioned at the first third of the walls height. For those placed at 2/3 of the height, they are spaced 40 cm far from each other and each one is also 40 cm far from one of the wall laterals. According to the numbering system used, the LVDTs are numbered in an increasing manner, according to the following order: LVDTs at higher places have smaller numbers and for LVDTs at the same height level, they increase in number from the left to the right. Figure 3.4 shows the positioning of all LVDTs used for the compressive test on the first wall. The basic experimental configuration described above is given by the LVDTs numbered 2 and 3 (at 2/3 of the height) and LVDTs 4, 5, 6, 7 and 8 (at 1/3 of the height).

The first LVDT has varied in the positioning of the masonry specimens because it was necessary to measure the adequacy of the load application frame, as the aim of this research consists in the evaluation of the mechanical behavior of specimens subjected to concentric load. In this particular experiment, the first LVDT was placed vertically in contact with a steel plate connected to the bottom web of the steel profile used as the spreader beam. Therefore, it was possible to register the vertical displacement of the spreader beam and load application structure. Figure 3.5 registers the exact position of the first LVDT, among the others. The last LVDT used, numbered 9, is used to measure the global shortening of the specimen. It was attached to a long stem so that it is possible for the tip of the LVDT to measure the global shortening of the wall. The LVDTs are supported on steel beams that cross the frame, however they do not play any role in the mechanical test.

For the load application in all masonry tests, the instrumentation was made of a steel profile as a spreader beam, as mentioned, and with a 3 cm thick layer of Neoprene. The hydraulic jack has a 500 kN capacity. A picture of the setup for the first masonry wall test is shown in the Figure 3.4. Finally, it is just highlighted that the wall was painted white for the cracks to become more apparent and that as can be seen, a strong floor was cast before each of the walls was built. It intended to provide a rigid base for the test. This first wall specimen was loaded 4 months after construction. The reason for it is that the system of load application used had never been prepared for such experimental test in the laboratory of the university, and it took more time than the

predicted to solve all the security as well as mechanical details of the experiment.

Figure 3. 4 - First masonry wall test detail.

Figure 3. 5 - Position of LVDT 1 for the masonry wall W1 test.

3.2.3 Second masonry wall setup

The second masonry wall specimen was also evaluated with the same load application common to all masonry tests, and it was settled with 9 LVDTs, in which the ones from number 2 to 8 belong to the basic instrumentation described in the previous subsection.

The particularity of this test regards the positioning of the first LVDT. In this

case, it was decided to place it near the top of the wall for it to register the displacement at the location expected to displace the most, given the support conditions of the test. Below, the positioning of the LVDT 1 is shown in Figure 3.6 and in Figure 3.7 displays the entire setup. The wall was tested at 28 days of mortar age.

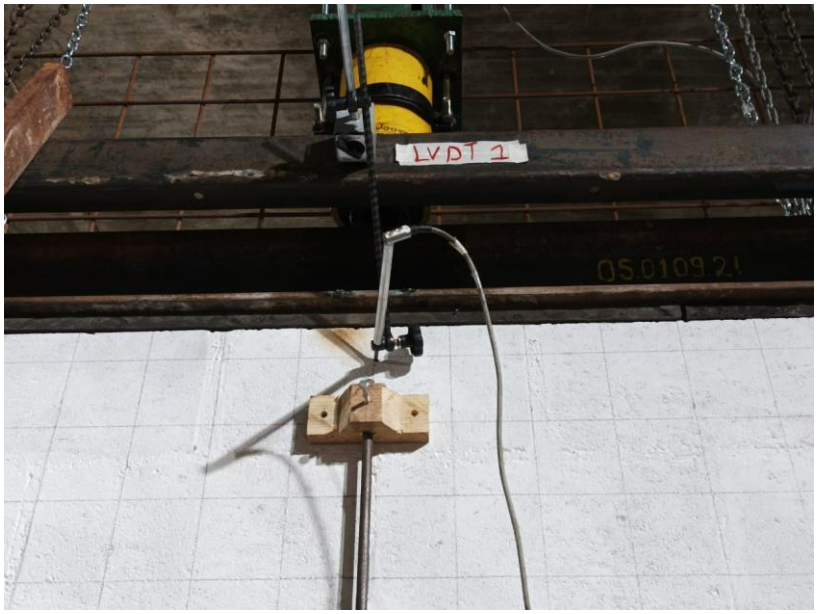

Figure 3. 6 - LVDT 1 positioning.

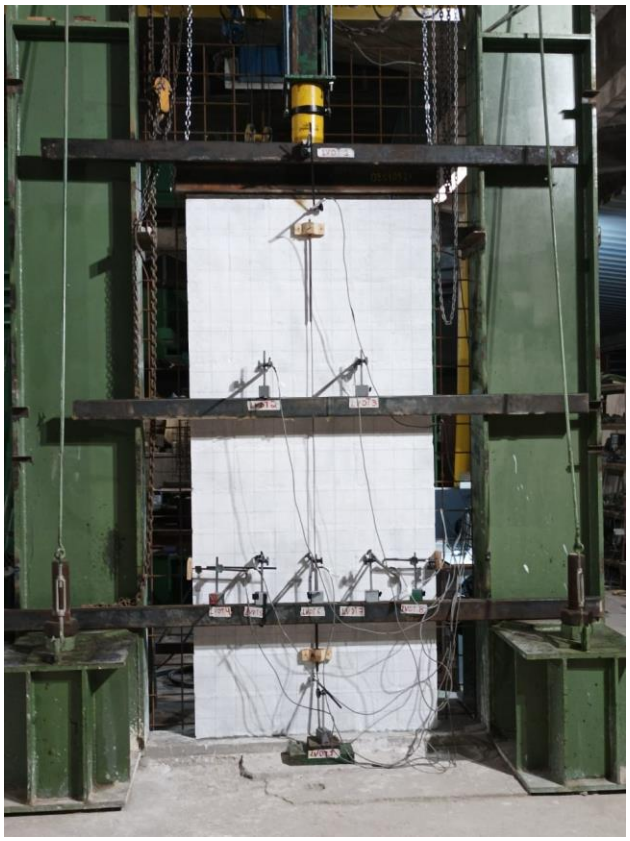
Figure 3. 7 - Experimental setup.

3.2.4 Third masonry wall setup

The third test carried out on the unreinforced masonry wall was done with the same disposition of the LVDTs numbered from 2 to 9. However, as highlighted in the previous section about the tests on the other masonry walls specimens, the position of the first LVDT has varied, for the purpose of registering specific details and information about the proper adequacy of the experimental setup and load application system. The horizontal displacement of the load application system has been registered, with regard to the displacement of the it the right extremity of the steel distribution beam. It was chosen that the first LVDT in this specimen should be placed in this a way, therefore allowing it to track the rotation of the distribution beam below the hydraulic jack. The wall was loaded at 28 days of age.

3.2.5 Mortar mechanical properties

The determination of both compressive and tensile strength in diametral compression of the mortar used in the masonry walls as well as in the wythes of the precast sandwich panels was given by the procedures of the ABNT NBR 5738 - Concreto — Procedimento para moldagem e cura and ABNT NBR 7222 – Concreto e Argamassa – Determinação da resistência à tração por compressão diametral de corpos de prova cilíndricos. Six specimens were collected for each test. They were conducted in the laboratory of structures and materials of the instituto Federal Samambaia (IF Samambaia). The machinery used is shown in Figure 3.8. Tables 3.2 and 3.3 display the values of both tests.

Table 3.2 - Values of compression tests of mortar.

Number of specimen	1	2	3	4	5	6
Compressive strength (MPa)	28.79	26.70	28.75	25.20	27.26	29.14

Table 3.3 - Values of tension in diametral compression tests of mortar.

Number of specimen	1	2	3	4	5	6
fct, sup (MPa)	2.26	2.78	3.66	3.67	2.55	2.45

a) **b)**

Figure 3. 8 - Machine used in mortar compression and tensile tests (tension in diametral compression).

3.2.6 Concrete blocks mechanical properties

The hollow concrete blocks used in the test of the reference walls are classified according to ABNT NBR 6136: Blocos vazados de concreto simples para alvenaria – Requisitos, having nominal dimensions of 190 mm x 190 mm x 390 mm, and class C, of according to table 2 of the standard. In this way, it is required as a requirement for class C of hollow concrete blocks, that the compressive strength (f_{bk}) equal to or greater than 3 MPa. The tests on the blocks were carried out in the materials and civil engineering laboratory of the University Center of Brasília (UniCeub), Taguatinga Campus.

The criteria for meeting the geometric configurations of the blocks were met. Thus, the tolerance of each measurement taken was smaller than the required one of 1 mm for each wall of the block taken individually. The compressive strength of hollow concrete blocks for use in masonry walls were determined from a sample of 6 blocks, as permitted by ABNT NBR 6136, for a number of blocks in a batch of less than 5000 units, tested under compression according to ABNT NBR 12118 – Blocos vazados de

concreto simples para alvenaria – Método de ensaio. The applied voltage was controlled with a focus on maintaining the loading speed established in the norm, equal to 0.15 MPa/s. The faces of the blocks where contact with the experimental apparatus occurred were smoothed using cement paste, with an average thickness not exceeding 3 mm, ensuring the flatness of the smoothing layer. Photos of the described procedure (Figures 3.9 and 3.10), as well as the press apparatus used to compress the blocks, are presented below. Table 3.4 is shown, as a summary of the results obtained for the compressive strength of the blocks, which obtained an estimated characteristic strength of 8.42 MPa ($f_{bk,est}$), as well as the normative equation used to calculate this characteristic strength.

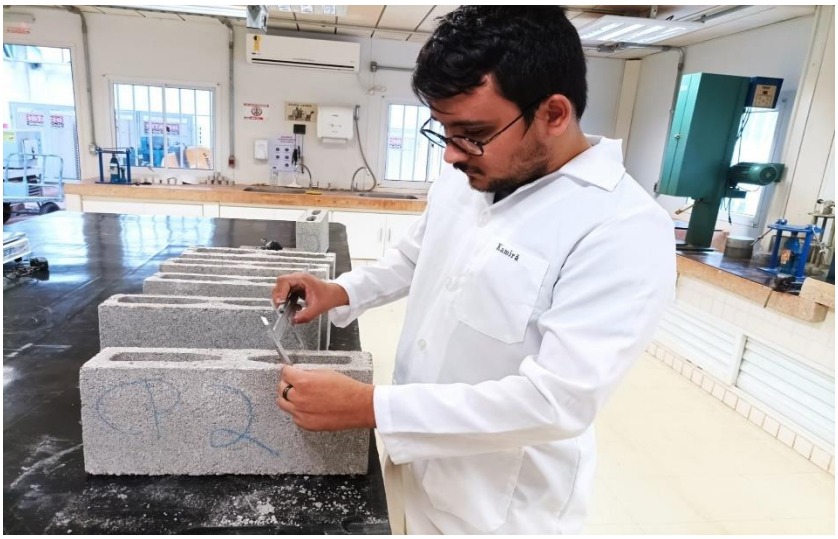

Figure 3. 9 - Measurement of concrete block dimensions.

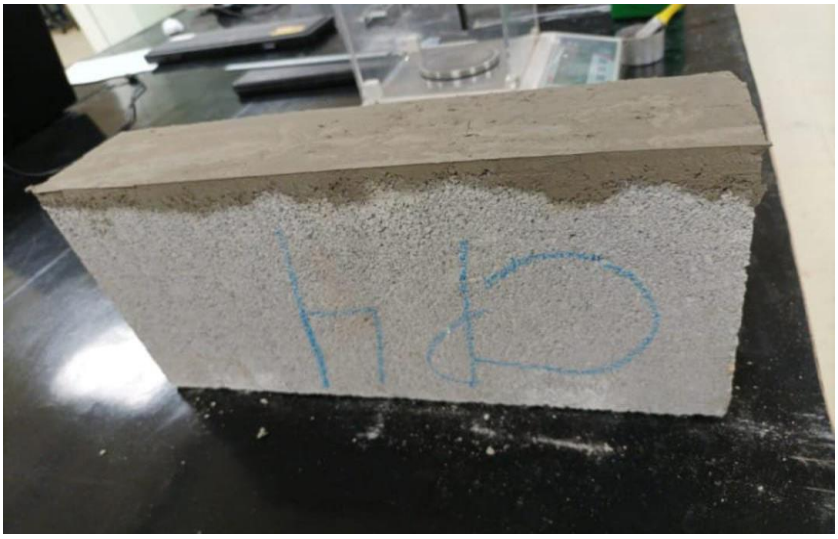

Figure 3. 10 - Regularization layer of cement paste, cast in the hollow concrete blocks for the compressive test.

Table 3.4 - Results of compressive strength of the concrete blocks.

Number of specimen	1	2	3	4	5	6
Compressive strength (MPa)	8.44	9.00	9.02	10.03	10.23	10.23
Mean resistance (MPa)	9.49					
Standard deviation	0.768					

$$f_{bk,est} = \frac{2[f_{b(1)} + f_{b(2)} + \ldots + f_{b(i-1)}]}{i-1} - f_{b(i)} \quad (31)$$

Where:
n = Number of blocks in the sample;
i = n/2, if n is even;
i = (n-1)/2, if n is odd;
$f_{b(1)}, f_{b(2),} \cdots f_{b(i)}$ = The resistance values of individual blocks tested, ordered in an increasing manner;
$f_{bk,est}$ = The characteristic compressive strength of the sample, in MPa.

The standard ABNT NBR 6136 also requires that the value of $f_{bk,est}$ calculated above shall not be smaller than ψ times $f_{(1)}$, ψ being used according to Tables 3.5 and 3.6, varying with the number of blocks in the sample. Therefore, ψ is equal to 0.89. Therefore, the characteristic strength must be bigger than 7.5116 MPa. The value determined to $f_{bk,est}$ was 8.42 MPa, then this is the characteristic strength.

Table 3.5 - Values of ψ. Source: ABNT NBR 6136.

Number of blocks	6	7	8	9	10	11
ψ	0.89	0.91	0.93	0.94	0.96	0.97

Table 3.6 - Values of ψ. Source: ABNT NBR 6136.

Number of blocks	12	13	14	15	16	18
ψ	0.98	0.99	1.00	1.01	1.02	1.04

3.3 Tests on Precast Sandwich Panels

3.3.1 Panels geometry

A series of 3 full-scale precast sandwich panel specimens were built and tested. The panels tested had a single geometrical configuration, as presented in detail

in Table 3.7. The load conditions investigated were centered axial loads for all panels evaluated (PA1, PA2, PA3). Panels PA1 and PA2 were tested at 28 days after casting, while panel PA3 was tested at 3 months after casting.

Table 3.7 - Specimens Tested.

Panel	H (mm)	B (mm)	t (mm)	H/B	H/t	t_1 (mm)	t_2 (mm)	c (mm)
PA1	2600	1200	140	2.16	18.57	25	90	10
PA2	2600	1200	140	2.16	18.57	25	90	10
PA3	2600	1200	140	2.16	18.57	25	90	10

Where, *H* is the panel height; *B* the width; *t* the overall thickness; t_1 the thickness of each mortar wythe; t_2 the thickness of insulation layer; *c* the mortar cover; (*H/B*) the aspect ratio and (*H/t*) slenderness ratio.

3.3.2 Experimental setup

The instrumentation used was 5 LVDTs (Linear Variable Differential Transformer) at each wythe, connected in the software Catman, from HBM. All LVDTs are designated according to their position as shown in Figure 3.12) a, and by a legend, which stands for whether the LVDT designated was positioned in the inner or outer wythe (letter I and O, respectively). The details on the capping beam at both ends of each panel, as well as the details on the reinforcement of the panels, are shown in Figure 3.11. In Figure 3.12 one can see the position of the LVDTs. The specimens tested were restrained to horizontal displacement and unrestrained to rotation at the height of the base of the top cap beam, by the positioning of two hinges, as shown in Figure 3.12) c, and unrestrained to rotation at the bottom. The bottom of the specimens was placed over a strong floor and of a 2 cm plaster layer. Figure 3.12) b also shows a front view of the experimental setup.

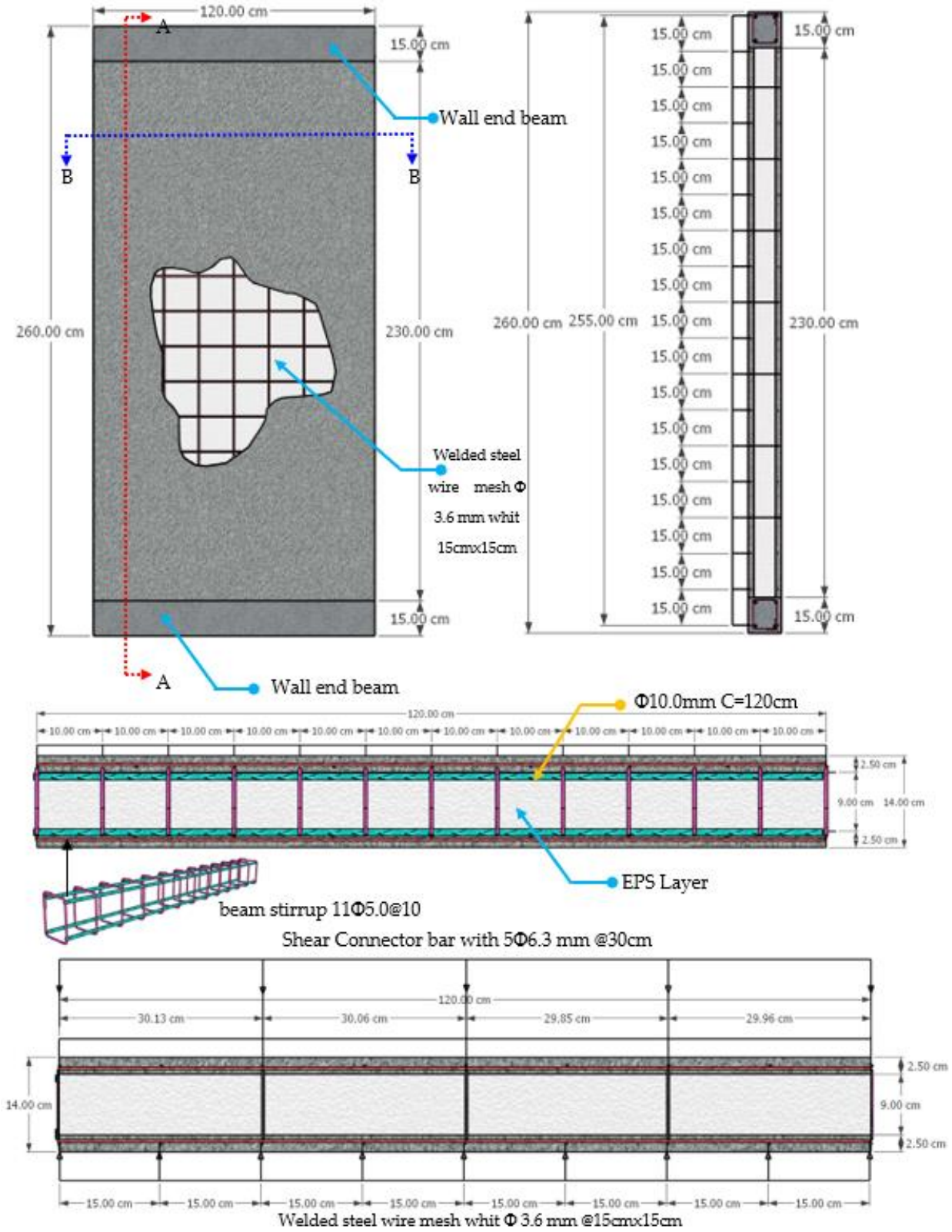

Figure 3. 11 - Details of reinforcement of the panels tested. Visualization of the wall with steel wires, with all measurements in centimeters.

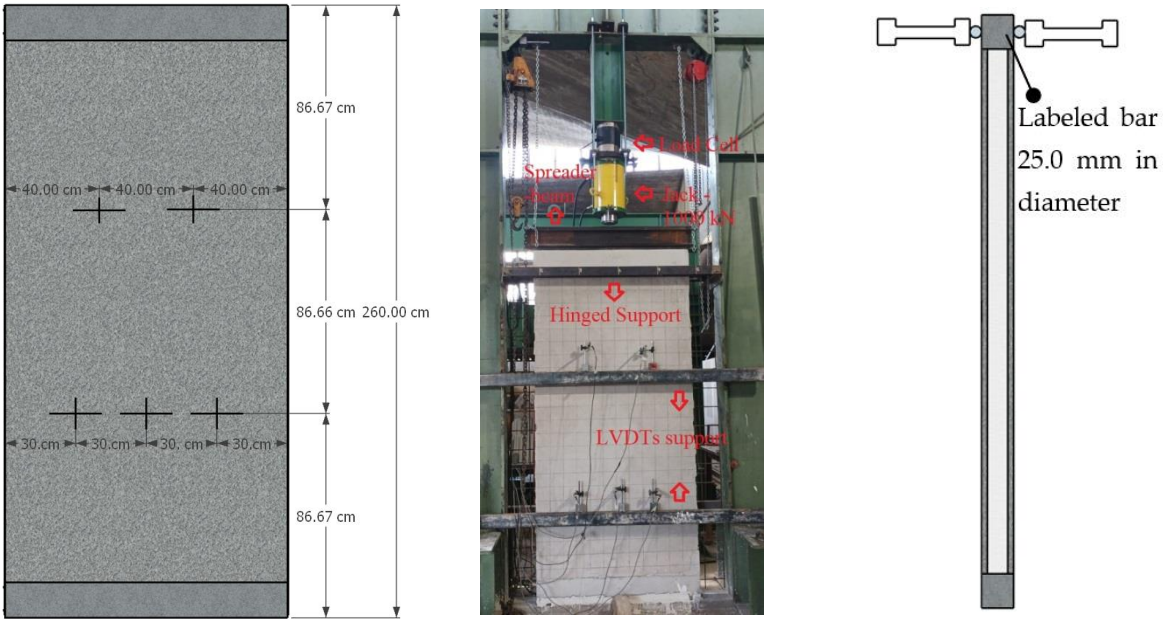

(**a**) (**b**) (**c**)

Figure 3. 12 - Experimental setup information. (a) Position of the LVDTs; (b) Reaction frame front-view; (c) Detail on the hinged supports at the top of the experimental setup.

3.3.3 Materials description

A square welded galvanized steel wire mesh of 3.6 mm diameter wires with 15 by 15 mm spacing was used as the longitudinal and transverse reinforcement of both wythes. The wire mesh described was connected to the insulation core by means of steel connectors made of steel with different mechanical properties as those of the wire mesh. They were 6.3 mm in diameter anchored at the extremities in the steel wire mesh, and spaced spanning 30 cm in both directions. A total number of 16 steel shear connectors were used for each square meter of the panel.

The insulation core material was EPS with 0.14 kN/m^3 nominal density. The wythes were composed of mortar with 1:2 cement to sand trace. The cement used is a Portland cement named CPII – Z32, according to the classification and criterion presented in the Brazilian standard ABNT NBR 16697. The mortar was produced in concrete mixers, and the panels were cast on place. Six cylindrical mortar specimens were collected and subjected to cure as a means to determine the mortar compressive strength of the wythes. No additive was used in the mortars. The panels were built in steps, given respectively by: 1) positioning and distribution of the steel wire mesh; 2) placement of the steel shear connectors bars, maintaining the proper cover; 3) cast of the mortar of inner wythe, and further cast of the mortar in the outer wythe; 4) later transportation of the panels in the loading frame

through an overhead crane, after the mortar of the wythes have 28 days age. The mortar tested obtained a characteristic compressive strength of 25.10 MPa, as it was done with the same trace as the masonry walls mortar, whose strength results are present in subsection 3.2.5. During the cast of the mortar in the wythes, it was given special attention to the correct maintenance of the mortar clear cover of 10 mm. It was done by the positioning of square pieces with 10 mm thickness of mortar with the same properties as the used for wythes, however already hard, above the welded wire mesh, aiming to keep the cover as close as possible to the desired value. Figure 3.13 is representative of the procedure aforementioned described.

Figure 3. 13 - Placement of sleeves to keep mortar clear cover.

The properties of square welded galvanized steel wire mesh are presented in Table 3.8. One concrete beam was cast at bottom and the top of the panel in an effort to better distribute the loads, in conformity with previous experimental works cited (BENAYOUNE *et al.*, 2007; BENAYOUNE *et al.*, 2006; GARA *et al.*, 2012). Both concrete beams were reinforced longitudinally with 4 steel bars of 10 mm diameter, and with a total of 11 stirrups of steel bars of diameter 5 mm. The mechanical properties of the following reinforcements are the same as those presented in Table 3.9.

Table 3.8 - Welded steel wire mesh mechanical properties.

Diameter (mm)	f_y (MPa)	f_u (MPa)	E_s (MPa)	ε_{cu} (%)
3.6	492	649	21000	0.93

Table 3.9 - Bar of the reinforced longitudinally and Stirrups with mechanical properties.

Diameter (mm)	Bar type	f_y (MPa)	f_u (MPa)	E_s (MPa)	ε_{cu} (%)
5.0	Stirrups	598	684	21000	0.98
10.0	Longitudinal bars of the beam	587	671	21000	0.10

Where: f_y is the nominal yield strength of steel; f_u is the ultimate strength of steel; E_s is the steel modulus of elasticity; ε_{cu} is the ultimate strain at failure.

Finally, an image of the reinforcement of the concrete beams cast in the top and bottom of panels is shown in Figure 3.14) a. The details of it are present in figure 3.11. The other figure below, 3.14) b show the concrete beam reinforcement before it was assembled to the panel.

a) **b)**

Figure 3. 14 - Concrete beam reinforcement: a) connected to the rest of the panel; b) in perspective.

CHAPTER 4

4 RESULTS AND DISCUSSION

In this chapter, a detailed discussion and presentation of the results of this research are written. In the context of the experimental data regarding the masonry walls specimens, there are subsections which deal with the load-displacement curves for the LVDTs positioned throughout the wall. Also, a discussion about the crack pattern and failure modes of the masonry walls is developed.

For the subsections with respect to the experimental data obtained by tests on the precast sandwich wall panels, there are some relative to the exhibition of displacement registered by the LVDTs and arranged in various ways. Further analysis and investigation are carried out about other aspects of the results collected, which have not yet been addressed in the literature, such as the cross-section displacement profile, the load-displacement profile not only for the middle part of the sections. Finally, the crack pattern and failure mode are scrutinized and the comparison of empirical equations of both concrete solid-wall and sandwich panels with regard to experimental results is presented.

4.1 Results on Masonry Walls

4.1.1 Load-displacement curves for LVDTs

For the main displacements obtained, which are the ones for LVDTs 2, 3, 5, 6 and 7, the results are depicted below in Figure 4.1. The displacements for LVDTs 2 and 3 show that the first and second masonry walls tested have reached displacements about 20 mm for W1 and even 30 mm for LVDT 3 of W2. The wall W3 has, however, displaced at most approximately 10 mm in absolute value. The first wall, W1, displays a stiffer behavior, as it requires a higher applied load to reach the maximum values for W2 and W3. It is attributed to the fact that this specimen was tested 4 months after its construction, leading to more mortar strength. It was also noticed that for the wall W1, it has concentrated the displacement at the top three concrete block layers, as one can notice in the next section, where pictures of the cracks developed in that wall are shown. Therefore, with that being said and the additional resistance of the mortar, it is

reasonable that it has displaced considerably less than W3 for the LVDTs at the first third of wall height.

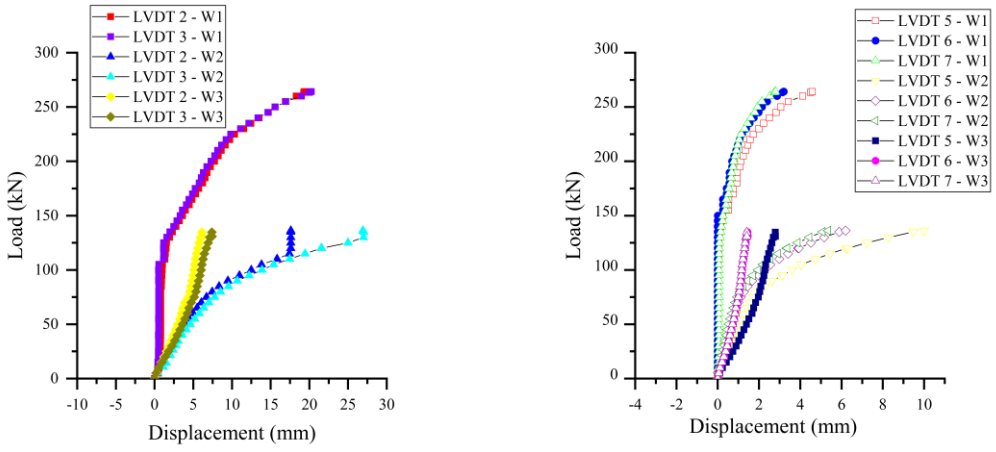

(a) **(b)**

Figure 4. 1 - Load-deflection response for walls W1, W2 and W3 for LVDTs: (a) 2 and 3; (b) 5, 6 and 7.

The LVDT 1 also contains interesting information regarding the functioning of the load application system. As described in the third section, about the experimental program, the LVDT 1 in the first wall has registered the vertical displacement of the steel distribution beam during the test. It shows that this displacement has a maximum absolute value of approximately 6 mm, in the downward direction. This curve is shown Figure 4.2) a, as well as the one showing the displacements versus load applied at the highest point of wall W2, in Figure 4.2) b.

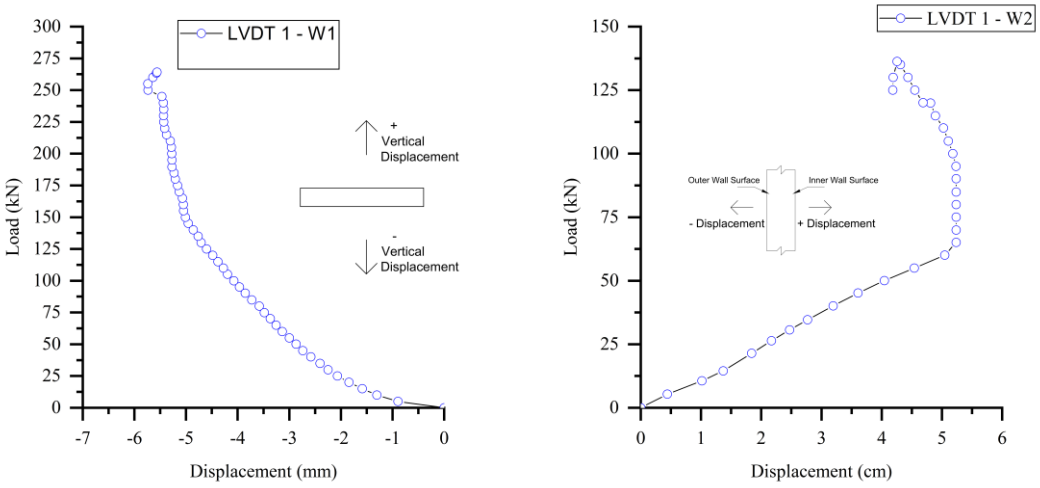

(a) **(b)**

Figure 4. 2 - Load-deflection response for LVDT 1 in: (a) W1; (b) W2.

For the LVDT 1 in the W3, it shows (Figure 4.3) a) that the steel distribution beam has not significantly displaced in its right extremity. Even though it is not a sufficient observation to assure that the beam has not rotated (as it is possible for it to rotate through the point where the LVDT 1 was positioned, or a near one), it gives indication that this hasn't rotated, because the movement described above is extremely unlikely to happen.

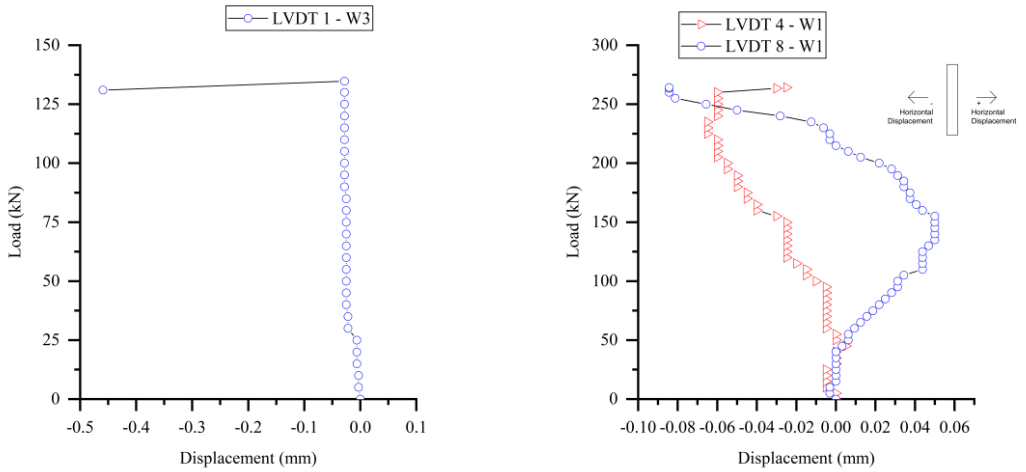

(a) **(b)**

Figure 4. 3 - Load-deflection response for: (a) LVDT 1 in W3; (b) LVDTs 4 and 8 in W1.

The displacements registered for LVDT 4 and 8 of W1 are shown in Figure 4.3) b. The ones for W2 and W3 are displayed in Figure 4.4) a and 4.4) b. One can notice that they are insignificant, not even reaching an absolute value close to 1 mm.

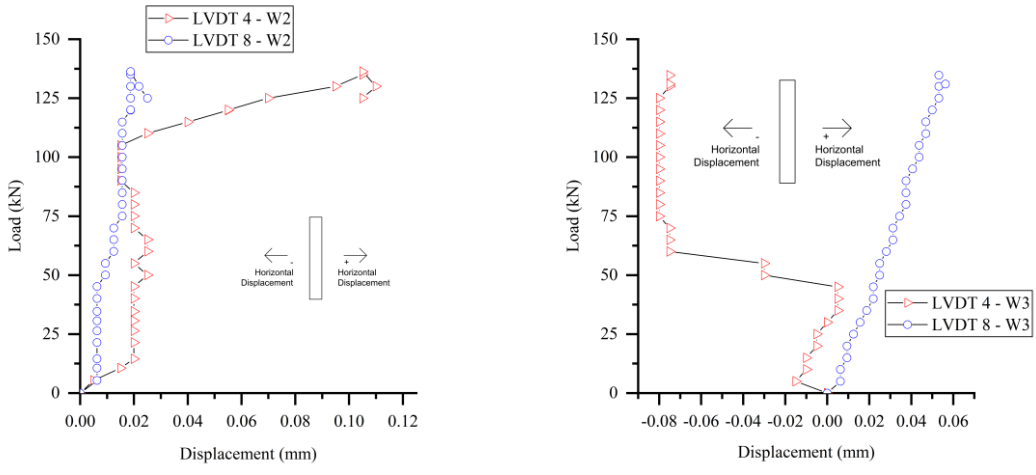

(a) **(b)**

Figure 4. 4 - Load-deflection response for LVDTs 4 and 8 in: (a) W2; (b) W3.

Now the load displacement curves for the LVDT 9 for walls W1 and W2 are presented in Figure 4.5. They indicate the overall shortening of those walls. The sign convention adopted in this figure is the same as in figure 4.2) a. For the wall W3, it has registered zero for all loads, therefore is not shown.

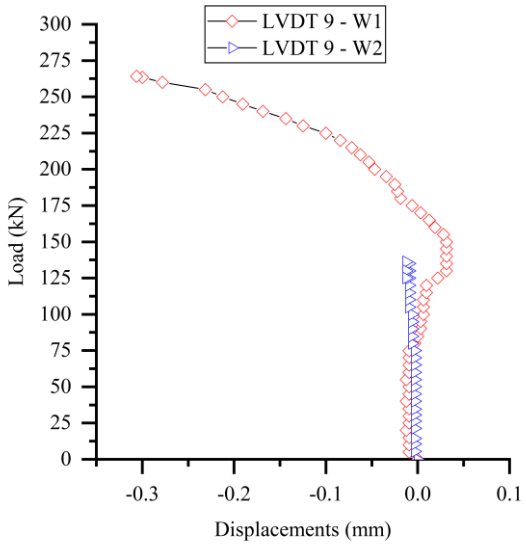

Figure 4. 5 - Load-deflection response for LVDT 9 in W1 and W2.

4.1.2 Failure mode and cracking pattern

The cracks developed in the masonry walls followed a common pattern with regards to the formation of vertical cracks on at least one side of the wall, along the row of blocks in contact with the neoprene layer below the steel distribution beam. Those cracks were all formed at a load of 12 tf. For masonry wall W1, additional horizontal, and inclined cracks were observed on the inner surface of the wall. They appeared, respectively, at loads 24 for the horizontal one and at 22 and 17 tf for the inclined ones. In this wall, one could also notice the relative detachment of the concrete block on the right side, leaving a gap between it and the block at its left. The cracks were registered and are depicted in Figures 4.6 and 4.7. All failures were abrupt and happened with concrete block crushing. In the following, Table 4.1, with the first crack loads, as well as the failure loads, failure loads per unit width and stress in failure (considering the gross area of the section) is presented.

Figure 4. 6 - Crack pattern of wall W1.

(a) **(b)**

Figure 4. 7 - Crack pattern of walls: a) W2; b) W3.

Table 4.1 - First crack and failure loads, as stress in failure for all walls.

Wall designation	Slenderness ratio *(H/t)*	First crack load (tf)	Failure Load (kN)[a]	Failure Load (kN/m)[b]	Stress in Failure (MPa)
W1	28.89	12	264.21	220.17	2.45
W2	28.89	12	136.26	113.55	1.26
W3	28.89	12	134.73	112.27	1.25

[a]Failure Load for whole width (1.2m); [b] Failure Load per 1m width.

4.2 Results on PCSPs

4.2.1 Load-deflection response

This section presents the load deflection curves for the specimens PA1 through PA3 for data acquired by the LVDTs at the positions shown in Figure 3.11. The nomenclature in the legend of the figures was created to designate the position of the displacement measured, the panel tested, and the given wythe for which the displacement was registered. These are represented respectively by the number from 1 to 5, the letter O (for outer wythe) or I (for inner wythe), and panel PA plus the number of the specimen tested. The largest displacements observed for the LVDTs at 1/3 of panel 2 height differ in the order of 4 mm, as the displacements registered in the inner wythe extend to 10 mm, while only reaching 6 mm at the outer wythes. The load response for panel 2 is noticeably linear to approximately 300 kN, which represents about 50% of the panel strength. Then one notices the presence of a nonlinear response until failure loads. For the outer wythes of panel 2, it is observed that LVDT 3 continues to displace in the negative direction. However, for the same LVDT at the inner wythe, Figure 4.8 shows that the displacement was kept constant while the load increased in the final part of the response curve until the ultimate load was reached. Comparing the largest values of displacements in both wythes for panel 2, one notices that the difference between them is not negligible and approaches 4 mm. This tendency has not been seen in the articles in literature who have made measurements of load-displacement profile. For example, BENAYOUNE *et al.* (2007) presents in figure 7 of that work a compilation of lateral deflection for several loads. In this figure, the largest displacements (compiled for panel PA5 of this work) reaches approximately 10 mm for both wythes, yet the displacements profile is kept symmetrical. One reason for this may

be the fact that, as the wythes were cast one after the other, it was necessary to wait for one wythe to harden, before turning the panel and casting the other wythe. This slight difference of age in wythes may be responsible to generate mortar layers with different resistances, which may cause the panels to laterally displace in an uneven way. The uneven propagation of cracks in the wythes may also have played a role in this fact. Other possible cause of this might be the presence of eccentricities in load applications, even though BENAYOUNE *et al.* (2006, 2007) tested same experimental program under axial and eccentric load and has not observed differences in displacement from one wythe to the other, just an increase in panel displacement, when loaded eccentrically. GARA *et al.* (2012) also tested the same specimens in both loading cases, yet the authors have only recorded the displacements in one wythe. The results for mid-height displacement show little difference in total displacements for the panels with 8 mm thickness, but the panels with 12 and 16 mm thickness EPS core have recorded about 10 mm more displacements for the panels eccentrically loaded, at mid-height. Interestingly, the panels with non-undulated EPS core and the one with half the number of shear connectors also did not observe significant differences in displacement for the two cases of load application.

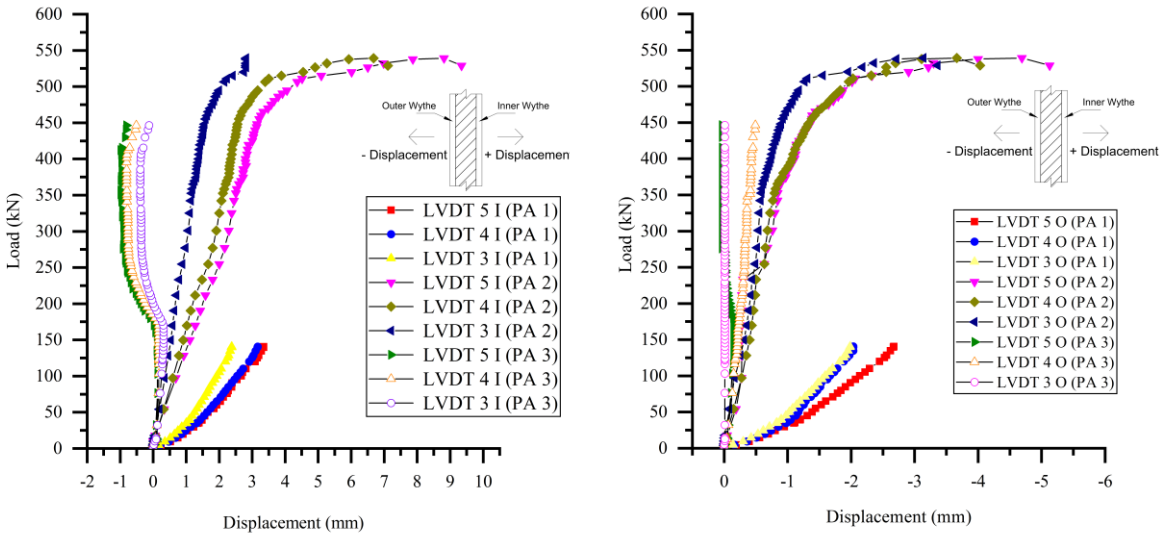

(a) **(b)**

Figure 4. 8 - Load-deflection response of LVDTs at 1/3 of height (LVDTs 3, 4 and 5): a) Response at inner wythe LVDTs; b) Response at outer wythe LVDTs.

For the first panel, the displacements measured have notably increased faster than in the cases of the other two specimens tested. The load-displacement curves for

1/3 of the panel height are observed to be linear and resemble a bilinear curve response, whose second linear part starts at around 25 kN.

At last, the behavior at 2/3 of panel height is observed to be linear in the outer wythe for the third panel tested, but some nonlinearity is noticed for the displacement curves at this height for the inner wythe. In Figure 4.9, the inner and outer behavior of all panels show a high degree of composite action at those sections, as the displacements observed are clearly symmetric. As already commented, this conforms to the literature results.

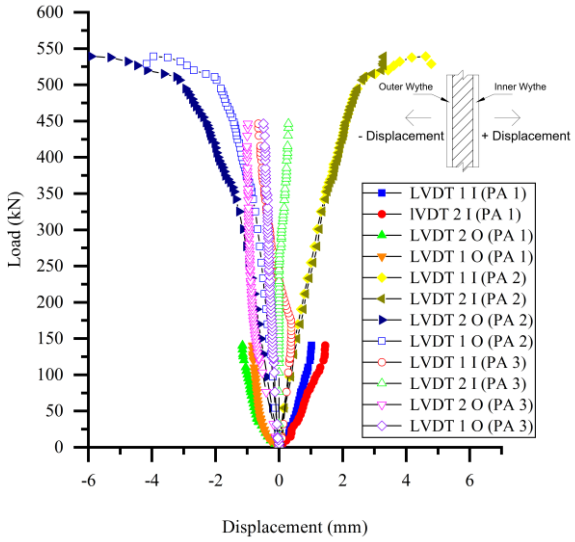

Figure 4. 9 - Load-displacement response for LVDTs at 2/3 of panel height.

4.2.2 Load-deflection response at cross-section level

The results from Figures 4.10 to 4.12 were assembled in a more appropriate manner to illustrate displacements at the cross-sectional level. The positive displacements indicate displacements in the outward direction of the external face of the inner wythe, while negative displacements indicate displacements in the outward direction of the external face of the outer wythe. This convention sign is the same as the ones in Figure 4.8 and 4.9, and distinction between inner and outer wythe can be seen in the details of Figure 4.9, for example. The figures are presented here as a way to determine the level of displacement and rotation of the cross-sections of the panels tested at different loads. One can observe the difference in the shape of deformation, in general, at 2/3 and 1/3 of height cross-sections. For the first panel, increasing load

led to displacements directed outward from the wythes. It can be seen that the displacements in Figure 4.10) a for the right LVDT (at 800 mm) are slightly bigger than those at the left, but for Figure 4.10) b this behavior shifts, and the biggest displacements are measured at the left part of the section (at 300 mm), for the positive displacements, but remained bigger at the right side of the section (at 900 mm) for negative displacements. This may be related to a rotation of the panel through its longitudinal axis. It's also noticed that the displacements in Figure 4.10) b approximately doubles compared to Figure 4.10) a. As the LVDTs were removed just after the first crack for the caution with the experimental material, as it was not known whether the rupture would damage the equipment, the displacements for the first panel were limited to a load far from its ultimate load. However, it is noticed that displacements at the first third of height is larger than the ones at the top third of height. AMRAN *et al.* (2016, 2017, 2019) also recorded the load-displacement profile along all the height of the panels tested. For this profile for the panel GA1, in AMRAN *et al.* (2016), which had slenderness ratio equal to 14, the displacement observed in the bottom third of height displaced more than the rest of the panel for the initial loads, but this behavior changes for higher loads, that is, the greatest displacements were closer to the top of the panel. This was also the case for the panel PA5 (slenderness ratio of 18.46), in BENAYOUNE *et al.* (2007). However, for all other panels in AMRAN *et al.* (2016, 2017, 2019), the load-displacements profile shows that the largest displacements are closer to the top of panels since the beginning of loading. For the panel PA1, tested in this dissertation, the tendency observed could not be compared to the ones described above. This panel showed that for the initial loads the largest displacements were found in the third of height closer to the bottom of it. However, as the LVDTs were removed at the first crack appeared, it was not possible to conclude whether the largest displacements continue at the first third of panel height or they turn to the third of height closer to the top of the panel.

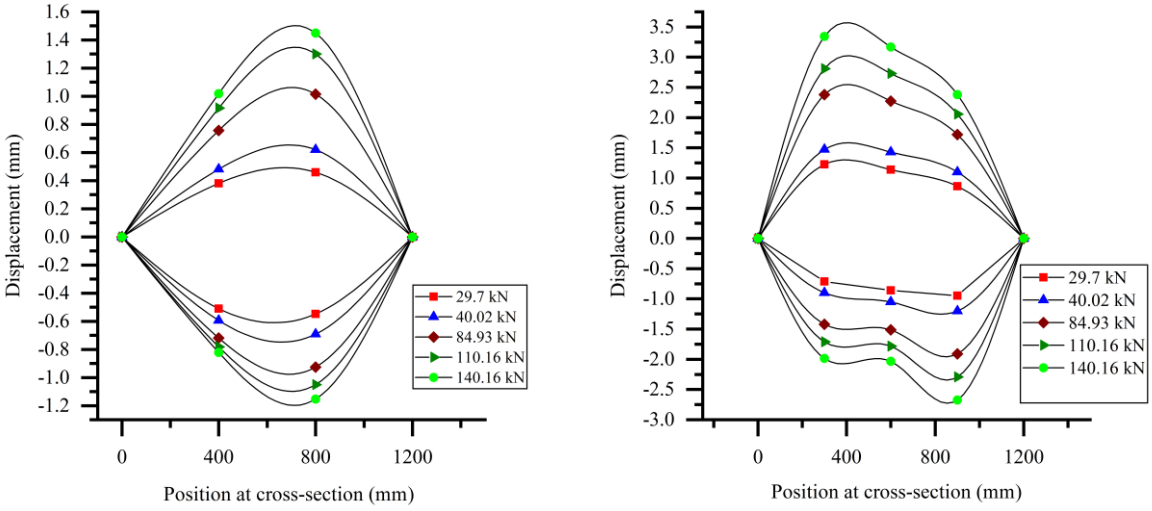

Figure 4. 10 - Cross-section displacements for panel PA2. (a) At the cross-section of 2/3 of panel height (LVDTs 1, 2); (b) At the cross-section of 1/3 of panel height (LVDTs 3, 4 and 5).

In Figure 4.11, it can be seen that for the load close to failure, as the curves for 510.09 kN and for 539.16 kN display, the positive displacements decrease while the magnitude of the negative displacements keeps increasing. This may be due to the accommodation of the specimen after or close to failure. For the cross-section at 1/3 of panel height, the positive displacements are larger. However, the negative displacements decrease, compared to the other section in Figure 4.11) a). The second panel tested, PA2, contradicts the general tendency mentioned above that the largest displacements are observed closer to the top of the panel (even when they are larger for the bottom third for initial load, it noticed that they become large at the top for higher loads). For panel PA2, except for the accommodation described above after rupture, the largest displacements are found in the bottom third of the panel. As observed in those articles, the hinged support is placed at the top of the panels. In this dissertation, the hinged support at the top was placed at a height corresponding to the base of the top concrete beam used to distribute the load. As the concrete beam is stiffer than the panel, the presence of such concrete beams at top should make the panel displace less close to the top of panel. This explanation seems to correspond to reality, as the panels of BENAYOUNE *et al.* (2007) did not have concrete beams at the top, therefore followed this tendency (higher displacements close to top of panel) the same way as the panels of AMRAN *et al.* (2016, 2017, 2019), which also hadn't concrete beams at top, but the lateral deflection profile presented by GARA *et al.* (2012) shows larger

displacements close to the mid-height of the panel, as they were cast with concrete beams at top and bottom of the panel. Therefore, it is reasonable that the largest displacements be found in this dissertation close to the third of height close to the bottom of the panels. This is also corroborated by the fact that the tests carried out in the present work have not used steel sections attached to the bottom of panels to create the support below, yet there was a layer of plaster with 2 cm thick, between the bottom of panels and strong floor of the laboratory. This layer of plaster may be less stiff than the other supports used in the other experimental tests in literature, therefore allowing the sandwich panel to displace more freely close to it.

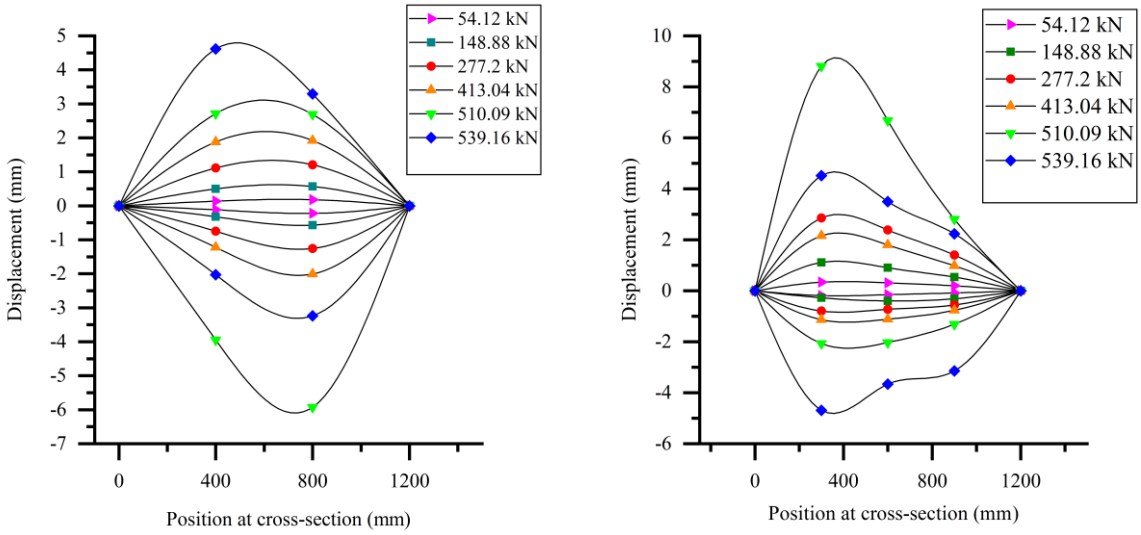

Figure 4. 11 - Cross-section displacements for panel PA2. (a) At the cross-section of 2/3 of panel height (LVDTs 1, 2); (b) At the cross-section of 1/3 of panel height (LVDTs 3, 4 and 5).

For the third specimen tested, it is possible to observe a rotation at both cross-sections analyzed in Figure 4.12. Even though this rotation increases with a positive increment of load, the magnitude of the displacements measured is negligible. It has to do with the fact that the LVDTs were removed far from the failure load for the sake of preservation of the equipment. This rotation had little or no influence on the ultimate load carried by panel PA3, as the panel reached higher resistance than the other two, which was expected given its higher age.

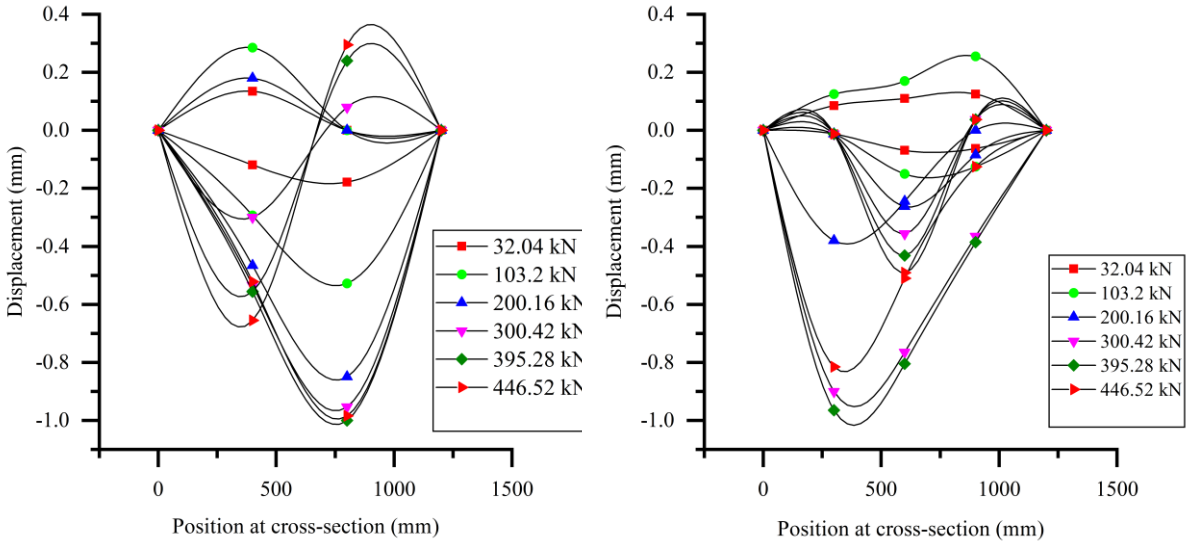

Figure 4. 12 - Cross-section displacements for panel PA3. (a) At the cross-section of 2/3 of panel height (LVDTs 1, 2); (b) At the cross-section of 1/3 of panel height (LVDTs 3, 4 and 5).

4.2.3 Crack pattern and failure modes

For panel PA1, the first cracks shown were two vertical cracks located close to the mid-height in the outer wythe and positioned at approximately 30 and 40 cm of the panel sides. This crack started as a minor one, and along with the increase in load has extended itself through the panel height, yet it has not developed across the whole height and stayed restricted about 60 cm up the mid-height and about 20 cm down this same reference. It is interesting to report that before panel transportation to the load application setup, a small width crack was observed close to the mid-height. This crack has been attributed to the shrinkage in the mortar layer after casting. Shrinkage or careless handling cracks have also been reported in BENAYOUNE *et al.* (2006). However, those authors state that this crack has closed during load and did not influence other existing cracks. That seems to be the case for the test in panel PA1, as was observed throughout the experiment.

Closer to the ultimate load, a horizontal crack started to form, extending itself across the whole panel width after failure. During the extension of those mentioned cracks, no visible one was detected in the inner wythe prior to failure. This behavior has a somewhat irregular manifestation in the literature. For example, in the articles of AMRAN *et al.* (2016, 2019), the authors write that the cracks formed in both wythes were symmetric. Even though this is the case in that experimental program, other works

have observed and described different patterns of cracking regarding the inner and outer wythes. For example, BENAYOUNE *et al.* (2007) states that cracks have formed in either or both concrete wythes. GARA *et al.* (2012) describes a completely different aspect of failure, as for their experimental tests the panels showed failure in the mesh in a tensioned wythe and due to crushing in the compressed one. Figure 4.13 shows the fully developed vertical cracks at the outer wythe. The load in which they first appeared was around 158 kN.

Figure 4. 13 - First cracks visible in panel PA1 test.

After the failure, two horizontal cracks were formed along all panel width at two different positions. One, already mentioned, was the extension of the horizontal crack which arises quite after the first vertical ones in the figure above. The other one was located between mid-height and bottom. This is attributed to the lateral instability and noticeable buckling of the load close to failure. Horizontal cracks were observed in the work of AMRAN *et al.* (2019), GARA *et al*. (2012), BENAYOUNE *et al.* (2007). Those authors have all explained this formation of horizontal cracks due to instability effects and/or buckling.

Figure 4.14 is presented following this paragraph, where Figure 4.14) a show the aspect of the panel after failure and Figure 4.14) b show the presence of minor inclined crack at the left-hand side of the top outer wythe. This inclined crack at the top or bottom of panel is also common in literature, not only for works which have not used capping beams, but also for ones which have used them. The first case is seen in: BENAYOUNE *et al.* (2007), where those cracks were also only present in the

slenderest panel tested, PA6; AHMAD & SINGH (2021), where a small-scale panel with capping beam was tested. Therefore, it seems unlikely that these inclined cracks formed due to the presence of the capping beam, since the first work cited above had not used capping beams, while the second work did. All the other cracks marked as blue were only developed after mortar crushing in the mid-height, not during loading.

a) **b)**

Figure 4. 14 - Panel PA1 after failure: a) front view; b) minor inclined crack at the top of panel

The lateral aspect of the panel PA1 is also presented, in Figure 4.15, as important information can be inferred from it. First, the surface of the EPS core at both sides was not crushed, as well as the welded wire mesh and shear connectors visible at both sides have not failed. Yet, in the figure only one is shown, but the visual inspection of the other side verified what is reported above. The intact aspect of the EPS suggests that the shear flow was kept during the whole test.

Figure 4. 15 - Side view of Panel PA1 after failure.

For the crack pattern in the test of panel PA2 and PA3, the first crack loads are registered in Table 4.2, however they were not marked, as a safety measure to avoid accidents for stepping close to the panel during load. They have been developed with a rather small width, which did not allow the perception of it through photos. The abrupt failure may also have been a consequence of wire or shear connector failure inside the panel. This could not be confirmed, as the visualization of the internal reinforcement has not been done.

The panel PA2 has crushed at bottom, in both sides of it. Differently from panel PA1, panel PA2 only presented one horizontal crack, which extended across the whole width. This was close to the bottom. It is possible to see in Figure 4.16 that the concrete beam at bottom has also crushed, not only the panel per say. Also, a detachment of a piece of concrete in the concrete beam at bottom was observed. Figure 4.16 shows the crushed surfaces as well as the detachment of concrete in panel PA2. Visual inspection of the sides of panel PA2 have found neither failure in the shear connectors nor the wire mesh. The failure was sudden and violent.

a) **b)** **c)**

Figure 4. 16 - Failure mode of panel PA2: a) and b) crushed concrete beam at bottom; c) horizontal crack formed after failure.

After failure the cracks formed were marked blue. The panel PA2 failed in the inner wythe, differently than panel PA1. The cracks developed after failure were mainly horizontal and vertical, however the presence of inclined cracks was also observed. Figure 4.17 shows the marked cracks.

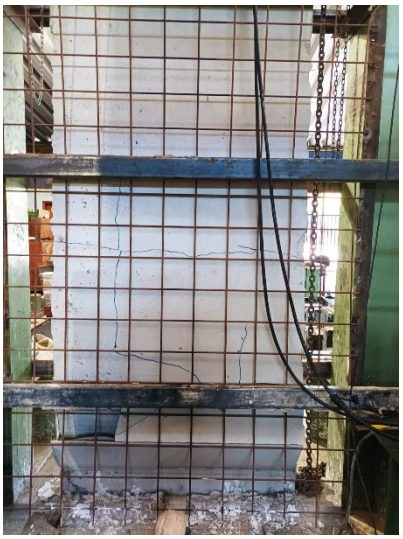

Figure 4. 17 - Cracks in panel PA2 after failure.

Panel PA3 has failed in a very similar way to panel PA2. The failure was sudden and violent. The pattern of cracks formed was also mainly horizontal and vertical, even though inclined cracks were seen. Regarding the presence of crushing of mortar in wythes or in the concrete beams, none was observed. Figure 4.18 shows the aspect of the panel sides after failure for the bottom of it.

a) **b)**

Figure 4. 18 - Panel PA3 bottom sides after failure: a) left side; b) right side.

The panel sides at the top are presented in Figure 4.19. One can observe that neither cracks nor crushing were developed. A main horizontal crack was created after failure, extended across whole panel width. This suggests that this panel has also failed due to instability and buckling, as observed in panel PA1 and PA2, however without crushing. Concrete or mortar crushing in wythe, or concrete distribution beam has been a constant aspect of failure in literature. For example, AMRAN *et al.* (2016, 2017, 2019) observed horizontal cracks and failure due to crushing; BENAYOUNE *et al.* (2007) and GARA *et al.* (2012) also did notice crushing for their panels tested under axial load, in either one or both extremities of panels. The explanation for the absence of crushing in PA3 may be better explained by the previous subsection, as the displacement profile along panel cross-sections is shown. There, it will be seen that those displacement profiles suggest the panel has suffered a rotation along it's longitudinal axis. This may have influenced the failure mode, or it may have been caused by a non-axial load application, which would change the failure mode. Figure 4.19 shows the aspect of the panel sides at the top after failure.

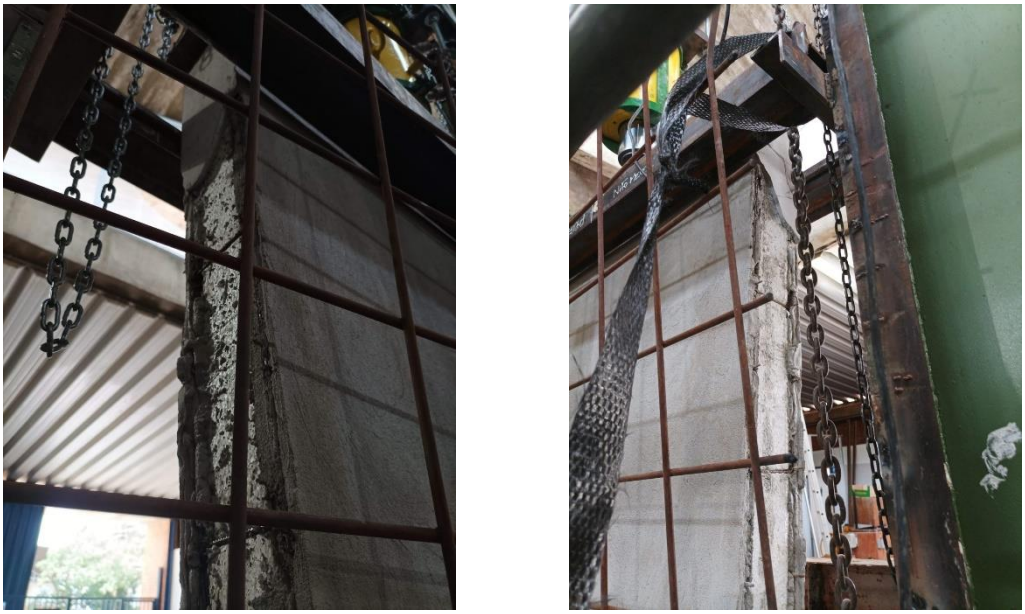

a) **b)**

Figure 4. 19 - Panel PA3 top sides after failure: a) left side; b) right side.

Figures 4.20) a and 4.20) b show the marked cracks in the inner wythe after failure as well as the horizontal crack crossing the cross-section, also formed after failure.

a) **b)**

Figure 4. 20 - Panel PA3 crack pattern after failure: a) marked in inner wythe; b) horizontal one in outer wythe.

Table 4.2, with first crack load, failure load and failure load per unit width of panel is presented. The stress in failure is calculated considering only the wythes

thickness, as the EPS core does not play an important role in the compression of the panels.

Table 4.2 - First crack and failure loads, as stress in failure for all panels.

Panel designation	Slenderness ratio *(H/t)*	First crack load (kN)	Failure Load (kN)[a]	Failure Load (kN/m)[b]	Stress in Failure (MPa)
PA1	18.57	≈158	490.32	408.6	8.17
PA2	18.57	≈221	538.98	449.15	8.98
PA3	18.57	≈274	709.02	590.85	11.82

[a]Failure Load for whole width (1.2m); [b] Failure Load per 1m width.

4.2.4 Displacement profile along panel height

As described in section 3(experimental program), the LVDTs have been positioned in the sandwich panels such that three were attached at each panel wythe in the first third of height (approximately 83.33 cm from the bottom) and two were attached at each panel wythe in the second third of height (approximately 173.33 cm from bottom). The LVDTs at the second third and the ones below did not match their positions regarding their distances to the sides of the panels. Therefore, to produce a series of figures displaying the displacement profile for a given load along the panel height at a same given distance from its sides, it was necessary that the displacement at the cross-section level for a chosen load (for the top LVDTs) was interpolated, such that with this interpolation equations, an estimate of the displacement at the second third of wall height could be calculated for distances at 300, 600 and 900 mm of panel side (which are the distances from panel side of the LVDTs close to the bottom third of panels), allowing a plot of the displacement profiles along the height of the panel for different positions at the cross-sections. The method used to interpolate the displacements points at top LVDTs was the Lagrange method. It was assumed that at the panel sides, the displacement was null, just as was done for the plotting of displacement profile at cross-section level.

For panel PA1, the chosen values of displacement for making the profiles were 29.7 kN, 40.02 kN, 84.92 kN, 110.16 kN, 140.16 kN. For the first load level, in Figure

4.21) a, it is observed that the most symmetrical displacement profile is the one for 900 mm distance of the left-hand side of cross-section, which corresponds to the position relative to panel side of LVDTs 5I or 5O; while 600 mm curves correspond same wise to LVDTs 4I or 4O distance to panel side and 300 mm curves correspond to LVDTs 3I or 3O distance to panel side. Even though differences in profiles for this load are visible along different vertical cuts of panel, they do not represent any significant behavior or discrepancies at this level, as the range of displacements is extremely low, reaching maximum values close to 1.5 mm. It has to do with the fact that the LVDTs for panel PA1 test were removed right after first crack, not registering displacements until failure. For the load level 40.02 kN, in Figure 4.21) b, the panel has also presented small displacements. It is interesting though that at the inner wythe the profile for 900 mm displaces more than the one at the center of the panel width (600 mm), while for curves of 300 mm and 600 mm they are only slightly different. Figure 4.21 shows those profiles for the load levels 29.7 kN and 40.02 kN.

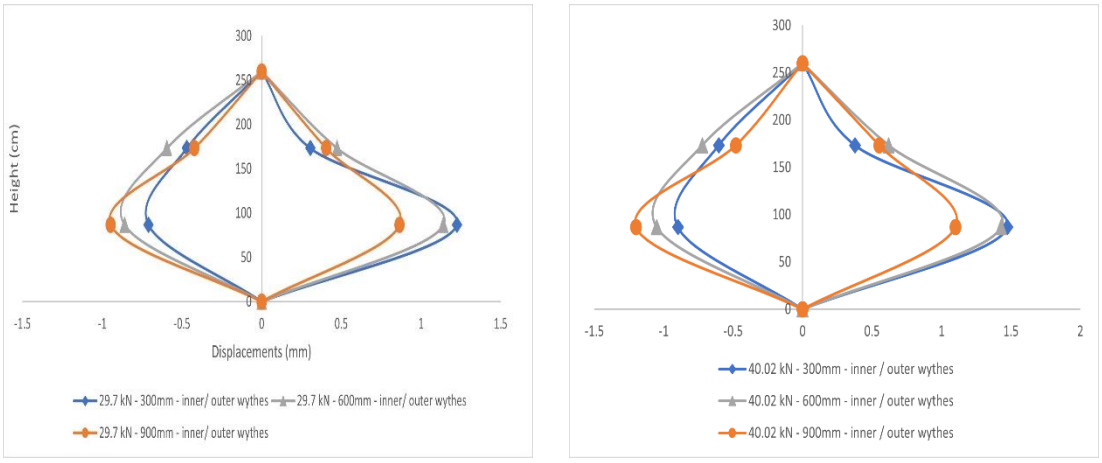

a) **b)**

Figure 4. 21 - Panel PA1 load-displacement profile for loads: a) 29.7 kN; b) 40.02 kN.

When the profiles for 84.93 kN (Figure 4.22) a) and 110.16 kN (Figure 4.22) b) are analyzed, it is possible to notice that as the previous profiles (in Figure 4.21), the displacements at the first and second third of height keep increasing in absolute value as the load increases. As the profile for 900 mm curve seems to remain symmetrical, this is not the case for the curve of 300 and 600 mm given the apparent increase in the difference of absolute displacements value for the inner and outer wythes. Those changes commented on are of a small scale, as the panels have not displaced so far more than 3 mm. Therefore, even though this difference appears to be significant

visually, it's rather not as much representative from the point of view of the mechanical behavior of the panel, but they can show interesting tendencies. For example, displacements at 900 mm curves have remained symmetrical (in Figures 4.21 through 4.23), while curves for 300 and 600 mm tend to displace more in the right hand side (or outer wythe) than left hand side (inner wythe) for each load observed and the second third displacement at 600 mm is larger than the one at 300 mm, while the displacement at 300 mm and 600 mm is practically the same for first third of height. For the profile for the load 140.16 kN (Figure 4.23), the maximum displacement reached about 3.5 mm.

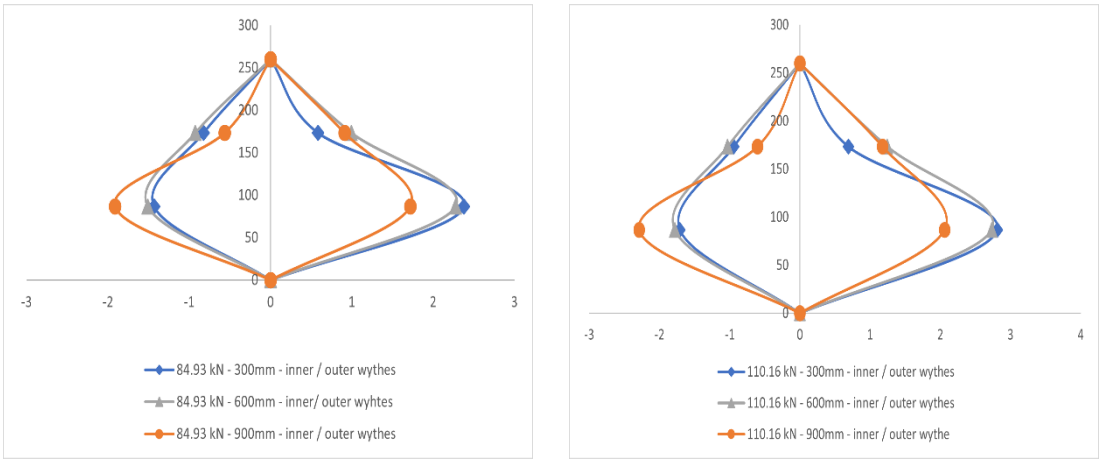

a) **b)**

Figure 4. 22 - Panel PA1 load-displacement profile for loads: a) 84.93 kN; b) 110.16 kN.

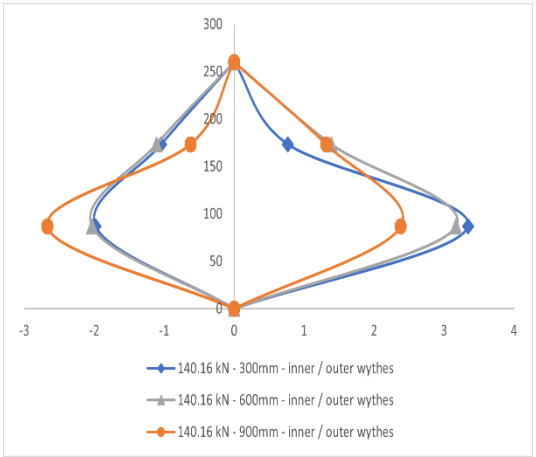

Figure 4. 23 - Panel PA1 load-displacement profile for loads 140.16 kN.

For the behavior of the load-displacements profile along panel PA2 height more information can be seen, as for this panel the LVDTs have registered displacement until panel failure. Again, the most symmetrical curves for initial loads of inner and outer wythes response have been the one for 900 mm (Figure 4.24, 4.25 and 4.26) a). The

only exception would be the profile for 900 mm at 539.16 kN (Figure 4.26) b), but this load represents failure and as already commented when the cross-section displacements were discussed, this panel suffered an accommodation subsequent to failure.

From the beginning, at load 54.12 kN (Figure 4.24) a), an initial displacement towards a buckling deformed profile is observable for the curves for 600 mm and 300 mm. However, until load 148.88 kN (Figure 4.4.24) b) this is not yet significant, and the displacements limit themselves to be as large as approximately 1 mm. For the profiles at load 277.2 kN (Figure 4.25) a), the inner wythes tend to concentrate displacement at the second third of height, while at outer wythe they start to increase displacement at first third of height. The curves for 900 mm remain somewhat symmetrical. Interestingly, at load 413.04 kN (Figure 4.25) b) the curves for the outer wythe at 600 and 300 mm retract, while those same curves for inner wythe displace slightly more.

For load 510.09 kN (Figure 4.26) a), maximum displacement at outer and inner wythe have reached, respectively, approximately 6 and 9 mm. They are found in the first third of height for outer wythe and in the second third of height for the inner wythe. After failure, the profiles change significantly. The one at 900 mm now appears as it has buckled and the other ones, at 600 mm and 300 mm turn into symmetrical curves for inner and outer wythes.

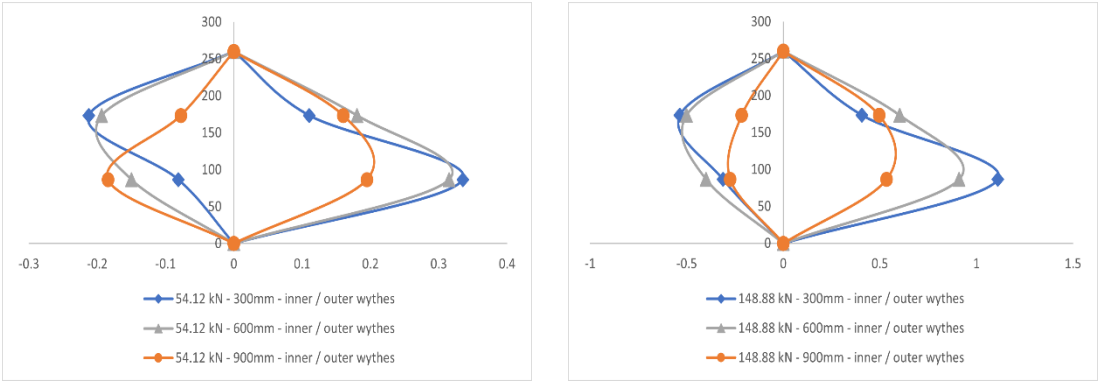

a) **b)**

Figure 4. 24 - Panel PA2 load-displacement profile for loads: a) 54.12 kN; b) 148.88 kN.

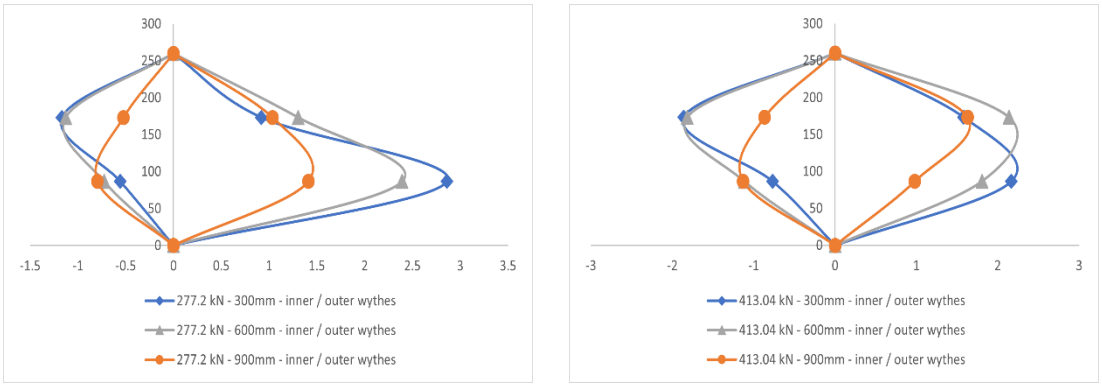

a) **b)**

Figure 4. 25 - Panel PA2 load-displacement profile for loads: a) 277.2 kN; b) 413.04 kN.

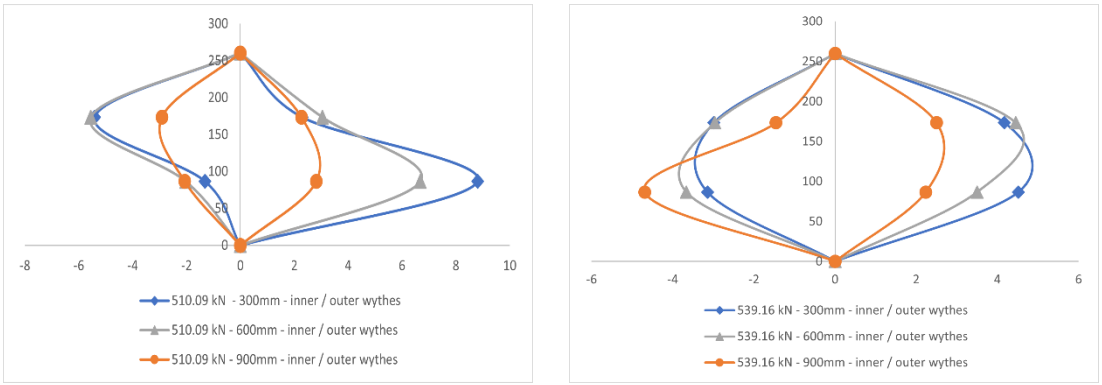

a) **b)**

Figure 4. 26 - Panel PA2 load-displacement profile for loads: a) 510.09 kN; b) 539.16 kN.

The behavior of panel PA3 is discussed. Even for low loads, such as 32.04 kN (Figure 4.27) a), the load-displacement profile for 900 mm already resembles the beginning of a buckling response in the wythes. As the load increases, the profiles for both 300, 600 and 900 mm show significant signs of instability, especially after 200.16 kN (Figure 4.28) a), where the displacement curves for the inner and outer wythes even start to cross each other, for 300 and 600 mm. The largest displacements registered in both inner and outer wythe are small, reaching in absolute value 1 mm. This is due to the fact that the panel has failed under a considerable higher load than the one at which the LVDTs were removed. Figure 4.29 shows the profiles for the loads 395.28 kN and 446.52 kN.

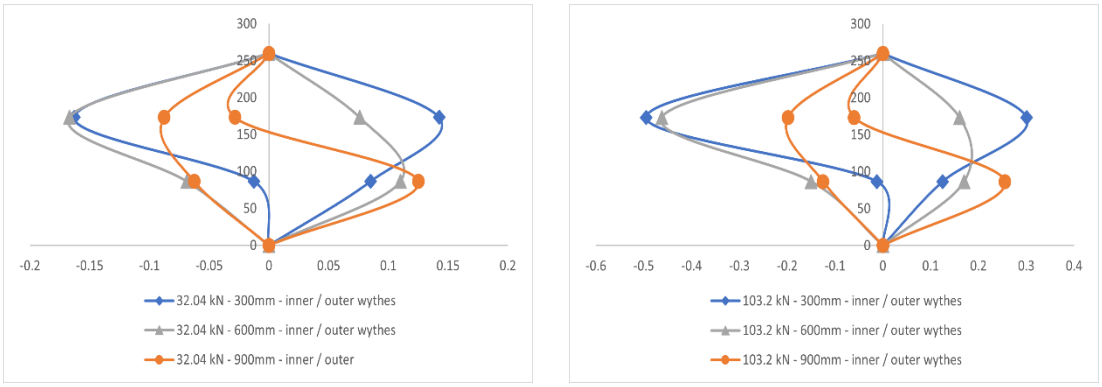

a) **b)**

Figure 4. 27 - Panel PA3 load-displacement profile for loads: a) 32.04 kN; b) 103.2 kN.

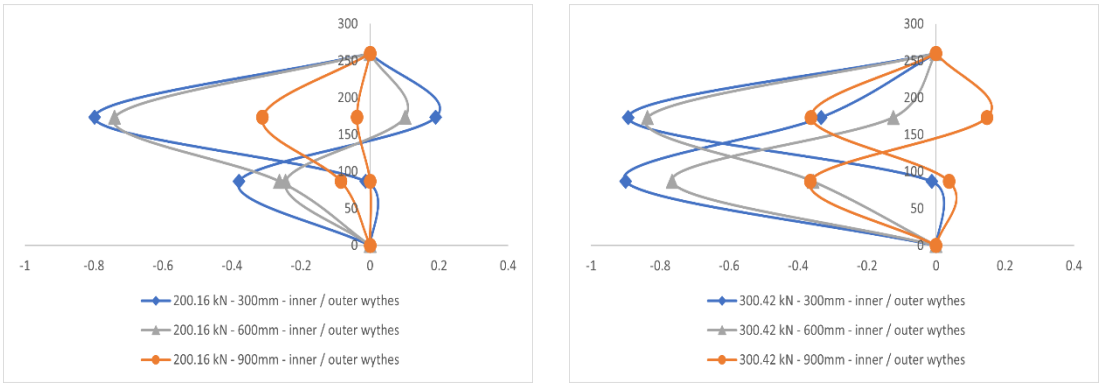

a) **b)**

Figure 4. 28 - Panel PA3 load-displacement profile for loads: a) 200.16 kN; b) 300.42 kN.

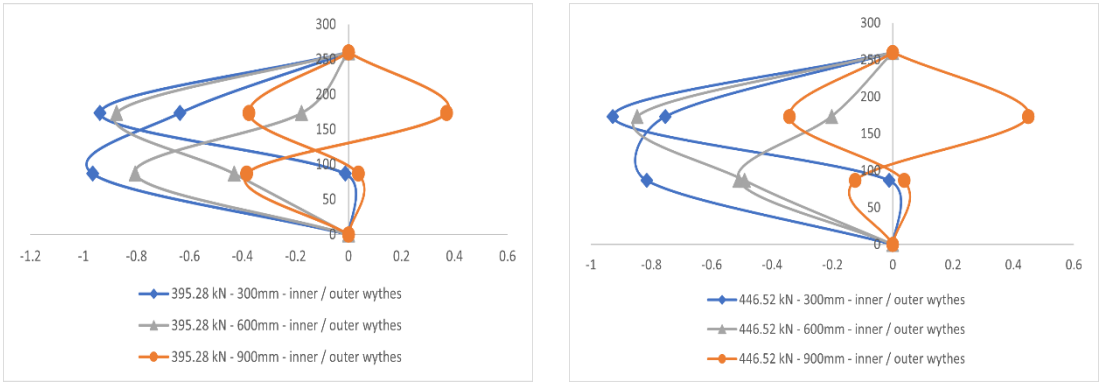

a) **b)**

Figure 4. 29 - Panel PA3 load-displacement profile for loads: a) 395.28 kN; b) 446.52 kN.

4.2.5 Comparison of empirical formulation and experimental results

A series of empirical formulations for both concrete-walls and PCSPs were detailed and presented in the literature review. As a way to evaluate the correspondence and validity of those equations to the experimentally obtained results of this dissertation, they were applied to the geometrical and mechanical characteristics of the panels tested here.

When the cross-section of the panels is considered, as shown in figure 3.11, a total amount of 18 vertical welded wires can be observed. They are the reinforcement which contributes to the formulations presented that incorporate it. The values calculated for the exact condition in which the panels were tested have resulted in 1) a conservative 384.52 kN for the ACI equation, numbered 11 in the text. This represents approximately 33.6 percent less than the mean experimental results and agrees with the same conservative behavior obtained in BENAYOUNE *et al.* (2007); 2) for equation 12 the theoretical result was approximately 271.05 kN, which is rather more conservative than the former equation result. This represents 47.7 percent of experimental mean strength; 3) 557.32 kN was the value for equation 13, representing about 96 percent of actual strength; 4) equation 14 reached 517.99 kN (about 89 percent of experimental results); 5) Equation 16 (used for this case, given that the aspect ratio of the panels tested is larger than 2) gives 406.36 kN (70 percent of experimental data); 6) 532.94 kN was obtained by the formulation in Eq. 19, proposed by BENAYOUNE *et al.* (2007), which differs about 8 percent of results; 7) finally, the equation 20, proposed by MOHAMMAD *et al.* (2012) supply an estimate value of 518.91 kN, less about 10.5 percent of mean panel test results. Therefore, among the formulations for PCSPs the closest one to the results was equation 19. Among the ones designed for concrete walls, the closest one was equation 13. For the ease in visualization of results of the equations just mentioned, Table 4.3 is presented below.

Table 4.3 – Values for equations mentioned applied to the panels tested geometrical and mechanical characteristics, and respective percentage to the mean value of experimental resistances.

	Value (kN)	Percentage to mean experimental results (%)
Eq. 11	384.52	33.6
Eq. 12	271.05	47.7
Eq. 13	557.32	96
Eq. 14	517.99	89
Eq. 16	406.36	70
Eq. 19	532.94	92
Eq. 20	518.91	89.5

Figure 4.30 is represented, but the results compiled now incorporate the experimental results obtained in this dissertation.

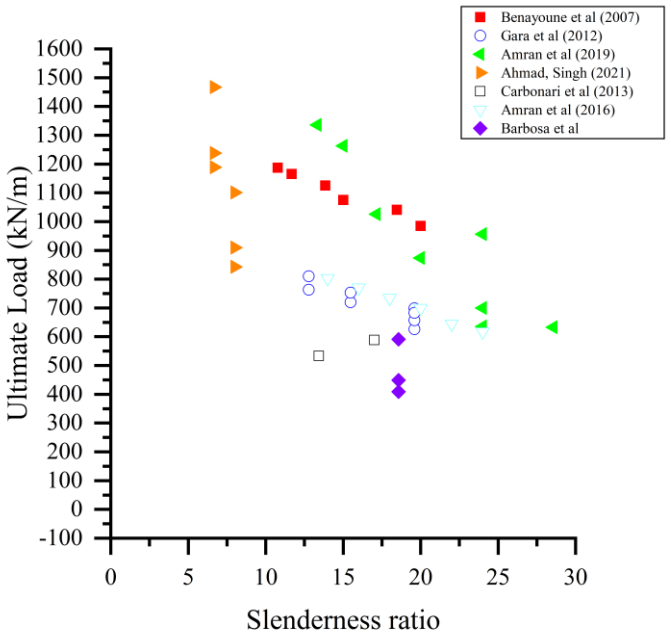

Figure 4. 30 - Ultimate load per unit width against slenderness ratio of data in literature and this dissertation.

CHAPTER 5

5 CONCLUSION, PERSPECTIVES AND RECOMMENDATIONS FOR FURTHER WORKS

Over the past two decades, increasing attention has been given to the compressive behavior of PCSPs. This dissertation described an evaluation of three axially loaded PCSPs with wythes slender by at least 15 mm, compared to the experimental programs found in the literature. The goal of this work was to analyze the compressive behavior of panels with reduced wythe thickness. In the experimental investigations done on PCSPs under compressive load, the displacements at the cross-section level were measured and reported. The main conclusions of the work are:

- The experimental program provided data showing that the panels have performed typically as a composite structure. The visual evaluation of the EPS at the sides of the panels has not shown signs of EPS failure. Therefore, shear connectors worked well until panel failure.
- The analysis of the displacements at the cross-sectional level has shown the rotation of the panels along its longitudinal axis (and throughout its height). This behavior has, however, not been associated with a decrease in the panel strength. Such rotations may be due to instabilities generated by small eccentricities in the application of the axial load as well as geometrical imperfections commonly observed in practice. Further investigations are recommended.
- Comparatively, in CARBONARI *et al.* (2013) a panel, named PMR-60 (with 2.55 m height and 150 mm thickness) showed an ultimate strength 8.53% smaller than the mean value strength of the panels tested in this research. Moreover, the slenderness of the PMR-60 panel is 8,45% smaller than the average slenderness of the three panels tested in this research. While panels are similar in slenderness, yet wythe thickness differs significantly between the two experimental programs. The panels in both studies had similar reinforcements, and mortar strength difference was less than 1%.
- Even though the wythe in CARBONARI *et al.* (2013) were thicker than the ones presented here by at least 15 mm, it is not possible to conclude that decreasing the wythe thickness while keeping the overall specimens thickness has any influence in

panel strength. Moreover, in the two studies, the inner and outer wythes have different values. The wythes of these two experimental programs are both 25 mm thick, which may have played an important role in the strength obtained by those authors.

- Finally, it is observed that the experimental results reported in the present research agree well with the other results shown in Figure 4.31, which is a compilation of experimental data on panels axially loaded available in the literature. Furthermore, it is suggested that more research be done on precast sandwich panels for the purpose of improving their use on such panels, which is so important in civil construction.

- Empirical equations specific for PCSPs, found in the literature, have reached less than 11 percent difference from experimental results. Therefore, reinforcing the validity of those equations for the design of PCSPs.

Regarding the challenges and outcomes presented at the moment for the design and analysis of PCSPs, the following suggestions are made for further academic works related to the topic:

- Investigation of the impact and influence on the choice of constitutive models of the insulation core material in the compression strength results and composite degree of the numerical finite element models for PCSPs under both axial and eccentric load applications.

- Empirical testing of the long-term shear transfer mechanism, evaluating the most common types of shear connectors present in literature, such as diagonal truss-shaped steel bars and steel bars placed perpendicular to the height of panels.

- Evaluation of the mechanism of absorption of water from the wythes material by the insulation core material and corresponding influence on the shear connectors deterioration process.

- Study on the optimization of design, with regard to the wire mesh and shear connectors spacing characteristics, diameter values, and shear connectors positioning across the insulation core (diagonal, horizontal, among others).

- Statistical analysis of the present literature data and proposition of an expression to fit those data and to establish one general design equation for PCSPs under axial load.

REFERENCES

Acharjee, D., Basu, D. J., & Bandyopadhyay, D. (2022). A numerical study on the through-thickness shear behavior of EPS sandwich panels. **Materials Today: Proceedings**.

Ahmad, A., & Singh, Y. (2021). In-plane behaviour of expanded polystyrene core reinforced concrete sandwich panels. **Construction and Building Materials,** 269, 121804.

Alchaar, A., & Abed, F. (2020). Finite element analysis of a thin-shell concrete sandwich panel under eccentric loading**. Journal of Building Engineering**, *32*, 101804.

Al-Rubaye, S., Sorensen, T. J., & Maguire, M. (2017). **Investigating composite action at ultimate for commercial sandwich panel composite connectors**.

Amran, Y. M., Ali, A. A., Rashid, R. S., Hejazi, F., & Safiee, N. A. (2016). Structural behavior of axially loaded precast foamed concrete sandwich panels. **Construction and Building Materials**, 107, 307-320.

Amran, M., Y. H., Rashid, R. S., Hejazi, F., Abang Ali, A. A., Safiee, N. A., & Bida, S. M. (2017). Structural performance of precast foamed concrete sandwich panel subjected to axial load. **KSCE Journal of Civil Engineering**, 22(4), 1179-1192.

Amran, M., Y.H. M., Alyousef, R., Alabduljabbar, H., Alrshoudi, F., Rashid, R. S. M. (2019). Influence of slenderness ratio on the structural performance of lightweight foam concrete composite panel. Case Studies in Const. Mater., Vol.10.

ASSOCIAÇÃO BRASILEIRA DE NORMAS TÉCNICAS**. NBR 5738: Concreto – Procedimento para moldagem e cura de corpos de prova**. Rio de Janeiro: ABNT, jun. 2016.

ASSOCIAÇÃO BRASILEIRA DE NORMAS TÉCNICAS**. NBR 5739: Concreto – Ensaio de compressão de corpos de prova cilíndricos**. Rio de Janeiro: ABNT, mai. 2018.

ASSOCIAÇÃO BRASILEIRA DE NORMAS TÉCNICAS. **NBR 7222: Concreto e argamassa – Determinação da resistência à tração por compressão diametral de corpos de prova cilíndricos**. Rio de Janeiro: ABNT, jun. 2011.

ASSOCIAÇÃO BRASILEIRA DE NORMAS TÉCNICAS. **NBR 12118: Blocos vazados de concreto simples para alvenaria – Métodos de ensaio**. Rio de Janeiro: ABNT, abr. 2013.

ASSOCIAÇÃO BRASILEIRA DE NORMAS TÉCNICAS. **NBR 6136: Blocos vazados de concreto simples para alvenaria – Requisitos**. Rio de Janeiro: ABNT, mai. 2016.

ASSOCIAÇÃO BRASILEIRA DE NORMAS TÉCNICAS. **NBR 16868-1: Alvenaria estrutural Parte 1: Projeto**. Rio de Janeiro: ABNT, ago. 2020

ASSOCIAÇÃO BRASILEIRA DE NORMAS TÉCNICAS. **NBR 16868-2: Alvenaria estrutural Parte 2: Execução e controle de obras**. Rio de Janeiro: ABNT, ago. 2020

ASSOCIAÇÃO BRASILEIRA DE NORMAS TÉCNICAS. **NBR 16868-3: Alvenaria estrutural Parte 3: Método de ensaio**. Rio de Janeiro: ABNT, ago. 2020

ASSOCIAÇÃO BRASILEIRA DE NORMAS TÉCNICAS. **NBR 16697: Cimento Portland – Requisitos. R**io de Janeiro: ABNT, ago. 2018

Basunbul, I. A., Saleem, M., & Al-Sulaimani, G. J. (1991). Flexural behavior of ferrocement sandwich panels**. Cement and Concrete Composites**, 13(1), 21-28.

Benayoune, A., Samad, A. A., Ali, A. A., & Trikha, D. N. (2007). Response of pre-cast reinforced composite sandwich panels to axial loading**. Construction and Building materials**, 21(3), 677-685.

Benayoune, A., Samad, A. A. A., Trikha, D. N., Ali, A. A. A., & Ashrabov, A. A. (2006). Structural behaviour of eccentrically loaded precast sandwich panels. **Construction and building Materials**, 20(9), 713-724.

BERTINI, A. A. (2002). **Estruturas tipo sanduíche com placas de argamassa projetada** (Tese de doutorado, Universidade de São Paulo).

Bush, T. D., & Stine, G. L. (1994). Flexural behavior of composite precast concrete sandwich panels with continuous truss connectors. **PCI journal**, 39(2), 112-121.

Carbonari, G., Cavalaro, S. H. P., Cansario, M. M., & Aguado, A. (2013). Experimental and analytical study about the compressive behavior of eps sandwich panels**. Materiales de Construcción**, 63(311), 393-402

Casini, M. (2016). **Smart buildings: Advanced materials and nanotechnology to improve energy-efficiency and environmental performance**. Woodhead Publishing.

Choi, I., Kim, J., & Kim, H. R. (2015). Composite behavior of insulated concrete sandwich wall panels subjected to wind pressure and suction. *Materials*, *8*(3), 1264-1282.

Chong, K. P., Wang, K. A., & Griffith, G. R. (1979). Analysis of continuous sandwich panels in building systems. **Building and Environment**, 14(2), 125-130.

Drysdale, R. G., Hamid, A. A., & Baker, L. R. (1994). **Masonry structures: behavior and design**.

Doh, J. H., Fragomeni, S., & Kim, J. W. (2001). Brief review of studies on concrete wall panels in one and two-way action. **International Journal of Ocean Engineering and Technology Special Issue**: Selected Papers, 4(1), 38-43.

Einea, A., Salmon, D. C., Fogarasi, G. J., Culp, T. D., & Tadros, M. K. (1991). State-of-the-art of precast concrete sandwich panels. **PCI Journal**, 36(6), 78-98.

Ellis Jr, R. W., & Cummings, S. D. (1970). **Concrete Sandwich Panels For Low Cost**

Housing Construction.

Fonseca, F. J. C. (1994). Projetos de painéis sanduíche de concreto pré-moldado (Tese de doutorado, Universidade de São Paulo).

Gara, F., Ragni, L., Roia, D., & Dezi, L. (2012). Experimental tests and numerical modelling of wall sandwich panels. **Engineering Structures**, 37, 193-204.

Gleich, H., "New Carbon Fiber Reinforcement Advances Sandwich Wall Panels." STRUCTURE Magazine April (2007): 61-63

Goh, W. I., Mohamad, N., Abdullah, R., & Samad, A. A. A. (2016). Finite element analysis of precast lightweight foamed concrete sandwich panel subjected to axial compression. **Journal of Computer Science & Computational Mathematics**, 6(1), 1-9.

Grzyb, K., & Jasiński, R. (2022, April). Parameter estimation of a homogeneous macromodel of masonry wall made of autoclaved aerated concrete based on standard tests. In **Structures** (Vol. 38, pp. 385-401). Elsevier.

Hendry, A. W., Sinha, B. P., & Davies, S. R. (2004). **Design of masonry structures**. CRC Press.

Hodicky, K., Sopal, G., Rizkalla, S., Hulin, T., & Stang, H. (2015). Experimental and numerical investigation of the FRP shear mechanism for concrete sandwich panels. **Journal of Composites for Construction**, 19(5), 04014083.

Juste, A. E. (2001). **Estudo da resistência e da deformabilidade da alvenaria de blocos de concreto submetida a esforços de compressão** (Tese de doutorado, Universidade de São Paulo).

Kinnane, O., West, R., Grimes, M., & Grimes, J. (2014**). Shear capacity of insulated precast concrete façade panels**. CERI-Civil Engineering Research Ireland.

Kripanarayanan, K. M. (1977, May). Interesting aspects of the empirical wall design equation. In **Journal Proceedings** (Vol. 74, No. 5, pp. 204-207).

Lee, B. J., & Pessiki, S. (2008). Experimental evaluation of precast, prestressed concrete, three-wythe sandwich wall panels. **PCI journal**, 53(2).

Lopes, G. M. (2014). **Estudo teórico e experimental de paredes esbeltas de alvenaria estrutural**.

Masonry Standards Joint Committee. (2002). **Building Code Requirements for Masonry Structures (ACI 530-02/ASCE 5-02/TMS 402-02) and Related Commentaries**. The Masonry Society, SEI of ASCE, and American Concrete Institute, l7l.

Mohamad, G., Fonseca, F. S., Vermeltfoort, A. T., Martens, D. R., & Lourenço, P. B. (2017). Strength, behavior, and failure mode of hollow concrete masonry constructed with mortars of different strengths. **Construction and Building Materials**, 134, 489-496.

Mohamad, N.; Abdullah, R.; Omar, W. (2012). Structural behaviour of precast lightweight foamed concrete sandwich panel as a load bearing wall. Int. J. of Sustain. Develop., vol. 5, no. 3, pp. 49-58.

Nalon, G. H., Ribeiro, J. C. L., Pedroti, L. G., da Silva, R. M., de Araújo, E. N. D., Santos, R. F., & de Lima, G. E. S. (2022). Review of recent progress on the compressive behavior of masonry prisms. Construction and Building Materials, 320, 126181.

Olsen, J. T. (2017). **Developing a general methodology for evaluating composite action in insulated wall panels**. Utah State University.

O'Hegarty, R., & Kinnane, O. (2020). Review of precast concrete sandwich panels and their innovations. **Construction and building materials**, 233, 117145.

O'Hegarty, R., Kinnane, O., Grimes, M., Newell, J., Clifford, M., & West, R. (2021). Development of thin precast concrete sandwich panels: Challenges and outcomes. *Construction and Building Materials*, *267*, 120981.

Pawar, P., Minde, P., & Kulkarni, M. (2022). Analysis of challenges and opportunities of prefabricated sandwich panel system: A solution for affordable housing in India. **Materials Today: Proceedings**.

Pessiki, S., & Mlynarczyk, A. (2003). Experimental evaluation of the composite behavior of precast concrete sandwich wall panels. **PCI journal**, 48(2), 54-71.

Pickard, S. S., & Ventures, N. (1990). Welded wire sandwich panels: an alternative to wood-frame construction. **Concrete Construction**, 35(4), 363-6.

Rahman, M. H. A., & Jaini, Z. M. (2013). The combined finite-discrete element analysis of precast lightweight foamed concrete sandwich panel (PLFP) under axial load. In ***Proceedings of the International Conference on Advances in Structural***.

Saheb, S. M., & Desayi, P. (1989). Ultimate strength of RC wall panels in one-way in-plane action. **Journal of Structural Engineering**, 115(10), 2617-2630.

Sandoval, C., Roca, P., Bernat, E., & Gil, L. (2011). Testing and numerical modelling of buckling failure of masonry walls**. Construction and Building Materials**, 25(12), 4394-4402.

Santana, M. R. C., Soares, R. A. B., & do Espírito Santo, K. N. A. (2020). Estudo de paredes, moldadas no local, constituídas por componentes de poliestireno expandido (EPS), aço e argamassa. **Brazilian Journal of Development**, 6(3), 16568-16586.

Silva, A. F. D. (2007). **Avaliação da resistência à compressão da alvenaria estrutural** (Dissertação de Mestrado, UNESP).

Standard, B. (2005). **Eurocode 6—Design of masonry structures—**. British Standard Institution. London, (2005).

Sulong, R., N. H., Mustapa, S. A. S., & Abdul Rashid, M. K. (2019). Application of expanded polystyrene (EPS) in buildings and constructions: A review. **Journal of Applied Polymer Science**, 136(20), 47529.

Zahra, T., Thamboo, J., & Asad, M. (2021). Compressive strength and deformation characteristics of concrete block masonry made with different mortars, blocks and mortar bedding types. **Journal of Building Engineering**, 38, 102213.